Investigation of the role of eukaryotic initiation factor 3f (eIF3f) and heterogeneous nuclear ribonucleoprotein K (hnRNP K) in stress induced RNA disruption in melanoma cells

By

Michayla Lizzi

A thesis submitted in partial fulfillment
of the requirements for the degree of
Master of Science (MSc) in Biology

Presented to the Faculty of Graduate Studies
Laurentian University
Sudbury, Ontario, Canada

THESIS DEFENCE COMMITTEE/COMITÉ DE SOUTENANCE DE THÈSE
Laurentian Université/Université Laurentienne
Office of Graduate Studies/Bureau des études supérieures

Title of Thesis
Titre de la thèse: Investigation of the role of eukaryotic initiation factor 3f (eIF3f) and heterogeneous nuclear ribonucleoprotein K (hnRNP K) in stress induced RNA disruption in melanoma cells

Name of Candidate
Nom du candidat: Lizzi, Michayla

Degree
Diplôme: Master of Science

Department/Program
Département/Programme: Biology

Date of Defence
Date de la soutenance: July 30, 2021

APPROVED/APPROUVÉ

Thesis Examiners/Examinateurs de thèse:

Dr. Amadeo Parissenti
(Co-Supervisor/Directeur(trice) de thèse)

Dr. A. Thomas Kovala
(Co-Supervisor/Co-directeur(trice) de thèse)

Dr. Jeffrey Gagnon
(Committee member/Membre du comité)

Approved for the Office of Graduate Studies
Approuvé pour le Bureau des études supérieures
Tammy Eger, PhD
Vice-President Research (Office of Graduate Studies)
Vice-rectrice à la recherche (Bureau des études supérieures)
Laurentian University / Université Laurentienne

Dr. Sherif Abou Elela
(External Examiner/Examinateur externe)

ACCESSIBILITY CLAUSE AND PERMISSION TO USE

Abstract

The incidence of skin cancer has been on the rise over the last few decades. While it only represents a small percentage of skin cancers, melanoma is the deadliest skin malignancy. Malignant melanoma is very aggressive and displays both primary and acquired resistance to most therapies. A recent clinical trial has demonstrated that high tumour ribosomal RNA (rRNA) degradation during neoadjuvant chemotherapy can predict complete tumour destruction and improved survival for breast cancer patients. This phenomenon of RNA degradation in response to chemotherapy has been termed RNA disruption, and has been shown to occur in various cancer cell lines, but never in melanoma cells. While the molecular mechanisms involved in RNA disruption remain unclear, studies conducted by other groups have provided evidence that eukaryotic initiation factor 3f (eIF3f) and heterogeneous nuclear ribonucleoprotein K (hnRNP K) may play a role. Under stress eIF3f has been shown to associate with hnRNP K, and it has been proposed that this results in the displacement of hnRNP K from rRNA, allowing it to be degraded by as of yet unidentified ribonucleases. We propose that this may be an underlying mechanism in chemotherapy induced RNA disruption. In this study, we provide the first evidence that chemotherapy and stress-induced RNA disruption can occur in malignant melanoma cells *in vitro*. We further demonstrate that chemical stressors inducing RNA disruption also promote the loss of eIF3f and hnRNP K expression in melanoma cells, and that similar to RNA disruption, this loss of expression is both dose- and time-dependent. However, our studies could not confirm prior studies that eIF3f binding to hnRNP K is increased in cells exposed to chemical stressors. Nevertheless, the dramatic reduction in cellular levels of hnRNP K (a ribosome associated protein) might facilitate rRNA degradation, by permitting greater ribonuclease binding to rRNA.

Key Words

Malignant melanoma, chemotherapy, RNA disruption, eukaryotic initiation factor 3f, heterogeneous nuclear ribonucleoprotein K

Abbreviations

ABC: ATP binding cassette

AMPK: adenosine monophosphate activated protein kinase

ATF6: activating transcription factor 6

ATP: adenosine triphosphate

CDK: cyclin-dependent kinase

CHK1: checkpoint kinase 1

CTLA: cytotoxic T-lymphocyte-associated protein

CYP: cytochrome P450

DMSO: dimethyl sulfoxide

DNA: deoxyribonucleic acid

eEF: eukaryotic elongation factor

eIF: eukaryotic initiation factor

ER: endoplasmic reticulum

FBS: fetal bovine serum

GAPDH: glyceraldehyde 3-phosphate dehydrogenase

GDP: guanosine diphosphate

GST: glutathione S transferase

GTP: guanosine triphosphate

hnRNP: heterogeneous nuclear ribonucleoprotein

HPDE: human pancreatic ductal epithelial

IRE1: inositol-requiring enzyme 1

KH: k homology

MAPK: mitogen-activated protein kinase

Met-tRNA: methionine transfer RNA

mRNA: messenger RNA

mTOR: mechanistic target of rapamycin

NAD: nicotinamide adenine dinucleotide

NGD: no-go decay

NRD: non-functional RNA decay

NSCLC: non-small cell lung cancer

P-bodies: processing bodies

P-gp: p-glycoprotein

p53: tumour protein 53

PARP: poly(ADP-ribose) polymerase

PBS: phosphate buffered saline

PD-1: programmed cell death protein 1

PD-L1: programmed cell death-ligand 1

PERK: PKR-like endoplasmic reticulum kinase

PKC: protein kinase C

PMSF: phenylmethylsulfonyl fluoride

Rb: retinoblastoma protein

RBD: RNA binding domain

RBP: RNA binding protein

RDA: RNA Disruption Assay

RDI: RNA Disruption Index

RIN: RNA integrity number

RNA: ribonucleic acid

RNase: ribonuclease

ROS: reactive oxygen species

RRM: RNA recognition motif

rRNA: ribosomal RNA

SDS: sodium dodecyl sulfate

S6K1: ribosomal protein S6 kinase beta-1

TBP: TATA-binding protein

tRNA: transfer RNA

UPR: unfolded protein response

4EBP: eIF4E binding protein

Acknowledgements

I would like to take this opportunity to thank the individuals who have supported me throughout this project. First, I would like to thank my supervisors Dr. Amadeo Parissenti and Dr. Tom Kovala, for allowing me to pursue this research, and for their continued support and guidance. I would also like to thank Dr. Jeffrey Gagnon for acting as a member of my thesis committee and for providing important feedback throughout this project. Many thanks to Dr. Baoqing Guo, Dr. Renee St. Onge, and Dr. Twinkle Masilamani of RNA Diagnostics for their support, expertise and assistance with experimental methods. I would also like to extend my gratitude to the other members of RNA Diagnostics and the Parissenti research group for sharing their knowledge and providing feedback and encouragement. Finally, I would like to thank my family and friends who have supported me throughout my Master's degree.

Table of Contents

List of Figures

List of Tables

1.0 Introduction

1.1 Malignant Melanoma

1.1.1 Epidemiology and Development

Cancer is a complex disease involving multiple genes, allowing it to overcome the many negative regulators of the cell cycle, grow uncontrollably, evade the immune system, resist apoptosis, and invade other tissues[1]. Understanding the mechanisms of cancer development and progression have led to advances in screening, early detection, novel therapies, and better patient outcomes; however, cancer remains to be a major public health problem worldwide[2]. Cancer is the leading cause of death in Canada, and it expected that nearly half of Canadians will be diagnosed with cancer in their lifetime[3]. The need for advancement in cancer therapy is further indicated by the growing and aging Canadian population, which has led to an increasing number of cancer cases and deaths each year[3].

The incidence of skin cancer has been steadily increasing over the last two decades, and it is now one of the most common forms of cancer[4,5]. While most subtypes of skin cancer are highly treatable and have excellent survival rates, malignant melanoma has a much higher morbidity and mortality rate[5]. Less than 5% of malignant skin tumours are melanoma, however, it accounts for nearly 60% of skin cancer related deaths[6,7]. Melanoma is among the cancers with the highest potential for metastasis and once it becomes metastatic the disease is often incurable, with a long-term survival rate of only 5%[5]. Melanoma develops from the malignant transformation of melanocytes, the pigment producing cells of the epidermis. Primary melanoma lesions develop most often on the skin epidermis, but can arise in any tissue containing melanocytes, including the oral mucosa, nasopharynx, paranasal sinuses, trachea, and eyes[5]. Melanocytes are dendritic cells found in the basal layer of the epidermis that have unique

melanin producing organelles known as melanosomes[7]. Melanin functions to protect skin cells from DNA damage by absorbing UV radiation and neutralizing reactive oxygen species (ROS)[8]. The dendritic processes of melanocytes extend between cells of the epidermis and transfer mature melanosomes to between 30 and 40 keratinocytes, the most abundant cell of the epidermis[8]. Keratinocytes are continuously renewed by stem cells in the basal layer of the epidermis; as they mature they accumulate melanin and migrate outwards, creating a barrier to UV radiation in the skin[8]. The transformation of melanocytes begins with the cell acquiring mutations that offer a proliferative and survival advantage, and a horizontal growth phase[9]. This is followed by a vertical growth phase, where tumour cells invade the dermis, and finally by metastasis, where cells pass through the endothelium into blood vessels and travel to distant sites[9]. The most frequent sites of metastasis are the liver, bone and brain[10].

1.1.2 Treatment

Melanoma treatment varies based on the location and stage of the cancer, but the most common interventions include surgical resection, chemotherapy, immunotherapy, and targeted therapy. For melanoma patients with early stage disease or a single metastatic tumour, surgery is the first line treatment; adjuvant immunotherapy, chemotherapy, or targeted therapy can be subsequently administered to improve survival[6]. The treatment of advanced melanoma with immunotherapy, chemotherapy, or targeted therapy is frequently complicated by an innate or acquired resistance. In addition, the lack of specificity of chemotherapy for cancer cells and the higher doses required for melanoma patients contribute to increased adverse events[6].

Chemotherapy was the first treatment option for advanced malignant melanoma, with the alkylating agent dacarbazine being the first chemotherapy agent to be approved. Several clinical

trials conducted with dacarbazine showed partial response rates of 15-28% and complete response rates of only 3-5%[11]. Despite the limited efficacy of this drug, it remains one of the most effective treatments for malignant melanoma, and a standard regimen to which other therapies are compared[11]. Temozolomide is a second alkylating agent approved for the treatment of advanced malignant melanoma, and has similar efficacy to dacarbazine[11]. Unlike dacarbazine, temozolomide can cross the blood-brain barrier, and therefore is often considered for patients with brain metastases, which occur in 30-40% of advanced melanoma cases[11,12]. Additional chemotherapy agents, including carboplatin, paclitaxel and docetaxel have also been tested in melanoma treatment both alone and in combination. The effects of these agents are comparable to dacarbazine, but result in more severe adverse effects[11]. Although chemotherapy with cytotoxic drugs is no longer the first line therapy for advanced metastatic melanoma, it is still frequently used when there is disease progression following immunotherapy or targeted therapy treatment[11].

Advancements in tumour biology have led to the development of newer therapies that have proven to be useful in the treatment of melanoma, including targeted therapies and immunotherapies. Cancer cells can evade the immune system by expressing CD80 or CD86, which bind to cytotoxic T-lymphocyte associated protein (CTLA-4) on the surface of T-cells to inhibit their activity[13]. Similarly, programmed cell death protein ligand 1 (PD-L1) is expressed by cancer cells to bind programmed cell death protein 1 (PD-1) on the surface of T-cells, to inhibit their activity[13]. This observation led to the development of immunotherapies to block these protein interactions and upregulate T-cell activity. Ipilimumab, an antibody to CTLA-4 was the first immunotherapy to be approved for melanoma treatment, followed by the anti-PD-1 agents nivolumab and pembrolizumab[12]. These therapies have led to significant improvements in

progression-free survival and overall survival for melanoma patients[12]. However, even in responsive cancers the success rate of these immunotherapies is often less than 50%, and primary and acquired resistance to immunotherapy is common[6].

Targeted therapy has also shown promise in the treatment of melanoma, as 70% of patient tumours have mutations in key cell signalling pathways[6]. Since these mutations are often associated with disease progression, targeted therapy uses small molecule inhibitors or antibodies to inhibit these mutated proteins. Mutations in BRAF, a serine-threonine kinase involved in the mitogen-activated protein kinase (MAPK) pathway[6], are associated with increased proliferation and are found in almost 45% of malignant melanomas[14]. The selective inhibitor of BRAF, Vemurafenib, was approved for the treatment of malignant melanoma and resulted in superior clinical response rates when compared to chemotherapy treatment alone in melanomas with BRAF mutations. However, acquired resistance to BRAF inhibitors is also common[12].

1.2 Chemotherapy for Cancer Treatment

1.2.1 Alkylating Agents

The alkylating agents are compounds frequently used as frontline chemotherapy for many cancers. These agents are highly reactive, and inflict DNA damage through the addition of an alkyl group to DNA molecules[15]. Alkylating agents can be classified into several categories, including the triazines, platinum based compounds, and oxazaphosphorines[16]. The triazines include dacarbazine and temozolomide, which are primarily used in the treatment of malignant melanoma. These agents are prodrugs, with dacarbazine being converted to its active form by cytochrome p450 (CYP) enzymes, and temozolomide being activated by the natural pH of the body[17]. These agents cause DNA breakage and apoptosis through the methylation of nitrogen

(N^7) and oxygen (O^6) on the guanine bases of DNA molecules[17,18]. Chemotherapy regimens can often result in severe adverse effects; for patients receiving dacarbazine and temozolomide these may include nausea, vomiting, fatigue, lymphopenia, thrombocytopenia, and neutropenia[17].

Platinum based alkylating agents used clinically in cancer treatment include cisplatin, carboplatin, and oxaliplatin. Platinating agents bind to the nitrogen (N^7) atoms of adenosine and guanine bases and create a crosslink between two DNA bases either on the same strand (intrastrand crosslinks) or different strands (interstrand crosslinks)[19]. The actions of these agents is believed to result in inhibition of DNA replication and subsequent cell death[20]. Cisplatin was first discovered in 1970 as an inhibitor of bacterial growth, and since then carboplatin and oxaliplatin have been developed[19]. Although these agents have similar mechanisms of action, their indications and toxicities vary. Cisplatin treatment has the most toxic effects on tissues and organs, including the nervous system (neurotoxicity), the organ of Corti (ototoxicity), and the kidneys (nephrotoxicity)[19,21]. Carboplatin treatment can result in myelosuppression, but displays relatively low organ toxicity, making it preferable to cisplatin[19,21]. Similar to carboplatin, oxaliplatin is not toxic to organs at conventional doses, but results in peripheral sensory neuropathy which is usually reversible[21].

Another important class of alkylating agents are the oxazaphosphorines, which are analogues of nitrogen mustard[22]. Oxazaphosphorines are prodrugs, and are metabolically transformed into active nitrogen mustards by CYP enzymes in the body[23]. Once transformed, these agents form crosslinks between strands of DNA by reacting with the nitrogen atoms of purine bases[22]. The two most widely used oxazaphosphorines are cyclophosphamide and ifosfamide, which are associated with nephrotoxicity, neurotoxicity, and cardiotoxicity[23].

1.2.2 Topoisomerase Inhibitors

DNA strands need to be separated for DNA and RNA polymerases to replicate and transcribe the genome, respectively. The double-helix structure of DNA results in DNA supercoiling at the points where the two strands of DNA separate[24]. DNA supercoiling ahead of the point of replication or transcription is referred to as positive supercoiling, while supercoiling behind the point of replication is referred to as negative supercoiling[24]. DNA topoisomerases are responsible for transiently cutting and then resealing DNA to relieve this tension, and without them positive supercoiling stalls replication while negative supercoiling results in abnormal DNA structures[24]. There are two types of topoisomerases, classified as type I and II, based on their mechanisms. Type I topoisomerases cleave one strand of DNA at a time, while type II topoisomerases cleave both DNA strands simultaneously[24]. Inhibition of DNA topoisomerase is a common mechanism of chemotherapy agents. The main classes of DNA topoisomerase inhibitors are the anthracyclines, epipodophyllotoxins, and camptothecins.

Anthracyclines are among the most effective anticancer agents, with few resistant cancer types[25]. They produce their cytotoxic effects primarily through their actions on topoisomerase II. Anthracyclines bind to and stabilize the cleaving complex of topoisomerase II, preventing the enzyme from re-ligating the phosphodiester backbone of DNA strands after cleaving to release supercoiling[25]. These agents promote DNA breaks and genomic instability, which eventually causes apoptotic cell death[25]. They have also been shown to intercalate in DNA preventing topoisomerase II activity, and generate ROS[25,26]. The first anthracyclines, daunorubicin and doxorubicin, are natural antibiotics isolated from a mutant strain of *Streptomyces peucetius*; while these were discovered almost 50 years ago, they remain important chemotherapy agents for cancer treatment today[25]. In fact, anthracycline-based therapy has reduced breast cancer

mortality by up to 30%, and has the highest response rate in malignant disease[25,27]. Limitations with these first generation anthracyclines include their toxicity on myocardial tissue, which is thought to be due to reactive oxygen species produced by these compounds[28]. Several derivatives of doxorubicin have since been developed, with epirubicin proving to be clinically useful and having a favourable toxicity profile[27]. However, in addition to cardiotoxicity, these agents can also result in alopecia, nausea, vomiting, leukopenia, and stomatitis[27].

Epipodophyllotoxin is a substance with anti-cancer properties, naturally found in the American Mayapple *Podophyllum peltatum*[29]. The semi-synthetic derivative of this natural product, etoposide, is an important chemotherapeutic used clinically[29]. Using one of the same mechanisms as the anthracyclines, etoposide inhibits topoisomerase II and prevents the re-ligation of DNA strands, causing DNA breaks, and ultimately leading to apoptosis[30]. Despite its potential benefits, treatment with etoposide may result in adverse effects, including myelosuppression, alopecia, nausea, vomiting, and weight loss[31].

Camptothecin is an alkaloid that was first isolated from the Chinese tree *Camptotheca acuminata*[32]. Several camptothecin derivatives were developed, but clinical trials revealed irinotecan and topotecan to be the most promising[32]. In contrast to the anthracyclines and epipodophyllotoxin derivatives, camptothecin and its derivatives exert their cytotoxic effects through the inhibition of topoisomerase I[32]. These compounds create covalent complexes between DNA and topoisomerase I, preventing both the initial cleavage of DNA and the re-ligation of DNA strands[24,32]. These events lead to double strand DNA breaks and the termination of DNA replication, leading to cell cycle arrest and cell death[32]. The major adverse effects associated with irinotecan and topotecan treatment are significant neutropenia, but can also include thrombocytopenia, anemia and gastrointestinal toxicity[32,33].

1.2.3 Microtubule Targeting Agents

Microtubules are polymers of tubulin proteins that are an essential component of the cell cytoskeleton[34]. They are required for cell movement, transport of vesicles, and the separation of chromosomes during mitosis[34]. Microtubules are dynamic in nature, and essential to their functions is the ability to assemble and disassemble[34]. Microtubules are essential for cell division and survival and there are several chemotherapy agents that target microtubules, including the taxanes and vinca alkaloids.

Paclitaxel was the first taxane to be discovered, and was isolated from the bark of the pacific yew tree *Taxus brevifolia*[35]. The extract from this tree was shown to have anti-tumour activity in mice, and the active component was identified to be paclitaxel[35]. Due to limited availability of paclitaxel and hypersensitivity reactions to its formulation, paclitaxel use was suspended for many years[35]. These issues have since been resolved, and synthetic paclitaxel has been developed and made available[35]. The discovery of paclitaxel resulted in the search for similar taxanes. Almost a decade later, 10-deacetylbaccatin III was isolated from the needles of the European yew tree *Taxus baccata*[35]. 10-Deacetylbaccatin III has no cytotoxic activity, but with modification by esterification, the semisynthetic taxane docetaxel was developed[35]. These two taxanes are chemically very similar, and have the same mechanism of action. Both paclitaxel and docetaxel bind to tubulin proteins, leading to the stabilization of microtubule structure, preventing disassembly and shortening[35]. Since the dynamic nature of microtubules is required for their function, microtubule stabilization results in the arrest of mitosis at the anaphase step, and leads to apoptotic cell death[35,36]. Although docetaxel is twice as potent as paclitaxel, they have comparable efficacy[36]. While these agents are effective treatments for many cancers, the toxicity of the taxanes can cause adverse effects including bone marrow suppression,

neurotoxicity resulting in peripheral paresthesia or hypoesthesia, arthralgia, myalgia and alopecia[36].

Vinca alkaloids are naturally extracted from the pink periwinkle plant, *Catharanthus roseus*[37]. When these compounds were first discovered they were investigated for their hypoglycemic effects, but were found to be much more useful for their cytotoxic effects[37]. There are several vinca alkaloids approved for clinical use, including the natural vinca alkaloids vincristine and vinblastine, and the semisynthetic vinorelbine[37,38]. In contrast to the taxanes, vinca alkaloids prevent microtubule assembly and elongation by binding to tubulin proteins in the mitotic spindle[38]. Similar to the taxanes, the effect of vinca alkaloids on microtubules results in the prevention of anaphase during mitosis, causing cell cycle arrest and apoptosis[38]. The toxicities associated with vinca alkaloids include nausea, vomiting, dyspnea, neuropathy, mouth sores, alopecia, and toxicity to blood cells[38].

1.3 RNA Disruption Assay

Even with the development of novel therapies such as immunotherapy or targeted therapies, chemotherapy continues to be the first-line treatment for many cancers, and a second-line therapy for others. Chemotherapy can not only result in severe toxic adverse effects as previously described, but certain chemotherapy regimens have even been linked to secondary malignancies, including leukemia[24,26]. Patients often endure the terrible side effects of several rounds of chemotherapy treatment, with no significant regression or even slowed growth of their cancer. This is a significant problem that indicates the need for a reliable biomarker to determine if patients will respond to chemotherapy treatment early on in the regimen.

A recent clinical trial investigated the relationship between response to chemotherapy treatment and various biomarkers in women with locally advanced or inflammatory breast cancer[39]. Patients were treated with epirubicin and docetaxel, and tumour biopsies were taken before and after treatment, as well as mid-treatment[39]. Investigators used capillary gel electrophoresis to evaluate the quality of RNA in tumour biopsies. Interestingly, this study found that low mid-treatment RNA integrity (RIN) was associated with achieving a pathological complete response[39]. These findings represent the first evidence that tumour RIN values during treatment may be a useful biomarker for predicting the outcome of neoadjuvant chemotherapy. This phenomenon of low RNA integrity in response to chemotherapy treatment, has since been termed "RNA disruption" and describes the unique formation of high molecular weight ribosomal RNA degradation fragments, which is distinct from the low molecular weight degradation products seen in autolytic RNA degradation. The RNA Disruption Assay (RDA) was developed by RNA Diagnostics, Inc. as a method of quantifying RNA disruption. This assay uses a proprietary algorithm to quantify the amount of degraded RNA as an RNA Disruption Index (RDI) using the electropherogram data obtained from capillary gel electrophoresis[40]. A follow up study of the above mentioned trial revealed that high mid-treatment tumour RNA disruption is associated with an increase in disease free survival, even in patients who did not achieve a pathological complete response[41].

The RDA represents a promising biomarker to predict chemotherapy response during treatment. This would provide an opportunity for physicians and patients to make decisions about chemotherapy regimens, and potentially substitute a therapy that may not be beneficial with a more effective one. This would not only improve treatment outcomes, but would avoid the unnecessary harm of ineffective chemotherapy regimens, improving the quality of life for cancer

patients. Over the last decade, immunotherapies have become a standard treatment for many cancers and has resulted in improved survival for cancers such as malignant melanoma. Preliminary *in vitro* studies currently being conducted in the Parissenti research lab suggest that RNA disruption can occur in tumour cells as they are targeted by natural killer cells. Therefore, the RDA may also prove to be a useful tool to predict outcomes from immunotherapy treatment.

1.4 Eukaryotic Ribosomes

1.4.1 Ribosome Structure and Biogenesis

About 80% of cellular RNA is ribosomal RNA, the major component of ribosomes that are responsible for translation and protein synthesis in the cell[42]. The eukaryotic ribosome is composed of a larger 60S subunit and a smaller 40S subunit, with the 'S' referring to their sedimentation coefficient. The 60S subunit is composed of the 5S, 5.8S and 28S rRNA, and 46 ribosomal proteins, while the 40S subunit is composed of the 18S rRNA and 33 ribosomal proteins[43]. In the mature ribosome, the main function of the 60S subunit is to catalyze the formation of peptide bonds, while the 40S subunit decodes messenger RNA (mRNA)[42]. Ribosomal subunits are synthesized in the nucleolus, through a process known as ribosome biogenesis. This is an energetically costly and complex process, involving all three RNA polymerases and more than 150 non-ribosomal factors to facilitate their assembly[44].

The first step in ribosome biogenesis is the synthesis of rRNA, which is tightly linked to the cell cycle. Transcription of rRNA is at its highest during the S and G2 phases of the cell cycle, reduced during mitosis, and increased in G1, reflecting the cells needs for protein synthesis and ribosomes for daughter cells[45]. Transcription of rRNA from rDNA occurs in the nucleolus, and is performed by RNA polymerase I. The rDNA genes residing on 5 different

chromosomes encode the 47S pre-rRNA, containing sequences for the 18S, 5.8S and 28S rRNA strands[42]. The 18S, 5.8S, and 28S rRNAs are separated by two internal transcribed spacers (ITS1 and ITS2), and external transcribed spacers (5'-ETS and 3'-ETS) are found on the ends of the transcript[43]. The gene for the 5S rRNA is separately located, and transcribed by RNA polymerase III[42]. Ribosomal proteins are transcribed by RNA polymerase II, translated in the cytoplasm, and transported into the nucleolus for ribosomal assembly[44]. Over 70 ribosomal proteins must assemble with rRNAs in the nucleolus to assemble functional ribosomal subunits. Ribosomal proteins are not only essential to facilitate the proper folding of rRNA, but are important for stabilizing ribosome structure, stabilizing domains in the mature ribosome, and may stabilize the interaction of ribosomes with mRNA during translation[45]. Following transcription, the pre-RNA is associated with ribosomal proteins, pre-ribosomal factors, and small nucleolar ribonucleoprotein particles[43]. This facilitates the removal of the internal and external transcribed spacers through the actions of several endonucleases and exonucleases, pre-rRNA folding and modification, and assembly with additional ribosomal proteins and the 5S rRNA[43]. The pre-40S and pre-60S subunits are then transported to the cytoplasm and dissociate from non-ribosomal factors, forming mature subunits ready for protein synthesis[44].

1.4.2 Ribosome Degradation and Recycling

The biogenesis and number of ribosomes in the cell is tightly regulated to maintain cellular homeostasis[46]. The production of ribosomal subunits is therefore controlled by cellular conditions including nutrient availability, stress, and the cell cycle[47]. While the control of ribosome production and assembly is well understood, the degradation and recycling of mature ribosomes is less clear[46]. It has been demonstrated that ribosomes can be degraded along with

other cell components during non-selective autophagy, however, they can also be selectively degraded through a process known as ribophagy[46]. Ribophagy is an autophagy-mediated process that has been shown to selectively target the ribosomal subunits in response to nutrient deprivation[48]. The Ubp3 ubiquitin protease is required for the degradation of the large ribosomal subunit, and is thought to remove ubiquitin from select ribosomal proteins, allowing the subunit to be recognized and degraded by autophagolysosomes[46,49]. While ribophagy of the small ribosomal subunit appears to occur through a pathway distinct from the large subunit, this pathway remains unclear[50].

Another ribosomal degradation pathway identified to be involved in ribosome quality control is the non-functional RNA decay (NRD) pathway[51]. Studies in yeast have demonstrated that mutated rRNA contained within mature ribosomes is selectively degraded by the NRD pathway, and there are two distinct pathways for each ribosomal subunit[46]. The 28S NRD is thought to be activated by mutations in the peptidyl transferase centre, while the 18S NRD is triggered by ribosomes with mutations in the decoding site, or that have stalled during translation[46]. In yeast, the 25S NRD pathway (the yeast equivalent of the human 28S NRD pathway) involves the ubiquitination of 60S ribosomal proteins by an E3 ubiquitin ligase complex[52]. The ubiquitination of proteins in the large subunit targets the proteins for degradation by the proteasome, and allows the rRNA to be accessed by RNases for degradation[52]. The 18S NRD appears to involve the proteins responsible for no-go mRNA decay (NGD) which eliminates abnormal mRNAs when a ribosome stalls during translation[50]. During mRNA NGD, a stalled ribosome triggers both endonuclease and exonuclease activity to digest the defective mRNA at the pause site[50]. Interestingly, 18S NRD and mRNA NGD substrates both accumulate in processing bodies, which are ribonuclear protein granules containing RNAs, while 25S NRD

substrates do not co-localize to p-bodies[50]. In contrast to the 25S NRD, it also appears that activation of the 18S NRD requires elongating ribosomes, further demonstrating that they are mechanistically distinct pathways[53].

1.5 Translation Control and Cancer

1.5.1 Translation Initiation and Eukaryotic Initiation Factors

The regulation of translation is primarily controlled during initiation, which is a complex process that is highly regulated by a group of proteins known as the eukaryotic initiation factors (eIFs)[54]. There are six eIFs that have been found to be involved in regulating translation, with most of them being complex proteins with multiple subunits[55]. The initiation of translation requires the assembly of the 60S and 40S ribosomal subunits into an 80S elongation-competent ribosome[54]. The first step in this process is the formation of a 43S preinitiation complex[56]. This involves the formation of a ternary complex of the initiating methionine tRNA (Met-tRNA), eIF2 and GTP[56,57]. This complex is then assembled with the 40S subunit and eIF1, eIF1a, eIF3, and eIF5, to form the 43S preinitiation complex[54,56]. The 43S complex is recruited to the 5' end of a mRNA marked with a 7-methylguanosine cap[54]. Association with the mRNA is mediated by the eIF4f complex, composed of a cap-binding protein (eIF4f) and an RNA helicase (eIF4a), as well as eIF3, eIF4b, and the poly(A) binding protein[54,57]. The 43S complex then scans the 5' untranslated region in a 5' to 3' direction until an AUG start codon is located[54,56]. Once the start codon has been located, the 43S complex is transitioned to a closed state, stabilizing the interaction between the mRNA and Met-tRNA and forming the 48S complex[56]. This is achieved by rejecting eIF1, and hydrolysis of eIF2-GTP to eIF2-GDP by eIF5. Joining of the 48S and 60S subunits to form the 80S initiation complex is mediated by eIF5b and eIF1a, and results in the

release of eIF2-GDP and other initiation factors (eIF1, eIF3, eIF4b, eIF4f and eIF5f). Finally, the release of eIF1a allows the ribosome to enter the elongation phase.

1.5.2 Eukaryotic Initiation Factors in Cancer

Translation plays an important role in tumorigenesis, as an increase in protein synthesis is required to sustain tumour cell growth[42]. Modifications in expression of initiation factors have been described in many different cancers. Of interest in this study is the largest and most complex eukaryotic initiation factor, eIF3, which is made up of 13 subunits (eIFa-m). The primary role of this initiation factor is to recruit mRNAs to form the 48S subunit, and prevent premature association with the 60S subunit[58]. It is also believed to act as a scaffold in translation initiation, as it is known to interact with other eIFs[59]. The roles of each of the eIF3 subunits have not been fully defined; however, many of them have been linked to poor prognosis in cancer patients and cancer progression. Expression of eIF3a fluctuates with the cell cycle, and reductions in its expression are associated with a reduction in cell proliferation. It has been found to be overexpressed in breast, colon, and lung cancers, and is associated with invasiveness in esophageal cancer[60]. The eIF3b subunit is highly expressed in colon cancer, while eIF3c and eIF3i are overexpressed in head and neck squamous cell carcinoma[60]. eIF3h has been associated with colorectal cancer risk, and is amplified in breast, prostate, liver, and lung carcinoma[60]. In contrast to the other eIF3 subunits, eIF3f expression is decreased in many human cancers, including melanoma, pancreatic cancer, and gastric cancer, and the loss of eIF3f expression is associated with a poor prognosis for cancer patients[61–63]. While its role is not well understood, this subunit it is believed to be a negative regulator of translation, explaining its reduced

expression in many cancers[64]. It has also been demonstrated that restoration of eIF3f expression in cancer cells results in rRNA degradation, inhibition of translation, and apoptosis[58].

1.6 Cell Cycle Control and Responses to Stress

1.6.1 Cell Cycle Control

The eukaryotic cell cycle is strictly regulated to ensure proper duplication of genetic material, and appropriate cell growth and division. Alterations in proliferative signalling pathways or cell cycle proteins can lead to uncontrolled growth and division, which is one of the hallmarks of cancer[1]. The cell cycle involves four phases: G1, S, G2 and M. The replication of DNA occurs during the S phase, and mitosis occurs during the M phase. The G1 and G2 phases are known as gap phases, occurring before DNA replication and before mitosis, respectively[65]. Transition through each phase is regulated by cyclin-dependent kinases (CDKs)[66]. CDKs are serine/threonine kinases that are activated by cyclin proteins; CDK activity is induced in response to mitogenic signals, and inhibited by cell abnormalities that lead to the activation of cell cycle checkpoints.

CDK4 and CDK6 are activated by cyclin-D in response to mitogenic signals, leading to the phosphorylation of the retinoblastoma (Rb) protein[66]. Rb is an important tumour suppressor, and its inactivation is required for progression through the cell cycle[67]. Inactivation of Rb allows E2F transcription factors to activate genes that are necessary for cell cycle progression from G1 to S phase[67]. E2F promotes the synthesis of cyclins E1 and E2, which bind CDK2; the cyclin E-CDK2 complex further phosphorylates Rb and leads to the progression of cells into S phase[66]. During the G2 phase, transcription of genes required for the progression through M phase occurs, including cyclin B which binds to CDK1; activation of cyclin B-CDK1 is required for entry into

mitosis[66]. There are cell cycle checkpoints at the G1 and G2 phase that will prevent cell cycle progression in response to DNA damage, and the cell will enter a reversible or permanent cell cycle arrest. The cyclin E-CDK2 complex is inhibited by the activation of the p53-dependent G1 DNA damage checkpoint, while cyclin B-CDK1 is inhibited by activation of the checkpoint kinase 1 (CHK1)-dependent G2 DNA damage checkpoint.

The transcription factor p53 plays an important role in regulation of the cell cycle, mediating the G1 DNA damage checkpoint and cell cycle arrest[68]. p53 is an important tumour suppressor, with alterations in the p53 protein or associated pathways being found in nearly every tumour[68]. Activation of p53 is also important in mediating cellular responses to stress. Depending on the type of stress, activation of p53 leads to the transcription of genes involved in cell cycle arrest, DNA repair, apoptosis and senescence[68]. Other p53 targets include genes that are involved in protecting the cell from oxidative stress, regulation of metabolic homeostasis, and autophagy[68].

1.6.2 Cellular Responses to Stress

One of the ways cells may respond to stress is by reducing protein synthesis. This is modulated by two main mechanisms: regulation of the mechanistic (or mammalian) target of rapamycin (mTOR) and phosphorylation of eIF2α[69]. mTOR is a serine/threonine protein kinase that coordinates cell growth and metabolism in response to nutrient availability and growth factors[70]. Regulation of protein synthesis by mTOR is achieved through its phosphorylation of eIF4E binding protein (4EBP) and p70S6 kinase (S6K1). 4EBP inhibits the initiation of translation by binding eIF4E and preventing the formation of the eIF4F complex[70]. Phosphorylation of 4EBP by mTOR triggers its dissociation from eIF4E and allows translation

initiation to proceed[70]. S6K1 is responsible for the phosphorylation and activation of several proteins involved in initiation of translation, including eIF4F[70]. In response to glucose deprivation, mTOR is inhibited by AMP-activated protein kinase (AMPK), a stress-response regulator[70].

Phosphorylation of eIF2α is another method that allows cells to stop translation. There are at least four distinct kinases in mammalian cells that can phosphorylate eIF2α under stress, inhibiting the recycling of eIF2 and translation initiation[69]. This is a particularly important pathway in response to endoplasmic reticulum (ER) stress. The endoplasmic reticulum (ER) is a network of tubules in the cytoplasm of eukaryotic cells, responsible for the folding, post-translational modification, and translocation of proteins. Under conditions of cell stress such as hypoxia, starvation, or acidosis, there is an alteration in protein homeostasis and misfolded proteins accumulate in the ER[71]. This is known as ER stress, and triggers the unfolded protein response (UPR). The UPR involves the initiation of adaptive mechanisms in an attempt to enhance the folding and clearance of proteins and restore homeostasis, as prolonged ER stress can result in cell death[71]. This response is mediated by activating transcription factor 6 (ATF6), PKR-like kinase (PERK), and inositol-requiring enzyme 1 (IRE1). ATF6 is a transcription factor that is activated during ER stress. Upon activation it is translocated to the Golgi apparatus where it is cleaved and translocated to the nucleus to activate the transcription of genes coding for ER chaperones[71]. PERK is responsible for halting mRNA translation during ER stress through the phosphorylation and inhibition of eIF2α, preventing additional proteins from entering the ER[71]. IRE1 is responsible for dictating cell fate, whether survival or cell death, based on the level of ER stress[71]. If the UPR cannot re-establish homeostasis, ER stress can eventually lead to cell death as a result of calcium overload, cessation of protein synthesis, or apoptosis[72].

Reactive oxygen species are by-products of oxygen metabolism that are generated by normal cellular processes and play an important role in signal transduction. For instance, hydrogen peroxide is known to play a role in the regulation of cell differentiation, proliferation, migration, and apoptosis[73]. However, ROS can also react with cellular components, resulting in protein oxidation, lipid peroxidation, and/or DNA damage. In order to maintain REDOX homeostasis, cells have antioxidant enzymes which include superoxide dismutase, catalase, glutathione peroxidases, and thioredoxin peroxidases, that function to detoxify ROS and recycle oxidized molecules[73]. Oxidative stress results when there is an imbalance in the cellular REDOX system, and the production of ROS exceeds the cells antioxidant capabilities. Oxidative DNA damage can lead to mutations that contribute to tumorigenesis, or can ultimately result in cell death[73]. Poly(ADP-ribose) polymerase (PARP) is an enzyme activated in response to oxidative DNA damage, and can mediate apoptosis or necrosis based on the extent of DNA damage[74]. Hyperactivation of PARP with severe oxidative DNA damage results in complete depletion of the REDOX coenzyme NAD, leading to energy failure and necrosis; with less severe DNA damage activation of PARP results in the ADP-ribosylation of chromatin, promoting the turnover of chromatin proteins and allowing apoptosis related proteins, such as p53, to bind to DNA[74].

1.7 RNA-Binding Proteins

1.7.1 Structure and Function of RNA Binding Proteins

RNA binding proteins (RBPs) play an important role in the control of gene expression. These proteins are responsible for the differential splicing of pre-mRNAs, facilitating the expression of multiple proteins from a single gene[75]. They are also responsible for the

maturation, stability, transport, and degradation of RNA molecules. RPBs contain one or more highly conserved RNA binding domains, that facilitate RNA binding[76]. The most common RNA binding domain (RBD) is the RNP motif or RNA recognition motif (RRM), which is composed of 90 to 100 amino acids that form four antiparallel β sheets and two perpendicular α helices[76]. Some RPBs facilitate the localization of mRNAs to specific areas of the cell, while others are involved in promoting or repressing the translation of certain mRNAs. While many RPBs have one specific cellular function, the heterogeneous nuclear ribonucleoprotein (hnRNP) family represents an example of RBPs that can facilitate multiple diverse processes[75]. These proteins are able to bind RNA sequences on multiple RNAs, and facilitate many important functions. Interestingly, alterations in the expression of several members of this protein family have been implicated in tumorigenesis[75].

1.7.2 Heterogeneous Nuclear Ribonucleoprotein K

Heterogeneous nuclear ribonucleoprotein K (hnRNP K) is a DNA and RNA binding protein that is involved in gene expression by regulating transcription, RNA splicing, and translation[77]. hnRNP K is a poly(C)-binding protein, with three K homology (KH) domains that facilitate binding to RNA and DNA[78]. The interaction of hnRNP K with other proteins is mediated by an unstructured region called the K-protein-interactive (KI) domain. In addition, hnRNP K contains a nuclear localization signal and a nuclear shuttling domain, which facilitate its bi-directional transport through nuclear pores[79]. hnRNP K is one of the most abundant proteins in the nuclear matrix, playing a role in stabilizing the nuclear matrix network. It is associated with areas of chromatin containing highly expressed genes, and is known to act as both an activator and repressor of transcription[79]. To stimulate transcription, it interacts with the

TATA-box binding protein (TBP), while to inhibit translation it binds the translational repressor Zik1[79]. It is known to regulate genes for the μ opioid receptor, eIF4e, and the nicotinic acetylcholine receptor[79].

hnRNP K has been shown to be an important protein involved in malignant transformation. Several studies have shown that hnRNP K can activate oncogenes including c-src, which leads to the activation of translation pathways[80]. hnRNP K can also bind the CT-element of the c-myc oncogene promoter and results in increased gene transcription and translation, which is associated with increased cell proliferation[80]. Levels of tumour hnRNP K can be associated with tumour stage and aggressiveness, indicating a relationship with tumour progression[79]. Rapidly dividing cells have a higher level of hnRNP K, and it has been found to be overexpressed in breast, esophageal, head and neck, lung, pancreatic, and colorectal cancer[77,81,82]. Recently, it has been shown that downregulation of hnRNP K in lung cancer cells reduces the formation of metastases in mice[83]. Together these observations suggest that hnRNP K plays and important role in suppression of tumorigenesis by regulating protein synthesis.

1.8 A Potential Pathway Involved in RNA Disruption

Some studies have suggested rRNA degradation occurs as a result of the activation of apoptosis[84,85], while others have demonstrated that rRNA can be degraded independently of apoptosis[86,87]. However, the exact pathway and molecular mechanisms involved in rRNA degradation in eukaryotic cells remain unclear. A study conducted by Wen et al. demonstrated the potential role of eIF3f and hnRNP K in regulating rRNA degradation[64]. Studies by the same group have described reduced eIF3f expression[58,62,63], and increased hnRNP K expression[82,88] in many cancers. They have also demonstrated that restoration of eIF3f expression in cancer cells

leads to rRNA degradation and induces apoptosis[58]. Stable knock down of eIF3f in normal cells results in features malignant transformation, including an increase in cell size, nuclear pleomorphism, aneuploidy, cell-cycle abnormalities, and resistance to apoptosis[64]. Furthermore, they showed that hnRNP K binds to the 28S rRNA, and found that overexpression of hnRNP K in normal cells was protective against rRNA degradation[64]. These findings suggest that loss of eIF3f promotes tumorigenesis by allowing increased translation, while overexpression of hnRNP K prevents ribosome degradation to facilitate increased protein synthesis.

Experiments looking at the interaction between eIF3f and hnRNP K revealed that these two proteins associate under stress. Cell fractionation experiments revealed that treatment of A375 malignant melanoma cells with staurosporine caused eIF3f to be co-localized with hnRNP K[64]. This association was also demonstrated in human pancreatic duct epithelial (HPDE) cells treated with 10 μM etoposide using co-immunoprecipitation studies. Based on these observations, Wen et al. proposed that eIF3f inhibits translation by interfering with the protective function of hnRNP K. Specifically, they hypothesized that eIF3f interacts with hnRNP K, dissociating it from rRNA, leaving the rRNA unprotected and able to be degraded by ribonucleases (RNases). Although it is likely that there is more than one molecular mechanism involved in the regulation of rRNA degradation, this study provides convincing evidence that eIF3f and hnRNP K are involved. We propose that this mechanism of stress-induced rRNA degradation may also play a role in chemotherapy-induced RNA disruption.

1.9 Hypothesis and Research Aims

Although studies have suggested that measuring tumour RNA disruption may be an important biomarker for predicting the outcome of chemotherapy treatment, the mechanism

behind this phenomenon is not well understood. Chemotherapy-induced RNA disruption has been shown to occur in several ovarian and breast cancer cell lines *in vitro*, in response to mechanistically distinct chemotherapy agents[89]. The aim of this study was to assess whether chemotherapy agents and other forms of cell stress can induce RNA disruption in melanoma cells, and to investigate the potential role of eIF3f and hnRNP K in this phenomenon. While A375 malignant melanoma cells were primarily selected based on their use in previous studies to demonstrate the association of eIF3f and hnRNP K under stress, this cell line is also of interest as RNA disruption has never been evaluated in melanoma cells. In this study, we assessed for the first time whether chemotherapy and cellular stress can induce RNA disruption in melanoma cells *in vitro*. We hypothesize that treatment of A375 cells with various structurally and mechanistically distinct chemotherapy agents will result in RNA disruption. We further hypothesize that other forms of stress, including metabolic stress, ER stress, oxidative stress, and inhibition of protein synthesis will promote RNA disruption. Finally, we propose that the expression of hnRNP K and eIF3f and/or the association between these two proteins are involved in regulating rRNA levels under stress, and we expect to see changes in the expression and interaction of these proteins with treatments that induce RNA disruption. To investigate the above hypotheses, four specific project objectives were set:

1) Determine if chemotherapy induced RNA disruption can occur in A375 cells and demonstrate the response is both dose- and time-dependent.
2) Assess whether RNA disruption can be induced by other forms of cell stress in A375 cells.
3) Evaluate the expression of eIF3f and hnRNP K with treatments that induce RNA disruption.

4) Optimize a co-immunoprecipitation protocol to assess whether there is an association of eIF3f and hnRNP K in A375 cells, which changes under stress and upon induction of RNA disruption.

2.0 Methods

2.1 Cell Culture

The A375 human malignant melanoma epithelial cell line was purchased from the American Tissue Culture Collection (Burlington, ON, Canada) to be used as an *in vitro* model of malignant melanoma. Cultures were maintained in 75 cm^2 vented tissue culture flasks (Starstedt, Nümbrecht, Germany) with Dulbecco's Modified Eagle's Medium (DMEM) (Gibco, Thermo Fisher Scientific, Waltham, MA) supplemented with 10% fetal bovine serum (FBS) (Gibco, Thermo Fisher Scientific, Waltham, MA). Cell stocks were prepared in DMEM containing 5% dimethyl sulfoxide (DMSO) and 30% FBS and cryopreserved in liquid nitrogen. The A2780 ovarian carcinoma cell line was previously obtained from the European Collection of Cell Cultures (Salisbury, UK), and was used as a positive control for RNA disruption in select experiments. A2780 cultures were maintained in 75 cm^2 vented tissue culture flasks (Corning, New York, USA) with RPMI-1640 medium (Gibco, Thermo Fisher Scientific, Waltham, MA) containing 10% FBS. All cells were grown in a humidified incubator at 37°C with 5% CO_2, and allowed to reach 70-90% confluency before subculturing every 2-3 days.

2.2 Chemotherapy Treatment

Nine chemotherapy agents were used in this study: two alkylating agents (cisplatin and carboplatin), four topoisomerase inhibitors (irinotecan, etoposide, doxorubicin, and epirubicin), and three microtubule targeting agents (vincristine, paclitaxel, and docetaxel). All chemotherapy drugs were obtained from the pharmacy at Health Sciences North (Sudbury, ON, Canada) and stored in amber vials at 4°C. A series of experiments were conducted to determine if chemotherapy-induced RNA disruption can occur in malignant melanoma cells *in vitro*. A375

cells were seeded at a density of 150,000 cells per well in 6-well tissue culture plates (Starstedt, Nümbrecht, Germany) and supplemented with 3 mL of cell culture medium. The plate was incubated for 24 hours to allow cells to adhere; the medium was then replaced with 3 mL of drug-free medium or 3 mL of treatment medium. Treatment medium was prepared by performing serial dilutions of the various chemotherapy drugs in cell culture medium. Cells were treated for 72 hours, then total RNA was isolated for analysis. The concentrations of chemotherapy drugs and treatment time was selected based on observations of RNA disruption in other cancer cell lines[89].

To determine the effects of chemotherapy drugs on protein expression and protein-protein interactions, A375 cells were seeded in 10 cm tissue culture plates (Starstedt, Nümbrecht, Germany) and supplemented with 10 mL of cell culture medium. For untreated controls, cells were seeded at a density of $1x10^6$ cells per plate, and for treatment conditions cells were seeded at a density of $2x10^6$ cells per plate, as cells die at higher rates and do not replicate as well during treatment. Seeded cells were allowed to adhere to their flasks for 24 hours before the cell culture medium was replaced with either 10 mL of fresh medium, or fresh medium supplemented with chemotherapy. Cells were treated for 48 or 72 hours, after which whole cell protein lysates were prepared from the cells. To obtain an adequate amount of protein with high dose treatments (1 μM doxorubicin and 200 μM etoposide), two plates each with $2x10^6$ cells were seeded and the whole cell lysates from the two plates were pooled (see section on preparation of whole cell lysates).

2.3 Staurosporine Treatment

Staurosporine is a non-selective inhibitor of protein kinases, known to cause apoptosis and the association of eIF3f with hnRNP K in A375 cells[64]. In this study, staurosporine was assessed for its ability to cause RNA disruption and for its effects on eIF3f and hnRNP K expression. It was also used as a positive control for monitoring the association of eIF3f with hnRNP K. Staurosporine was purchased from Abcam (Cambridge, MA, USA) and dissolved in DMSO according to the manufacturers recommendation. To assess the effects of staurosporine on RNA disruption, cells were seeded at a density of 150,000 cells per well in 6-well tissue culture plates and incubated for 24 hours. After 24 hours, cells were treated with cell culture medium supplemented with staurosporine for 72 hours.

For protein expression and immunoprecipitation experiments, control plates were seeded at a density of $1x10^6$ cells per plate, and treatment plates were seeded at a density of $2x10^6$ cells per plate. Plates were incubated for 24 hours before the cell culture medium was replaced with either 10 mL of fresh medium or fresh medium supplemented with staurosporine for 36 to 72 hours. Following treatment, whole cell protein lysates were obtained. For treatment with 1 μM staurosporine, two plates each were seeded with $2x10^6$ cells and the whole cell lysates from the two plates were pooled.

2.4 Activation of Cell Stress Pathways

Several agents were used to determine if activation of cell stress pathways can lead to RNA disruption in malignant melanoma cells. ER stress was simulated by treatment of cells with thapsigargin (Sigma-Aldrich, Oakville, ON, Canada) or tunicamycin (Sigma-Aldrich, Oakville, ON, Canada). Tunicamycin inhibits N-linked glycosylation of proteins in the ER, disrupting the

maturation of proteins, and triggering ER stress[90], while thapsigargin results in ER stress by altering ER calcium levels[91]. Cycloheximide (Sigma-Aldrich, Oakville, ON, Canada) was used as an inhibitor of protein synthesis and palbociclib (Cedarlane, Victoria, BC, Canada) was used to selectively inhibit CDK4 and CDK6. For treatment, cells were seeded at a density of 150,000 cells per well in a 6-well tissue culture plate and supplemented with 3 mL of fresh medium. After 24 hours, the medium was replaced with treatment medium and plates were incubated for 72 hours. Treatment medium was prepared by serial dilutions of each agent in fresh cell culture medium immediately before use.

2.5 Hydrogen Peroxide Treatment

Hydrogen peroxide treatment was used to determine the effects of oxidative stress on RNA disruption. A2780 cells were used as a positive control in these experiments as A375 cells were found to be resistant to low doses of hydrogen peroxide in preliminary experiments. In 6-well tissue culture plates, A375 cells were seeded at a density of 150,000 cells per well, while A2780 cells were seeded at a density of 250,000 cells per well. After a 24 hour incubation, 3 mL of cell culture medium supplemented with hydrogen peroxide (Sigma-Aldrich, Oakville, ON, Canada) was added to the plates and cells were treated for 24 hours.

2.6 Cell Culture Media Dilution

Whole cell culture medium dilution with sterile PBS was used to induce cellular stress by reducing cellular nutrients and growth factors, in order to determine whether this would have an effect on RNA disruption. Cells were plated and incubated for 24 hours as described above. Prior to the addition of treatment medium, each well was washed with 3 mL of sterile PBS in order to

remove excess media. Then, 3 mL of fresh medium, diluted medium or PBS alone were added to the plate for 72 hours.

2.7 RNA Isolation

Total RNA was isolated from treated and untreated cells using the RNeasy® Mini Kit (Qiagen, Mississauga, ON, Canada). First, the spent medium was removed from each well and transferred to a 15-mL conical tube. Adherent cells were washed with 3 mL of PBS, and the wash was transferred to the corresponding tube. Any floating cells were pelleted by centrifugation at 500 x g for 5 minutes, and the supernatant was discarded. Then, 350 µL of RLT Lysis Buffer supplemented with β-mercaptoethanol were added to each well, and any adherent cells were lifted using a sterile cell scraper. Lifted cells were transferred to the tube containing the corresponding cell pellet, and cells were sheared by seven passages through a 21G needle. The lysate was mixed with 350 µL of 70% ethanol and transferred to an RNeasy® Mini spin column. The spin column was centrifuged at 12,000 x g for 15 seconds, binding the RNA. The column was then washed once with 700 µL of RW1 Wash Buffer, and twice with 500 µL RPE Buffer to wash away any biomolecules and salts. Finally, the RNA was eluted from the column with 35 µL of RNase-free water and stored at -80°C until analysis.

2.8 RNA Quantification and Integrity Analysis

The RNA concentration of each sample was used to assess the response of cells to each treatment, and was determined using a NanoDrop™ One (Thermo Fisher Scientific, Waltham, MA) spectrophotometer. RNA integrity was also assessed by capillary gel electrophoresis using the RNA 6000 Nano kit (Agilent Technologies, Santa Clara, CA, USA). All RNA samples were

heat-denatured at 70°C for 3 minutes, and loaded onto an RNA Nano chip according to the manufacturers protocol. Electrophoresis and data depiction were performed using an Agilent 2100 Bioanalyzer and 2100 Expert Software (Agilent Technologies, Santa Clara, CA, USA). The RNA Disruption Index (RDI) was computed for each sample using its electropherogram data exported from the Agilent 2100 Expert Software and a proprietary algorithm from RNA Diagnostics, Inc. (Toronto, ON, Canada). The RDI represents the mass ratio of abnormal ribosomal RNA degradation products to the normal 28S and 18S ribosomal RNAs.

2.9 Preparation of Whole Cell Lysates

Non-denaturing lysis stock buffer (20 mM Tris HCl, 137 mM NaCl, 2 mM EDTA, 0.2% NP-40, pH 8) was prepared and stored at 4°C. A protease inhibitor cocktail (Roche, Mississauga, ON), 10 µM sodium fluoride, 1 µM phenylmethylsulfonyl fluoride (PMSF), and 2 mM sodium orthovanadate were added to the stock buffer immediately before use. Following 36, 48, or 72 hours of treatment with or without various stress inducing agents, the tissue culture plates were removed from the incubator and placed on ice. Cell culture medium containing any floating cells was transferred to a 50-mL conical tube, and adherent cells were washed with 5 mL of cold PBS. The PBS wash was transferred to the corresponding tube and floating cells were collected by centrifugation at 500 x g for 5 minutes. Following centrifugation, the supernatant was discarded, and the cell pellet was placed on ice. Non-denaturing lysis buffer was added to each of the tissue culture plates and adherent cells were lifted from the plates using a sterile cell scraper. The cells were then transferred to the corresponding conical tube containing the cell pellet and sheared by seven passages through a 21G needle. The mixture was then transferred to a 1.5-mL microcentrifuge tube and incubated on ice for 30 minutes. Following incubation, the samples

were centrifuged at 15,000 x g for 20 minutes at 4°C. The supernatant containing isolated protein was transferred to a new 1.5-mL tube and stored at -80°C until use. The protein concentration of each whole cell lysate was quantified using the Pierce BCA Protein Assay Kit (Pierce, Rockford, IL, USA).

2.10 Immunoprecipitation

Whole cell lysates were thawed on ice, and 100 to 500 µg of protein from each cell lysate was transferred to a 0.5 mL microcentrifuge tube. Samples were diluted to equal volumes with non-denaturing lysis buffer, and the primary antibody was added to each tube. Primary antibodies for the immunoprecipitation of eIF3f (ab176853) and hnRNP K (ab52600) were purchased from Abcam (Cambridge, MA, USA). Samples were incubated with primary antibody overnight on a rocker at 4°C. Pierce™ Protein A/G Magnetic Beads (Thermo Fisher Scientific, Waltham, MA) were used for immunoprecipitation. To prepare the beads, they were washed with 175 µL and then 1mL of wash buffer consisting of tris-buffered saline with 0.05% Tween-20 (Sigma-Aldrich, Oakville, ON, Canada). For each wash, beads were mixed with wash buffer, collected on a magnetic stand, and the supernatant was discarded.

Following incubation with the primary antibody, each sample was transferred to a 1.5mL tube containing prepared magnetic beads and incubated with gentle agitation at room temperature for 1 hour. The magnetic beads bound to the primary antibody and protein of interest were then collected using a magnetic stand and the supernatant containing the remaining protein lysate was kept for analysis. The beads were then washed twice with 100 µL of wash buffer, and the wash buffer was collected for analysis. Both the supernatant and wash buffers were stored at

-20C until use. Finally, one of two different methods were used in this study to elute the protein of interest from the beads.

2.10.1 Glycine Elution

An elution buffer consisting of 0.2 M glycine (pH 2.6) was prepared and stored at 4°C. Bound proteins were eluted by adding 50 µL of glycine elution buffer to the magnetic beads and incubating them for 10 minutes on a shaker at room temperature. The beads were then collected on a magnetic stand, and the supernatant containing eluted proteins was transferred to a 0.5-mL tube. To neutralize the low pH, 50 µL of a 1M Tris (pH 8) neutralization buffer was added to each of the samples. This process was repeated for a total of 2 washes, and the immunoprecipitated proteins were stored at -20°C until analysis.

2.10.2 SDS Elution

To elute bound proteins, 25 µL of 2X sample buffer was mixed with the magnetic beads and the sample was heated at 100°C for 2 minutes. After heating, the beads were collected using a magnetic stand, and the supernatant was transferred to a 0.5-mL microcentrifuge tube. This process was then repeated a second time to elute any remaining proteins, and the samples were stored at -20°C until use.

2.11 Polyacrylamide Gel Electrophoresis

2.11.1 Protein Expression Western Blots

The proteins in whole cell lysates were resolved by polyacrylamide gel electrophoresis in order to determine the effects of treatment on the expression of various proteins. These samples

were prepared by mixing 25 µg of protein with an equal volume of 2X sample buffer, and heating at 100°C for 5 minutes. Proteins were resolved on a 12% polyacrylamide gel at 90V for 2 hours using a BioRad PowerPac™ power supply.

2.11.2 Co-Immunoprecipitation Western Blots

Immunoprecipitated proteins were resolved on a 12% polyacrylamide gel at 90V for 2 to 2.5 hours using a BioRad PowerPac™ power supply. For samples obtained by glycine elution, a 50 µL fraction of the immunoprecipitated proteins was prepared with 5X sample buffer and heated at 100°C for 5 minutes. For samples obtained by SDS elution, the immunoprecipitated proteins in each sample (already prepared in 2X sample buffer) were loaded onto the gel. Whole cell lysates prepared as previously described were used as a loading control. To evaluate possible loss of the protein of interest, remaining proteins in the supernatant or wash buffers were also resolved. To prepare these samples, 25 µL of the supernatant or wash buffer were mixed with an equal volume of 2X sample buffer, and heated at 100°C for 5 minutes.

2.12 Immunoblotting

Proteins were transferred from the polyacrylamide gel to a nitrocellulose membrane (GE Healthcare Life Sciences, Marlborough, MA, USA) at 12V for 90 minutes using a BioRad semi-dry transfer unit. The membranes were then blocked in a 5% milk solution in 0.1% TBST (tris buffered saline containing 0.1% Tween-20) for 1 hour with gentle agitation on a shaker. Then, a dilution of primary antibody was prepared in 5% milk in 0.1% TBST, and the membranes were incubated on a rocker overnight at 4°C. In this study, expression of eIF3f was determined using a rabbit polyclonal antibody (ab52600) obtained from Abcam (Cambridge, MA, USA). Two

antibodies were used for the detection of hnRNP K, one rabbit monoclonal antibody (ab52600) and one mouse monoclonal antibody (ab39975), both obtained from Abcam (Cambridge, MA, USA). GAPDH was used as a loading control, and was detected using a mouse monoclonal antibody (0411) from Santa Cruz Biotechnology (Dallas, TX, USA).

After incubation with primary antibody, the membrane was washed 3 times with 0.1% TBST for 5 minutes. The membranes were then incubated with the secondary antibody diluted in 5% milk in 0.1% TBST for 1 hour on a shaker at room temperature. Mouse primary antibodies were detected with an anti-mouse IgG secondary antibody (sc-2005) obtained from Santa Cruz Biotechnology, and rabbit primary antibodies were detected using an anti-rabbit IgG secondary antibody (70745) from Cell Signalling Technology (Danvers, MA, USA). To remove unbound secondary antibody, the membranes were again washed 3 times with 0.1% TBST for 5 minutes. Proteins of interest were visualized using the enhanced chemiluminescence (ECL) method using SuperSignal™ West Pico Plus reagents (ThermoFisher Scientific, Waltham, MA). Blot images were obtained using a Fluorchem™ gel documentation system (Protein Simple, San Jose, CA), and densitometry was performed using ImageJ software.

2.13 Statistical Analysis

Statistical analyses were performed using GraphPad Prism 8 software. For all RNA and protein densitometry data, the difference between the untreated control and each treatment condition was determined using a one-tailed paired Student's t-tests. A p value of < 0.05 was considered to be statistically significant. This statistical analysis was selected as it is more conservative than other methods, and there was a large amount of variance in the data obtained.

Furthermore, comparisons were made only between individual treatment doses and the untreated control.

3.0 Results

3.1 Chemotherapy Induced RNA Disruption in Malignant Melanoma

To address our first project objective, we assessed whether chemotherapy can induce RNA disruption in malignant melanoma cells using a variety of mechanistically distinct chemotherapy agents. Drug treatments were selected based on concentrations that have been shown to cause RNA disruption in other epithelial cell lines[89]. Recognizing that A375 cells may respond differently, a dose 10-fold higher and 10-fold lower than what was previously shown to cause RNA disruption was also included for each drug.

3.1.1 Alkylating Agents

Previous studies have demonstrated that 72 hour treatment with 20 μM carboplatin and 1.7 μM cisplatin were sufficient to cause RNA disruption in A2780 cells[89]. Therefore, A375 cells were treated with 2, 20, and 200 μM carboplatin and 0.17, 1.7 and 17 μM cisplatin for 72 hours. The effect of these agents on the cellular RNA integrity was determined by capillary gel electrophoresis using the Agilent 2100 Bioanalyzer (Figure 1A). The effect on total RNA was determined by spectrophotometric quantification of RNA isolated from treated and untreated cells (Figure 1B), while effect on RNA disruption (ribosomal RNA degradation) was quantified using the RDA (Figure 1C). There was a statistically significant decrease in total RNA upon treatment of cells with 20 μM ($p = 0.0016$) and 200 μM ($p = 0.0003$) carboplatin compared to the untreated control. There was no statistically significant change in RDI with carboplatin treatment; however, 200 uM carboplatin caused a 6.8-fold increase in RDI from the untreated control and some RNA degradation products can be observed on gel images at this dose (Figure 1A). Cisplatin treatment resulted in a statistically significant decrease in total RNA at 1.7 μM (p

= 0.0061) and 17 µM (p = 0.0007). RNA degradation products were visible on gel images with 17 µM cisplatin treatment (Figure 1A); this treatment was found to result in a statistically significant increase in RDI (p = 0.0142) and represents an 8.8-fold increase from the untreated control.

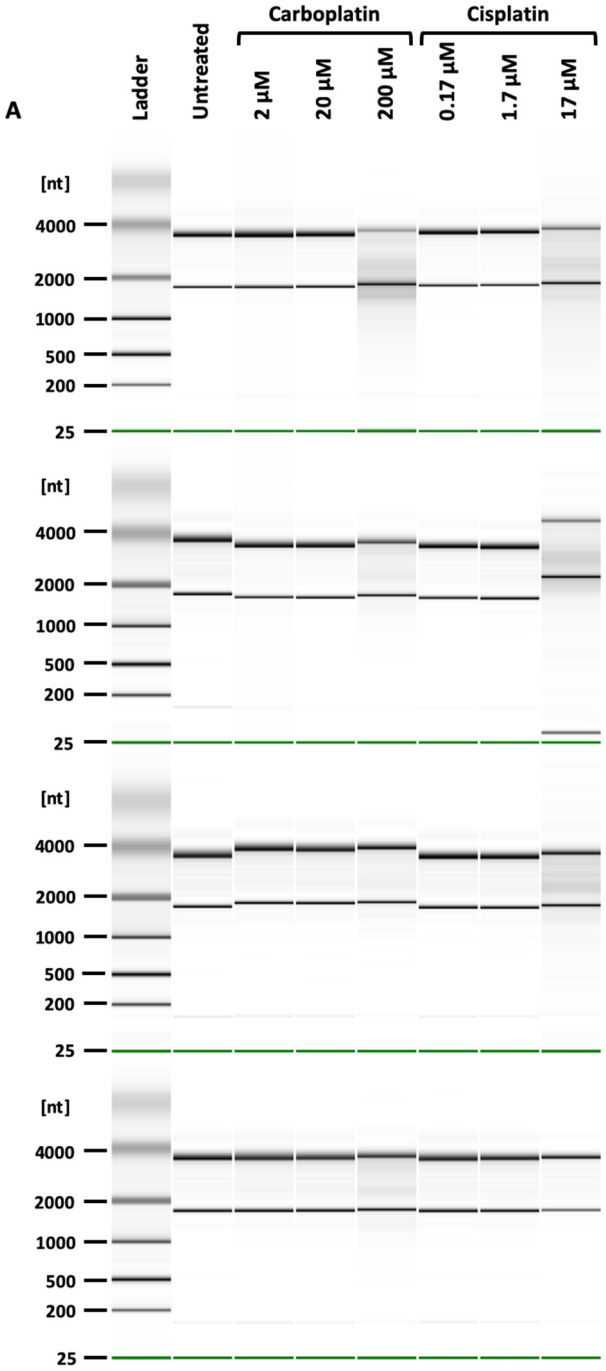

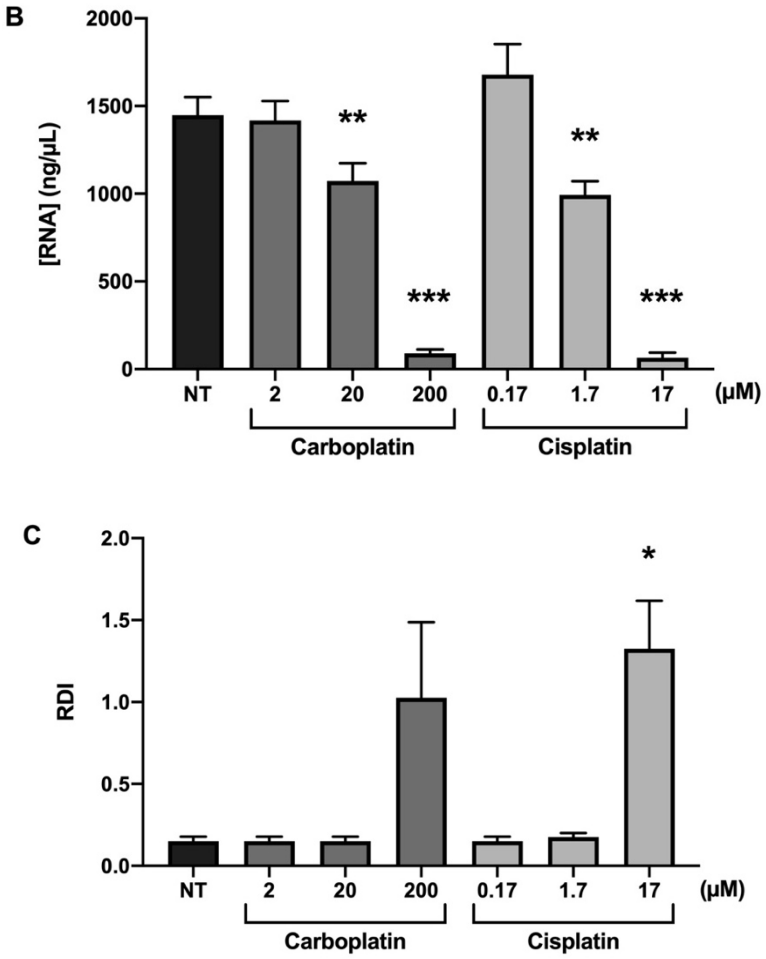

Figure 1. Effect of treatment with alkylating agents on RNA integrity after 72 hours. Cells were treated with 2, 20, and 200 µM of carboplatin and 0.17, 1.7, and 17 µM cisplatin for 72 hours. Total RNA was isolated and samples were quantified and analyzed using capillary gel electrophoresis. 'NT' indicates the untreated control. **(A)** Gel images demonstrating the effect on RNA integrity for four biological replicates. (**B)** Effect of treatment on total RNA. **(C)** RDI values determined by the RDA. Error bars indicate ±SEM (n = 4, *p < 0.05, **p < 0.01, ***p < 0.001).

Table 1. Effect of treatment with alkylating agents on total RNA and RNA disruption. Average RNA concentration, RDI value, standard deviation and p value are noted for each treatment condition. "FC" represents the average fold-change from the untreated control.

		RNA Concentration (µg/µL)			RNA Disruption Index			
		Avg.	SD	P Value	Avg.	SD	P Value	FC
Carboplatin	2 µM	1418.5	221.0	0.4492	0.2	0.1	0.5000	1.0
	20 µM	1072.0	203.7	0.0016	0.2	0.1	0.5000	1.0
	200 µM	90.9	42.4	0.0003	1.0	0.9	0.0835	6.8
Cisplatin	0.17 µM	1679.1	349.0	0.2033	0.2	0.1	0.5000	1.0
	1.7 µM	993.2	157.2	0.0061	0.2	0.1	0.1955	1.2
	17 µM	64.7	57.9	0.0007	1.3	0.6	0.0142	8.8

3.1.2 Topoisomerase Inhibitors

Treatment with 4 µM irinotecan, 10 µM etoposide, and 1 µM doxorubicin were previously shown to induce RNA disruption in A2780 cells[89]. Based on these observations, A375 cells were treated with 0.4, 4 and 40 µM irinotecan, 1, 10 and 100 µM etoposide, and 0.1, 1 and 10 µM doxorubicin. Epirubicin was not included in previous studies but was evaluated using the same concentrations as doxorubicin. The effect on RNA integrity was determined by capillary gel electrophoresis (Figure 2A), total RNA was quantified by spectrophotometry (Figure 2B), and RNA disruption was quantified using the RDA (Figure 2C).

There was a significant decrease in total RNA with 4 µM ($p = 0.0027$) and 40 µM ($p = 0.0003$) irinotecan treatment. Although the magnitude of the change was small (1.7-fold), there was a significant increase in RDI with 4 µM ($p = 0.0459$) irinotecan. Treatment with 40 µM irinotecan induced some visible RNA degradation products and resulted in an average 8.2-fold increase in RDI (Figure 2A); however, this increase in RDI was not found to be statistically

significant. Etoposide treatment resulted in a statistically significant decrease in total RNA with 1 μM ($p = 0.0002$), 10 μM ($p = 0.0004$), and 100 μM ($p = 0.0004$) treatment. Etoposide induced statistically significant increases in RDI values at concentrations of 10 μM ($p = 0.0281$) and 100 μM ($p = 0.0017$), representing a 5.8-fold and 20.5-fold increase from the untreated control, respectively. RNA degradation products and a decrease in the intensity of the 28S and 18S RNA bands could also be seen on the gel images with these treatments (Figure 2A).

There were statistically significant decreases in total RNA with 0.1 μM, 1 μM, and 10 μM doxorubicin treatment, and 0.1 μM ($p = 0.0001$), 1 μM ($p < 0.0001$), and 10 μM ($p < 0.0001$) epirubicin treatment. These agents were found to be the most effective of all surveyed chemotherapy agents at inducing RNA disruption in A375 cells. Although increases in RDI with doxorubicin treatment were not considered statistically significant due to large variation in the data, treatment with 1 μM and 10 μM resulted in an average 58-fold and 51.8-fold increase in RDI, respectively. Furthermore, RDI values cannot be calculated when RNA degradation is so extensive that there is a complete loss of the 28S or 18S bands. This resulted in only three RDI values being obtained for 1 μM and 10 μM doxorubicin treatments. Epirubicin treatment was found to result in significant increases in RDI at 1 μM ($p = 0.0187$) and 10 μM ($p = 0.0048$), representing a 12.3-fold and 64-fold increase from the untreated control, respectively. This magnitude of change in RDI and corresponding RNA banding pattern (Figure 2A) indicated that doxorubicin and epirubicin are able to induce strong RNA disruption in A375 cells.

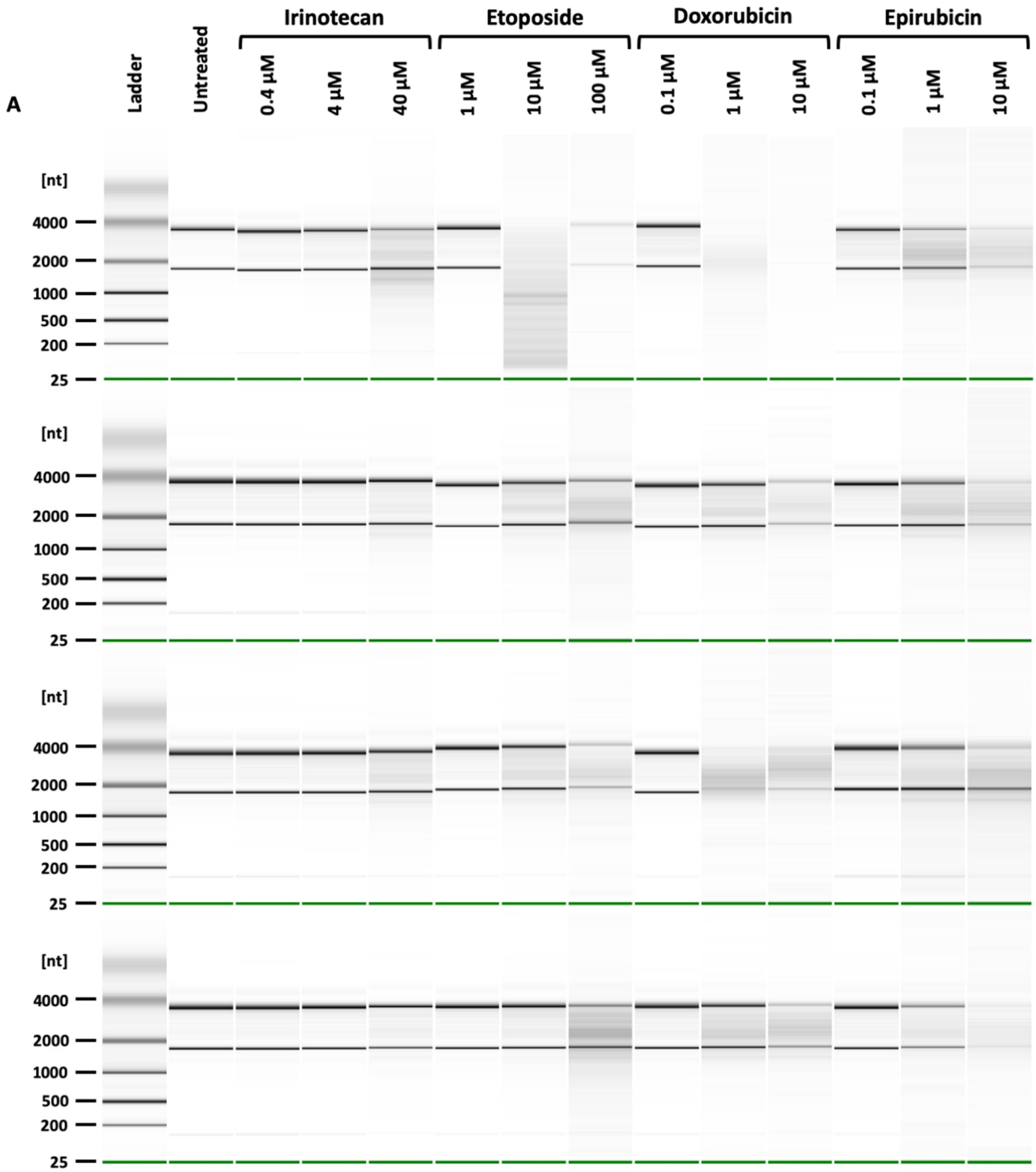
A
Ladder
Untreated
Irinotecan
0.4 µM
4 µM
40 µM
Etoposide
1 µM
10 µM
100 µM
Doxorubicin
0.1 µM
1 µM
10 µM
Epirubicin
0.1 µM
1 µM
10 µM
[nt]
4000
2000
1000
500
200
25

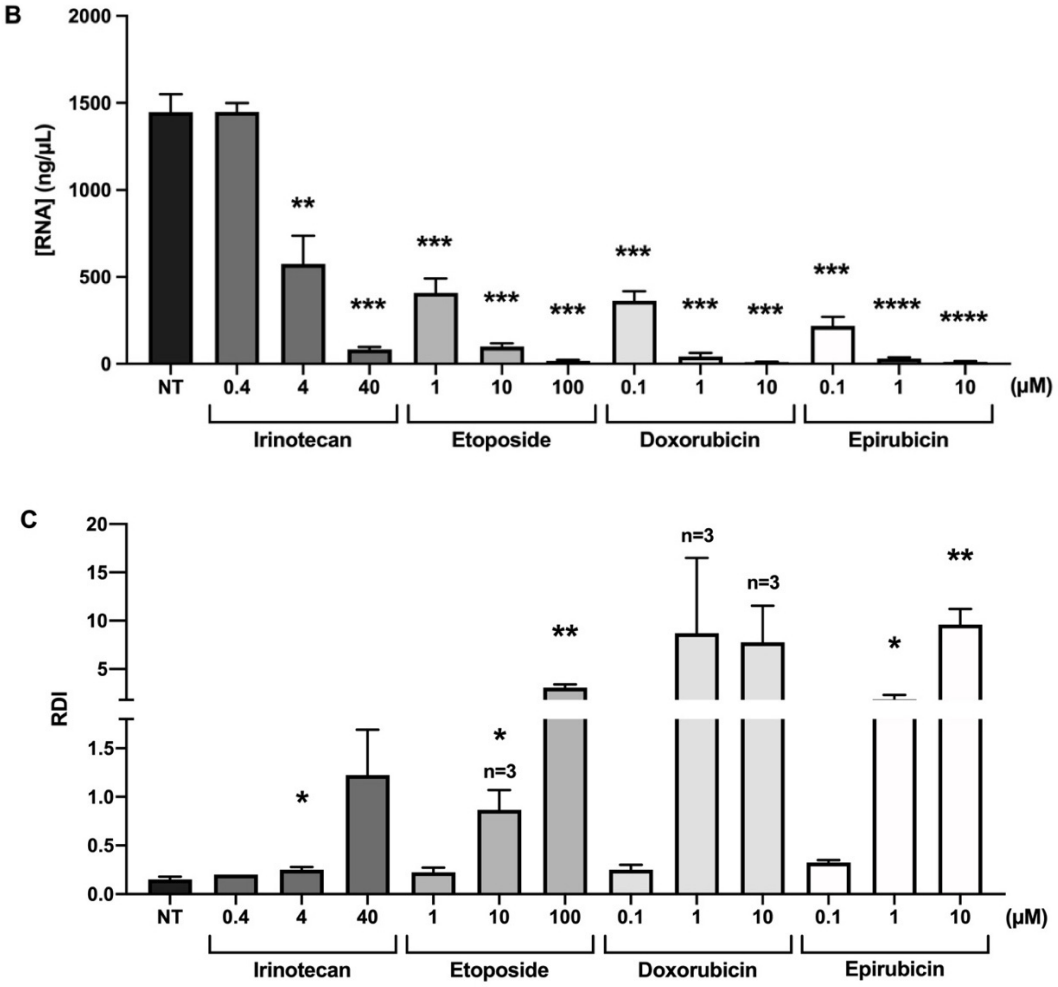

Figure 2. Effect of treatment with topoisomerase inhibitors on RNA integrity after 72 hours. Cells were treated with 0.4, 4, and 40 µM of irinotecan, 1, 10, and 100 µM of etoposide and 0.1, 1, and 10 µM of doxorubicin and epirubicin. Total RNA was isolated and samples were quantified and analyzed using capillary gel electrophoresis. 'NT' indicates the untreated control. **(A)** Gel images demonstrating the effect on RNA integrity for four biological replicates. (**B)** Effect of treatment on total RNA. **(C)** RDI values determined by the RDA. Error bars indicate ±SEM (unless otherwise indicated n = 4, *p < 0.05, **p < 0.01, ***p < 0.001, ****p < 0.0001).

Table 2. Effect of treatment with topoisomerase inhibitors on total RNA and RNA disruption. Average RNA concentration, RDI value, standard deviation and p value are noted for each treatment condition. "FC" represents the average fold-change from the untreated control.

		RNA Concentration (µg/µL)			RNA Disruption Index			
		Avg.	SD	P Value	Avg.	SD	P Value	FC
Irinotecan	0.4 µM	1448.6	100.0	0.4976	0.2	0.0	0.0908	1.3
	4 µM	572.5	326.8	0.0027	0.3	0.1	0.0459	1.7
	40 µM	83.7	26.0	0.0003	1.2	0.9	0.0556	8.2
Etoposide	0.1 µM	409.8	163.5	0.0002	0.2	0.1	0.1595	1.5
	10 µM	100.2	34.7	0.0004	0.9	0.4	0.0281	5.8
	100 µM	18.1	10.4	0.0004	3.1	0.7	0.0017	20.5
Doxorubicin	0.1 µM	362.4	113.5	0.0002	0.3	0.1	0.1261	1.7
	1 µM	42.9	42.9	0.0003	8.7	13.5	0.1938	58.0
	10 µM	10.4	5.6	0.0004	7.8	6.5	0.0901	51.8
Epirubicin	0.1 µM	218.2	105.9	0.0001	0.3	0.0	0.0107	2.2
	1 µM	31.6	14.9	<0.0001	1.9	0.9	0.0187	12.3
	10 µM	11.8	8.9	<0.0001	9.6	3.2	0.0048	64.0

3.1.2 Microtubule Targeting Agents

The optimal dose of vincristine for inducing RNA disruption in A2780 cells was previously found to be 5 nM[89]. In this study, A375 cells were treated with 0.5, 5 and 50 nM doses of vincristine for 72 hours. RNA integrity was analyzed by capillary electrophoresis (Figure 3A), total RNA was quantified (Figure 3B), and RDI values were determined (Figure 3C). Vincristine had little effect on RNA disruption, even at the highest dose. There was a significant increase in RDI values with 50 nM treatment ($p = 0.0305$); however, little RNA disruption can be seen on the gel images (Figure 3A) and the magnitude of change in RDI was relatively small (3.2-fold). There were statistically significant decreases in total RNA with 5 nM ($p = 0.0001$) and 50 nM ($p = 0.0003$) vincristine treatment.

For both paclitaxel and docetaxel, 0.2 μM treatment for 72 hours was able to induce RNA disruption in A2780 cells[89]. Therefore, A375 cells were treated with 0.02, 0.2 and 2 μM docetaxel and paclitaxel for 72h hours. Treatment with paclitaxel resulted in a statistically significant decrease in total RNA at 0.02 μM ($p = 0.0005$), 0.2 μM ($p = 0.0004$), and 2 μM ($p = 0.0004$). Gel images (Figure 3A) show some RNA degradation with paclitaxel treatment; there were significant changes in RDI values at 0.02 μM ($p = 0.0033$), 0.2 μM ($p = 0.003$), and 2 μM ($p = 0.0053$), representing a 3.8-fold, 6.5-fold, and 5.7-fold increase in RDI from the untreated control, respectively. Docetaxel treatment also resulted in noticeable RNA degradation on gel images for all three doses (Figure 3A). RDI values with docetaxel treatment were found to be significant at 0.02 μM ($p = 0.0001$), 0.2 μM ($p < 0.0001$), and at 2 μM ($p = 0.0162$), representing a 6.3-fold, 7.2-fold, and 5.2-fold increase from the untreated control, respectively. Docetaxel treatment resulted in a statistically significant decrease in total RNA ($p = 0.0004$) for all three doses. Although RNA disruption was considered significant with paclitaxel and docetaxel treatment, the banding pattern and magnitude of the changes in RDI indicate paclitaxel and docetaxel are not strong inducers of RNA disruption at these doses.

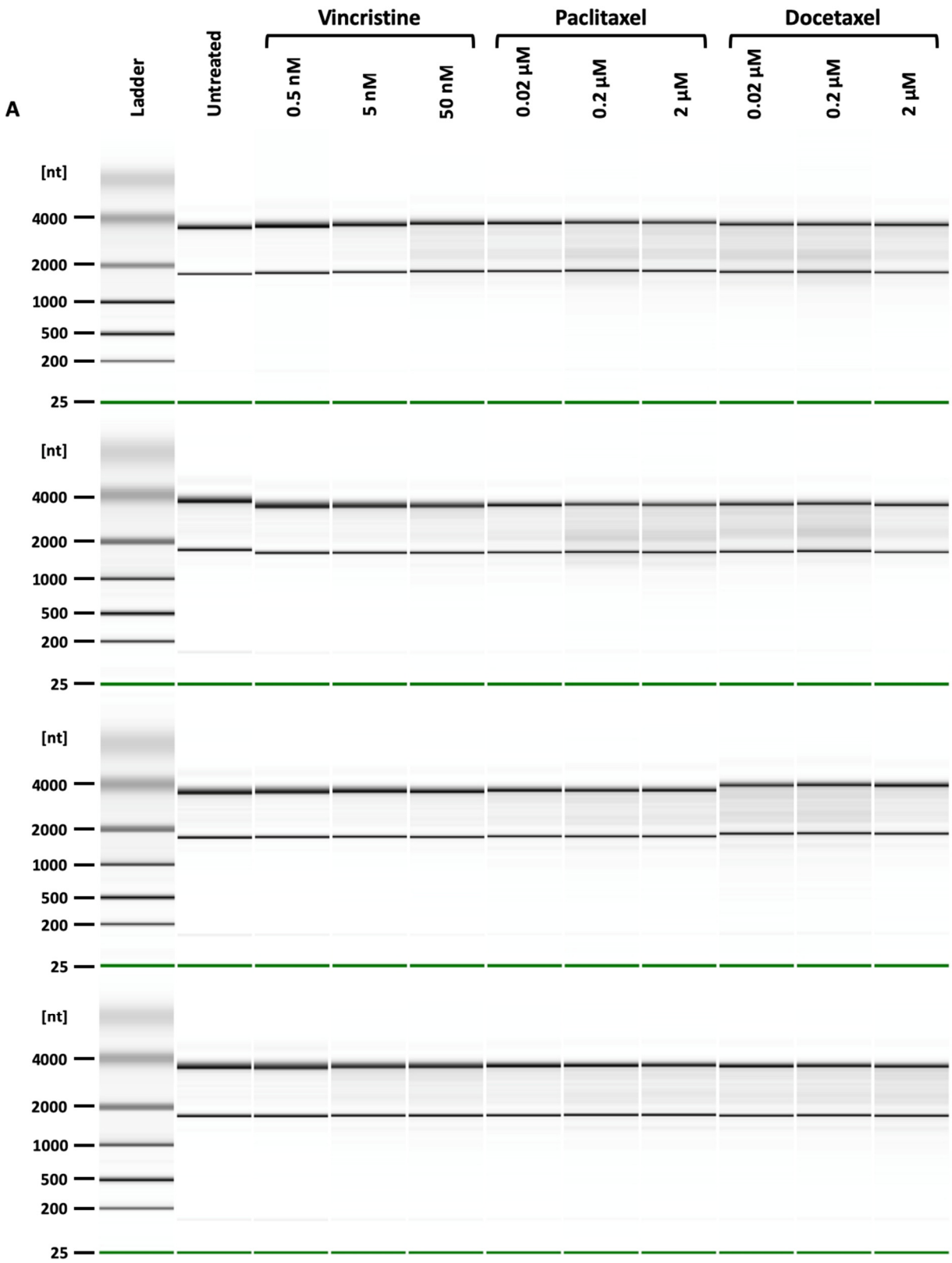
A
Ladder
Untreated
Vincristine
0.5 nM
5 nM
50 nM
Paclitaxel
0.02 µM
0.2 µM
2 µM
Docetaxel
0.02 µM
0.2 µM
2 µM
[nt]
4000
2000
1000
500
200
25

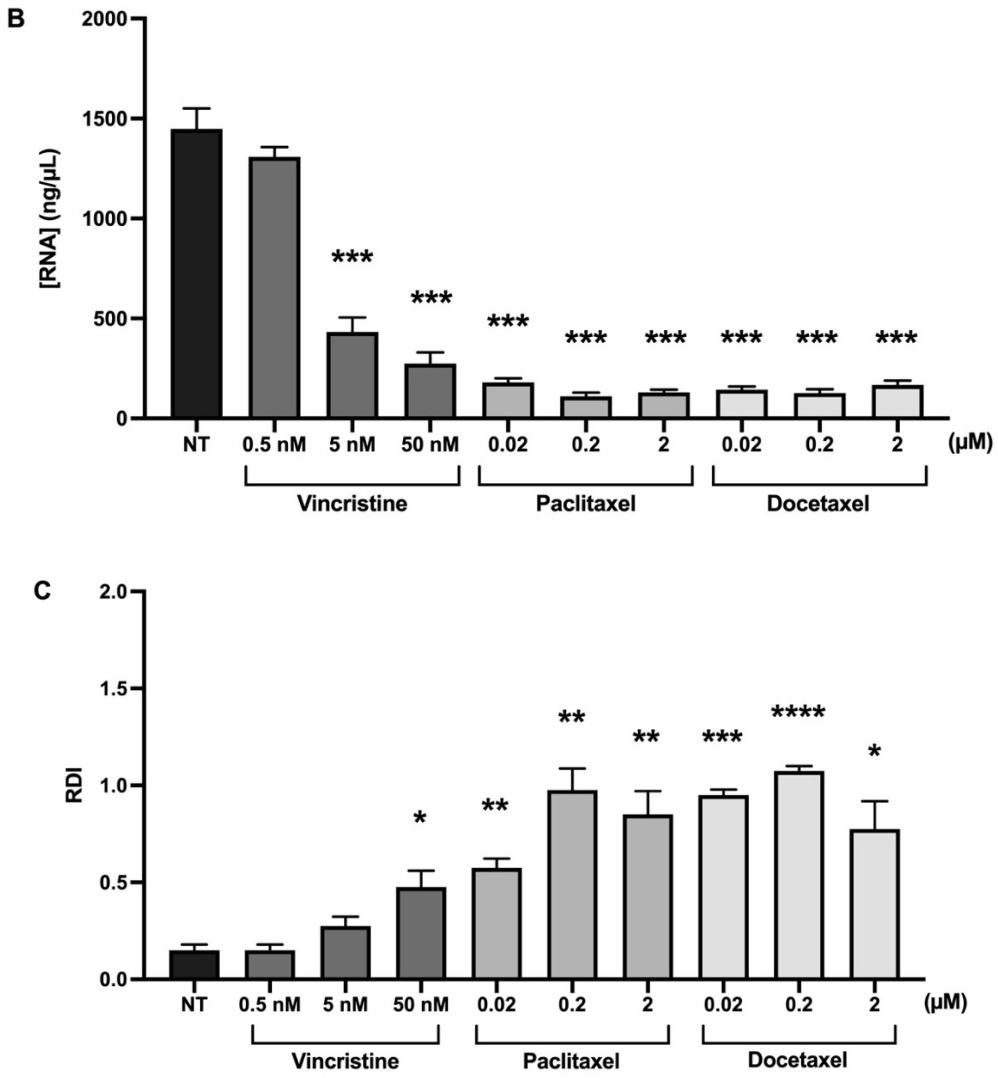

Figure 3. Effect of treatment with microtubule targeting agents on RNA integrity after 72 hours. Cells were treated with 0.5, 5, and 50 nM vincristine, and 0.02, 0.2, and 2 µM of paclitaxel and docetaxel. Total RNA was isolated and samples were quantified and analyzed using capillary gel electrophoresis. 'NT' indicates the untreated control. **(A)** Gel images demonstrating the effect on RNA integrity for four biological replicates. (**B)** Effect of treatment on total RNA. **(C)** RDI values determined by the RDA. Error bars indicate ±SEM (n = 4, *p < 0.05, **p < 0.01, ***p < 0.001, ****p < 0.0001).

Table 3. Effect of treatment with microtubule targeting agents on total RNA and RNA disruption. Average RNA concentration, RDI value, standard deviation and p value are noted for each treatment condition. "FC" represents the average fold-change from the untreated control.

		RNA Concentration (µg/µL)			RNA Disruption Index			
		Avg.	SD	P Value	Avg.	SD	P Value	FC
Vincristine	0.5 nM	1308.7	97.2	0.1166	0.2	0.1	0.5000	1.0
	5 nM	432.6	144.1	0.0001	0.3	0.1	0.0706	1.8
	50 nM	274.6	112.0	0.0003	0.5	0.2	0.0305	3.2
Paclitaxel	0.02 µM	180.7	39.7	0.0005	0.6	0.1	0.0033	3.8
	0.2 µM	109.7	39.1	0.0004	1.0	0.2	0.0030	6.5
	2 µM	130.1	28.6	0.0004	0.9	0.2	0.0053	5.7
Docetaxel	0.02 µM	144.1	32.3	0.0004	1.0	0.1	0.0001	6.3
	0.2 µM	127.4	37.5	0.0004	1.1	0.1	<0.0001	7.2
	2 µM	167.9	43.9	0.0004	0.8	0.3	0.0162	5.2

3.2 Kinetics of Chemotherapy Induced RNA Disruption in Malignant Melanoma

To address the second portion of the first objective, we determined if RNA disruption in response to chemotherapy treatment is both dose- and time-dependent in A375 cells. To accomplish this, cells were treated with 0.1, 1 and 10 µM doxorubicin for 8, 24, 48 and 72 hours. RNA integrity was analyzed by capillary gel electrophoresis (Figure 4A), total RNA was quantified (Figure 4B), and RDI values were determined (Figure 4C). Treatment with 0.1 µM doxorubicin had little effect at 8 hours, but resulted in statistically significant changes in total RNA after 24 ($p = 0.0120$), 48 ($p = 0.0005$), and 72 ($p = 0.0002$) hours. There was a small (2-fold) but significant increase in RDI ($p = 0.0288$) with 0.1 µM doxorubicin after 24 hours; however, 0.1 µM doxorubicin did not result in statistically significant changes in RDI at 48 or 72 hours.

Treatment with 1 μM doxorubicin resulted in significant increases in RDI at 8 ($p = 0.0288$), 24 ($p = 0.0052$), 48 ($p = 0.0235$), and 72 ($p = 0.0048$) hours. The magnitude of change in RDI values with 1 μM doxorubicin were small after 8 and 24 hours, representing a 2.4-fold and 2.8-fold increase from the untreated control, respectively. This increased to a 10.2-fold change after 48 hours, and a 6.7-fold change after 72 hours, with clear rRNA degradation products and loss of the 28S and 18S rRNA bands (Figure 4A). Decreases in total RNA with 1 μM doxorubicin treatment were found to be significant at 8 ($p = 0.0011$), 24 ($p = 0.005$), 48 ($p < 0.0001$), and 72 ($p < 0.0001$) hours.

Following treatment with 10 μM doxorubicin there was clear RNA degradation visible on the gel images (Figure 4A) after just 48 hours. After 72 hours, there were clear losses of the 28S and 18S rRNA bands, which is an indicator of strong RNA disruption. There was a 15.6-fold and 27.7-fold increase in RDI with 10 μM doxorubicin treatment after 48 and 72 hours, respectively. The increases in RDI at 10 μM were significant after 8 ($p = 0.0346$), 24 ($p = 0.0030$), 48 ($p = 0.0005$), and 72 ($p = 0.0121$) hours of treatment and there was a statistically significant decreases in total RNA after 8 ($p = 0.0067$), 24 ($p = 0.0029$), 48 ($p < 0.0001$), and 72 ($p < 0.0001$) hours. RNA disruption in malignant melanoma cells in response to doxorubicin treatment is dependent on both dose and time, with higher doses and longer treatment time increasing RNA disruption.

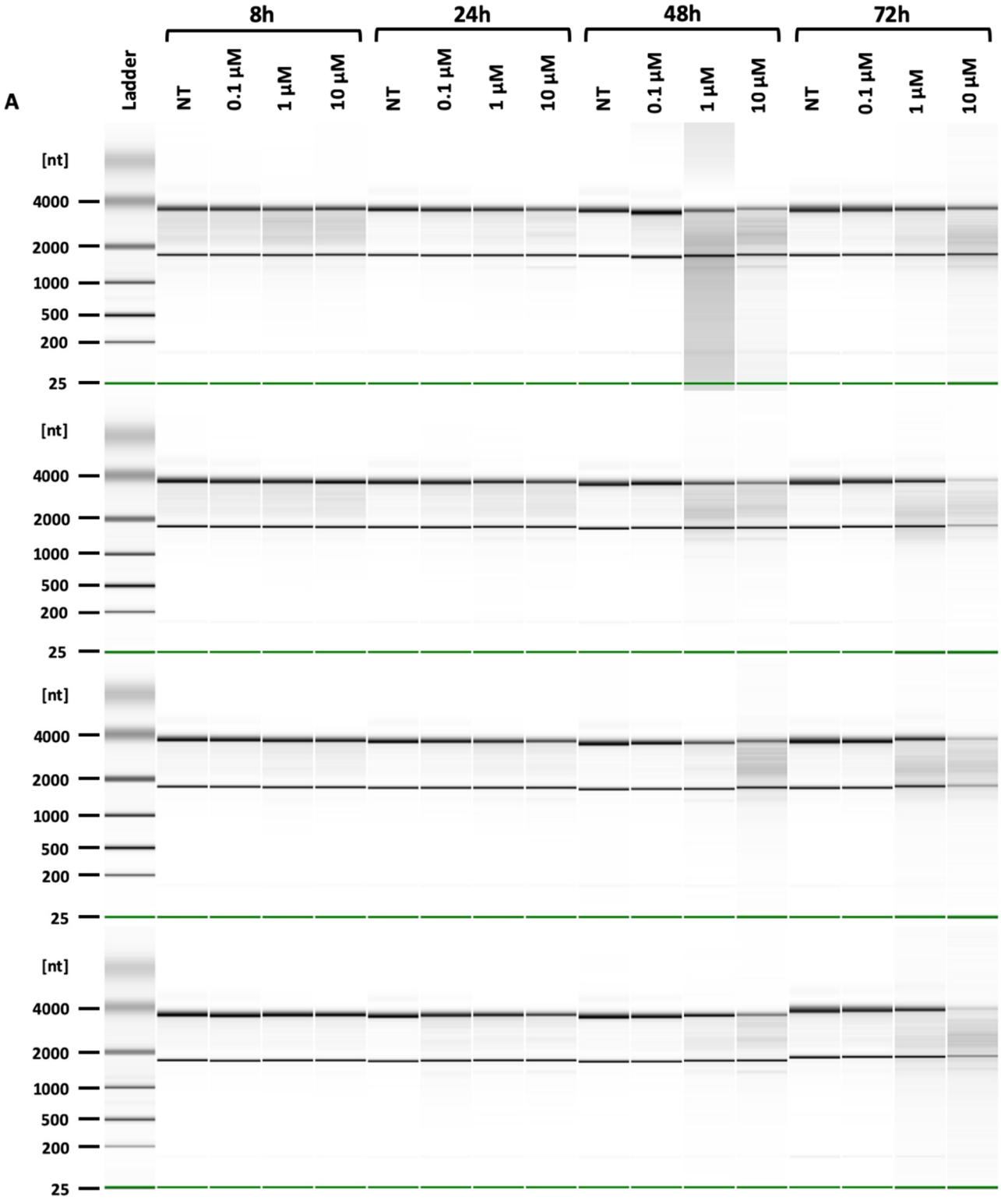
A
8h
24h
48h
72h
Ladder
NT
0.1 µM
1 µM
10 µM
[nt]
4000
2000
1000
500
200
25

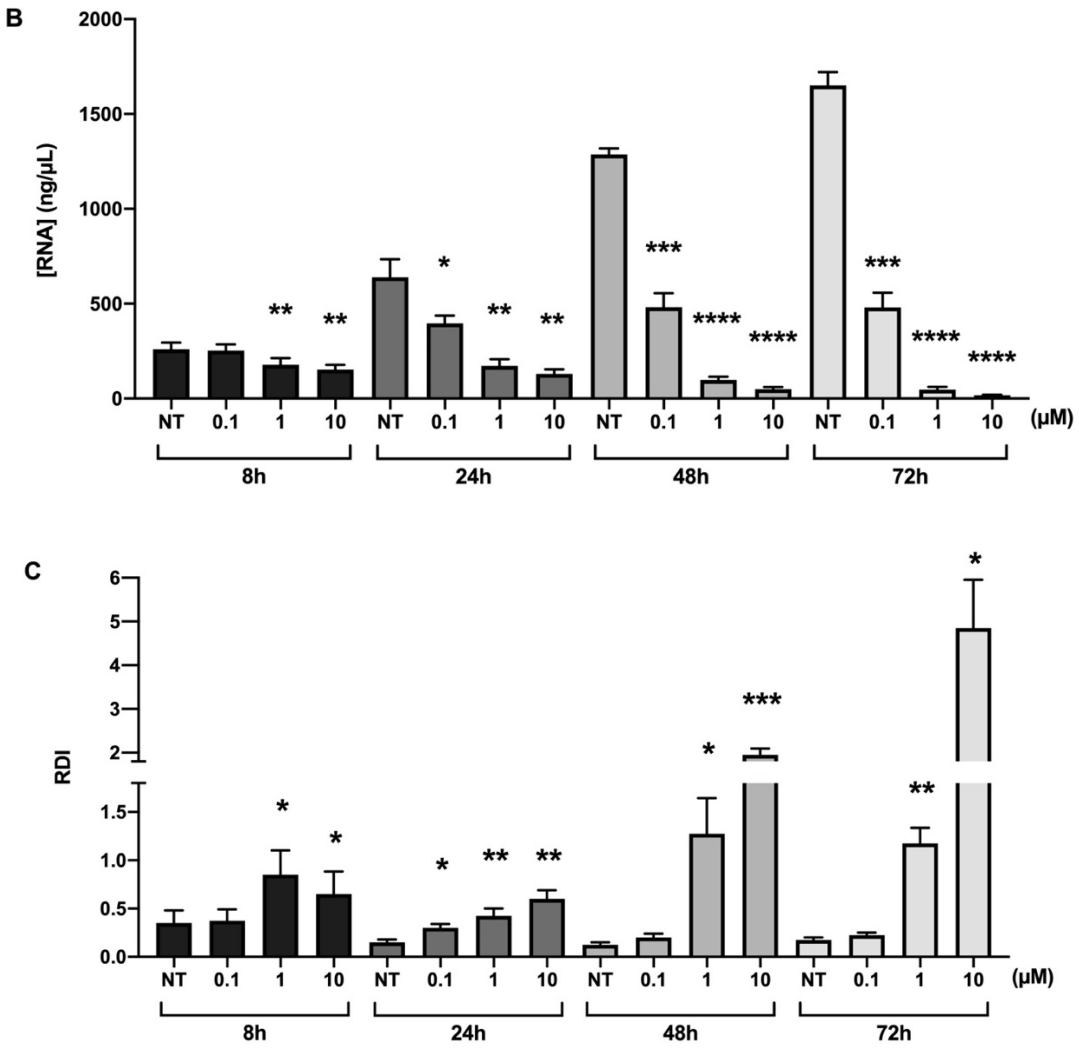

Figure 4. Effect of treatment with doxorubicin on RNA integrity after 8, 24, 48, and 72 hours. Cells were treated with 0.1, 1, and 10 µM of doxorubicin for 8, 24, 48, and 72 hours. Total RNA was isolated and samples were quantified and analyzed using capillary gel electrophoresis. 'NT' indicates the untreated controls. **(A)** Gel images demonstrating the effect on RNA integrity for four biological replicates. (**B)** Effect of treatment on total RNA. **(C)** RDI values determined by the RDA. Error bars indicate ±SEM (paired t-test, one-tailed, n = 4, *p < 0.05, **p < 0.01, ***p < 0.001, ****p < 0.0001).

Table 4. Effect of increasing dose of doxorubicin and treatment time on total RNA and RNA disruption. Average RNA concentration, RDI value, standard deviation and p value are noted for each treatment condition. "FC" represents the average fold-change from the untreated control.

		RNA Concentration (µg/µL)			RNA Disruption Index			
	[Doxorubicin]	Avg.	SD	P Value	Avg.	SD	P Value	FC
8 Hours	0.1 µM	252.5	67.2	0.1778	0.4	0.2	0.1955	1.1
	1 µM	178.4	70.6	0.0011	0.9	0.5	0.0459	2.4
	10 µM	152.9	49.6	0.0029	0.7	0.5	0.0346	1.9
24 Hours	0.1 µM	395.8	83.4	0.012	0.3	0.1	0.0288	2.0
	1 µM	171.7	70.6	0.005	0.4	0.2	0.0052	2.8
	10 µM	130.3	46.9	0.0067	0.6	0.2	0.0030	4.0
48 Hours	0.1 µM	481.1	149.3	0.1000	0.2	0.1	0.1076	1.6
	1 µM	97.8	34.7	<0.0001	1.3	0.7	0.0235	10.2
	10 µM	49.9	21.0	<0.0001	2.0	0.3	0.0005	15.6
72 Hours	0.1 µM	480.0	154.7	0.0002	0.2	0.0	0.0908	1.3
	1 µM	47.4	28.8	<0.0001	1.2	0.3	0.0048	6.7
	10 µM	17.8	4.2	<0.0001	4.9	2.2	0.0121	27.7

3.3 Stress Induced RNA Disruption

The second project objective was to determine if RNA disruption can occur in response to various forms of cell stress. To accomplish this, cells were subjected to treatments known to induce various stress response pathways, including inhibition of cell cycle progression, inhibition of protein synthesis, ER stress, metabolic stress, and oxidative stress, to determine the effect on RNA disruption.

3.3.1 DMSO Drug Vector Control

RNA integrity of untreated cells was compared to cells treated with 1% DMSO to determine the effect of the solvent used to dissolve palbociclib, staurosporine, thapsigargin and

tunicamycin. RNA gel images (Figure 5A) showed no visible RNA degradation products in response to DMSO. However, 1% DMSO did cause a small (1.3-fold) but significant ($p = 0.0033$) decrease in total RNA (Figure 5B), and a small (1.2-fold) but significant ($p = 0.0390$) increase in RDI (Figure 5C). The biological significance for these small DMSO-induced changes in total RNA and RNA integrity are unclear, and may represent a small amount of stress induced by the solvent.

3.3.2 Cycloheximide, Palbociclib, and Staurosporine

A375 cells were treated with cycloheximide, palbociclib and staurosporine, to determine if the stress response induced by these agents can cause RNA disruption in malignant melanoma cells. RNA integrity was assessed by capillary gel electrophoresis (Figure 6A), total RNA was quantified (Figure 6B), and RDI values were determined (Figure 6C). Cycloheximide treatment doses were selected based on observations in A2780 cells[92]. Cells were treated with 10, 100 and 1000 µM of cycloheximide for 72 hours. The decrease in total RNA with cycloheximide treatment was statisitcally significant at all three concentrations tested ($p \leq 0.0001$). The increase in RDI values was statistically significant at 10 µM ($p = 0.0352$), 100 µM ($p = 0.0083$), and 1000 µM ($p = 0.0133$). There were visible RNA degradation products at all doses of cycloheximide, however, treatment with 1000 µM induced particularly strong RNA disruption, reflected by the large magnitute increse in RDI (23.8-fold), and decreases in intensity of the 28S and 18S rRNA bands (Figure 6C).

Palbociclib treatment doses were selected based on the concentrations that have been used in cancer cells *in vitro* in other studies[93,94]. Cells were treated with 5, 10 and 20 µM palbociclib for 72 hours. There was mininal RNA disruption in response to palbociclib even with

20 μM treatment, with the magnitude of change in RDI being relatively small (5-fold). However, there was a visible decrease in intensity of the 28S and 18S RNA bands, and the increase in RDI at this dose was considered significant ($p = 0.0222$). There were significant decreases in total RNA with palbociclib treatment at 10 ($p = 0.0269$), and 20 ($p = 0.0030$) μM.

To assess the ability of staurosporine to induce RNA disruption, cells were treated with 0.02, 0.2 and 1 μM staurosporine for 72 hours. These doses were selected as treatment with 0.02 μM staurosporine has been shown to cause the association of eIF3f with hnRNP K[64] (which has been implicated in changes in cellular rRNA levels), and 0.2 and 1 μM staurosporine have been used to induce apoptosis in other studies[95,96]. The decrease in total RNA was significant with 0.02 μM ($p = 0.0008$), 0.2 μM ($p = 0.0002$), and 2 μM ($p = 0.0006$) staurosporine treatment. RNA integrity analysis showed that treatment with 1 μM staurosporine induced strong RNA disruption, causing visible RNA degredation and a decrease in the intensity of the 28S and 18S rRNA bands (Figure 6A). This is reflected by the large increase in RDI (31-fold) with 1 μM staurosporine treatment, however, this increase was not found to be statistically signifcant due to a large variation in the data. The increases in RDI values with 0.02 μM ($p = 0.0459$), and 0.2 μM ($p = 0.0412$) treatment were found to be statistically significant, representing a 1.6-fold and 3.6-fold increase from the untreated control, respectively.

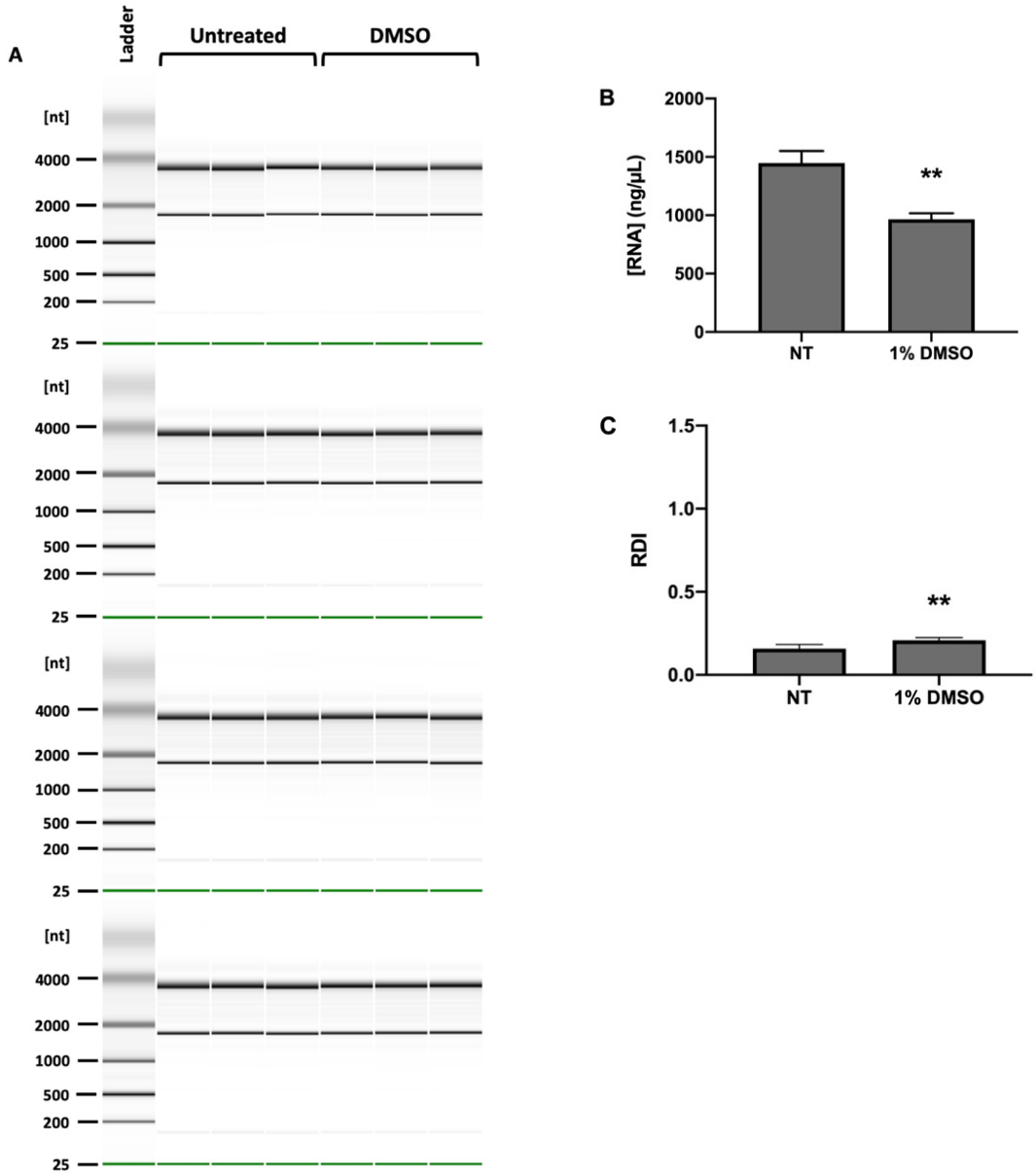

Figure 5. Effect of DMSO on RNA integrity. Cells were treated with 1% DMSO for 72 hours. Total RNA was isolated and samples were quantified and analyzed using capillary gel electrophoresis. 'NT' indicates the untreated control. **(A)** Gel images demonstrating the effect on RNA integrity for four biological replicates. (**B)** Effect of treatment on total RNA. **(C)** RDI values determined by the RDA. Error bars indicate ±SEM (paired t-test, one-tailed, n = 4, **p < 0.01).

Table 4. Effect of DMSO on total RNA and RNA disruption. Average RNA concentration, RDI value, standard deviation and p value are noted. "FC" represents fold change from the untreated control.

	RNA Concentration (µg/µL)			RNA Disruption Index			
	Avg.	SD	P Value	Avg.	SD	P Value	FC
1% DMSO	965.8	102.5	0.0033	0.15	0.03	0.0390	1.2

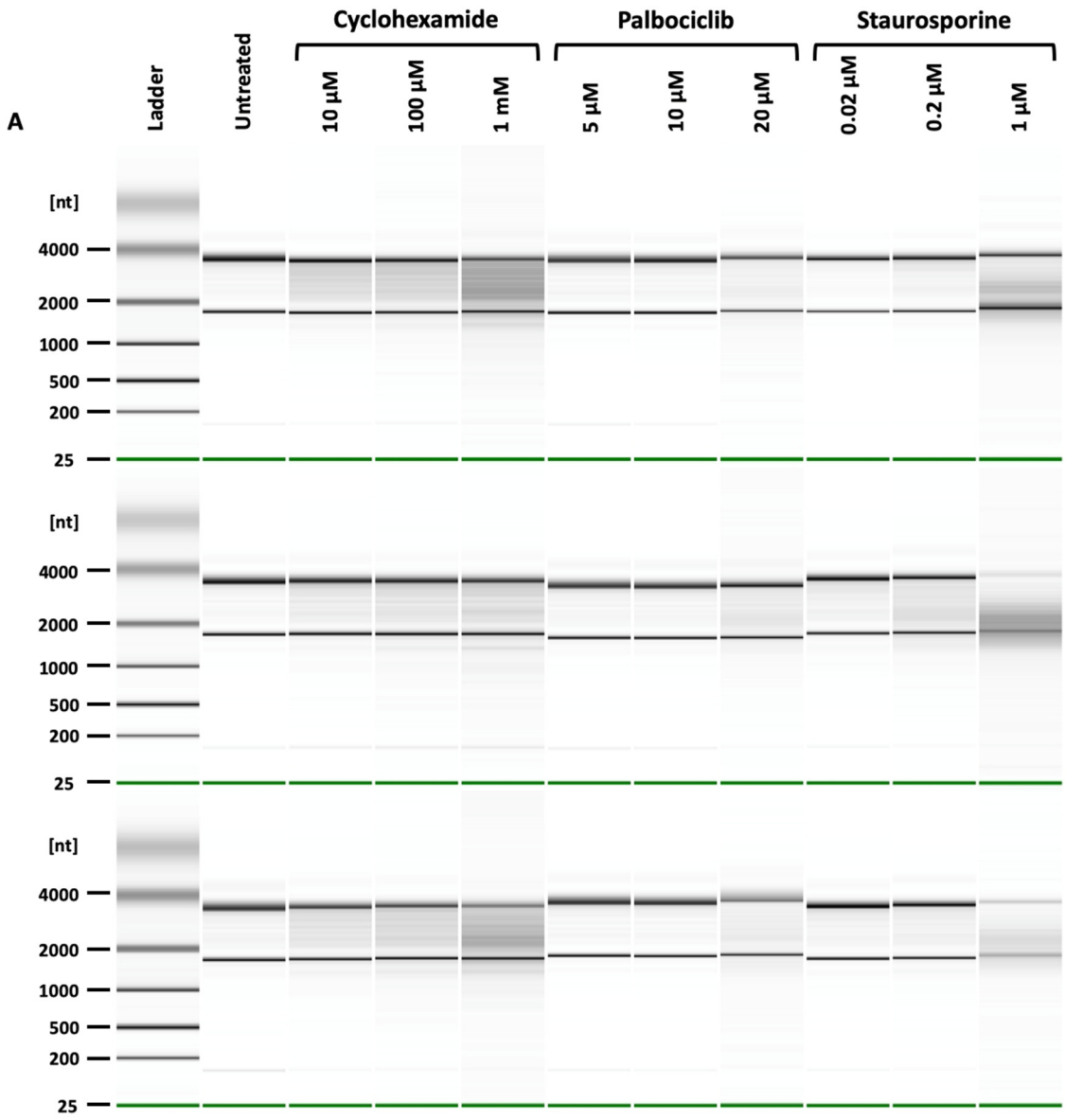

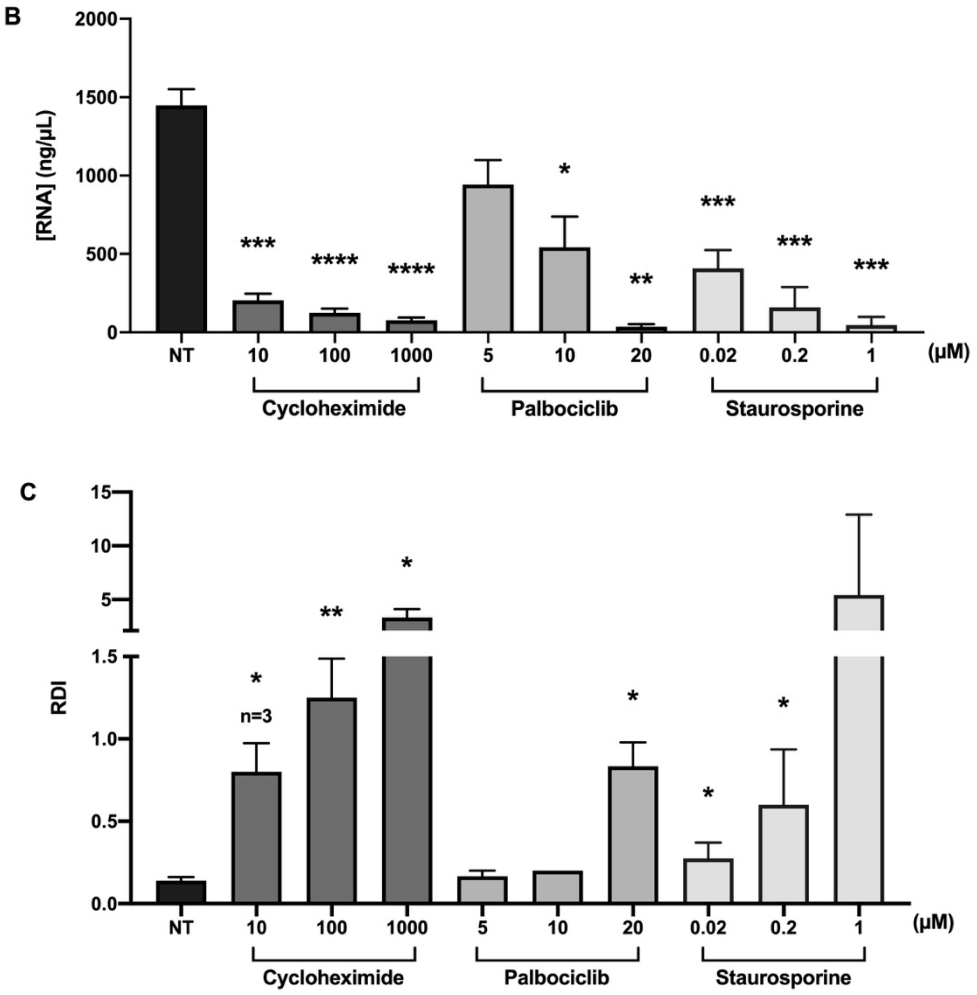

Figure 6. Effect of treatment with cycloheximide, palbociclib and staurosporine on RNA integrity after 72 hours. Cells were treated with 10, 100, and 1000 µM cycloheximide, 5, 10, and 20 µM palbociclib and 0.02, 0.2, and 2 µM staurosporine. Total RNA was isolated and samples were quantified and analyzed using capillary gel electrophoresis. 'NT' indicates the untreated control. **(A)** Gel images demonstrating the effect on RNA for three biological replicates. (**B)** Effect of treatment on total RNA. **(C)** RDI values determined by the RDA. Error bars indicate ±SEM (paired t-test, one-tailed, unless otherwise indicated n = 4, *p < 0.05, **p < 0.01, ***p < 0.001, ****p < 0.0001).

Table 6. Effect of cycloheximide, palbociclib, and staurosporine on total RNA and RNA disruption. Average RNA concentration, RDI value, standard deviation and p value are noted for each treatment condition. "FC" represents the average fold-change from the untreated control.

		RNA Concentration (µg/µL)			RNA Disruption Index			
		Avg.	SD	P Value	Avg.	SD	P Value	FC
Cycloheximide	10 µM	204.3	85.7	0.0001	0.8	0.3	0.0352	5.7
	100 µM	124.6	53.3	<0.0001	1.3	0.5	0.0083	8.9
	1 mM	76.8	37.3	<0.0001	3.3	1.6	0.0133	23.8
Palbociclib	5 µM	942.2	271.2	0.0513	0.2	0.1	0.4226	1.0
	10 µM	543.6	337.3	0.0269	0.2	0.0	0.1840	1.2
	20 µM	36.1	27.1	0.0030	0.8	0.3	0.0211	5.0
Staurosporine	0.02 µM	408.1	115.6	0.0008	0.3	0.1	0.0459	1.6
	0.2 µM	159.9	128.3	0.0002	0.6	0.3	0.0412	3.4
	1 µM	46.3	52.5	0.0006	5.4	7.5	0.1271	31.0

3.3.3 ER Stress

Thapsigargin and tunicamycin were used to determine if ER stress can lead to RNA disruption in A375 cells. Based on unpublished observations in A2780 cells, A375 cells were treated with 0.1, 1, and 10 µM thapsigargin, and 1, 10, and 25 µM tunicamycin for 72 hours. RNA integrity was analyzed using capillary gel electrophoresis (Figure 6A), total RNA was quantified (Figure 6B), and RDI values were determined (Figure 6C). There were statistically significant decreases in total RNA with 0.1 µM ($p = 0.0002$), 1 µM ($p < 0.0001$), and 10 µM ($p < 0.0001$) thapsigargin treatment, and 1, 10, and 25 µM tunicamycin treatment ($p < 0.0001$ for all doses). There was visible RNA degradation with these treatments, particularly with 10 µM thapsigargin and 25 µM tunicamycin treatment, which induced a 10.3-fold and 9.6-fold increase in RDI, respectively. Increases in RDI were considered to be significant with 0.1 µM ($p =$

0.0390), 1 µM (p = 0.0119), and 10 µM (p = 0.0003) thapsigargin, and 1 µM (p = 0.0078), 10 µM (p = 0.0291), and 25 µM (p = 0.0429) tunicamycin.

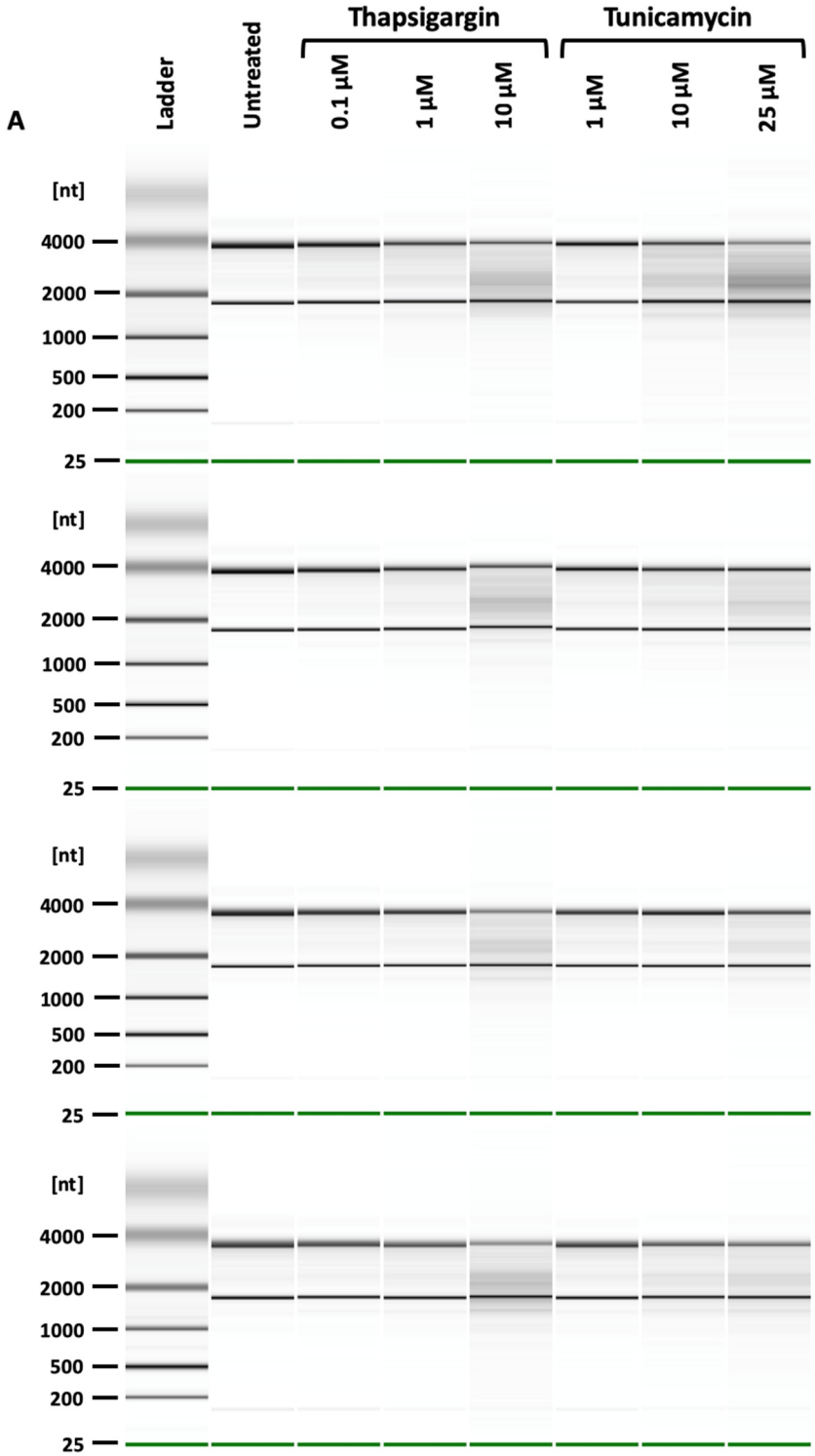

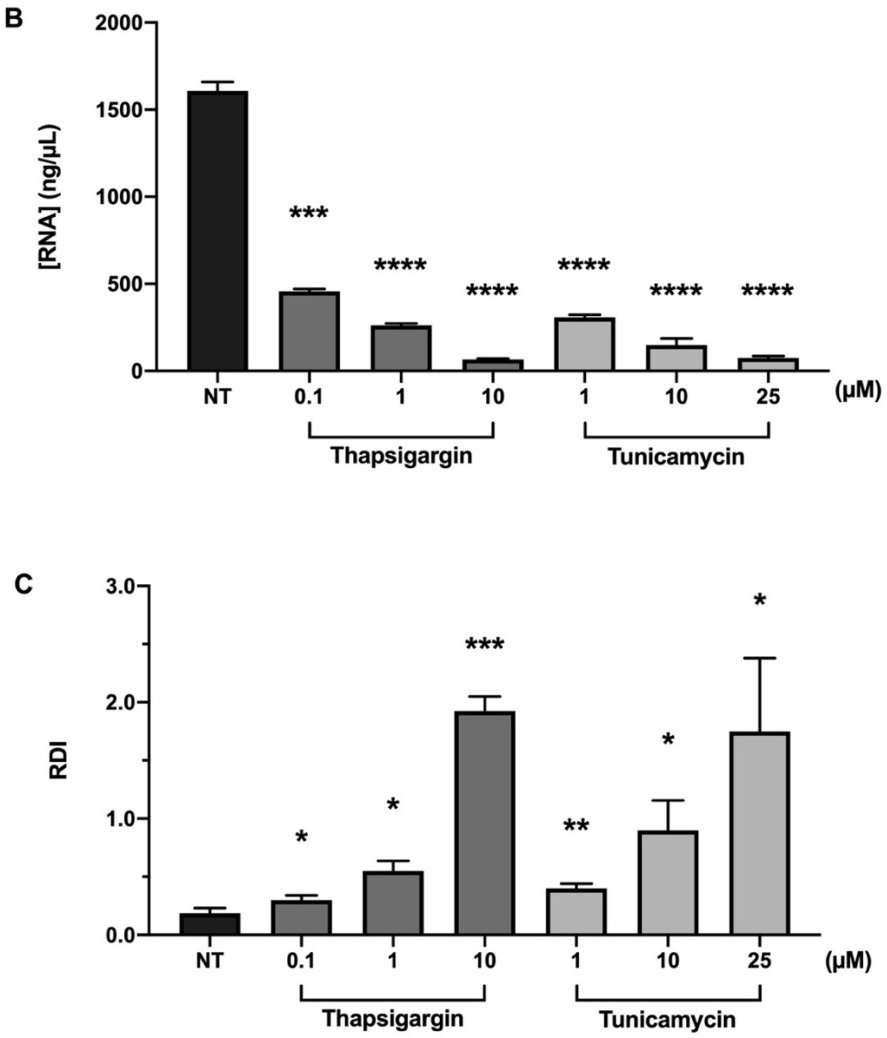

Figure 7. Effect of ER stress on RNA integrity after 72 hours. Cells were treated with 0.1, 1, and 10 µM thapsigargin and 1, 10, and 25 µM tunicamycin for 72 hours. Total RNA was isolated and samples were quantified and analyzed using capillary gel electrophoresis. 'NT' indicates the untreated control. **(A)** Gel images demonstrating the effect on RNA integrity for four biological replicates. (**B)** Effect of treatment on total RNA. **(C)** RDI values determined by the RDA. Error bars indicate ±SEM (paired t-test, one-tailed, n = 4, *p < 0.05, **p < 0.01, ***p < 0.001, ****p < 0.0001).

Table 7. Effect of thapsigargin and tunicamycin on RNA concentration and RNA disruption. Average RNA concentration, RDI value, standard deviation and p values for each treatment are noted. "FC" represents fold change from the untreated control.

		RNA Concentration (µg/µL)			RNA Disruption Index			
		Avg.	SD	P Value	Avg.	SD	P Value	FC
Thapsigargin	0.1 µM	456.7	27.1	0.0002	0.3	0.1	0.0390	1.6
	1 µM	261.9	21.6	<0.0001	0.6	0.2	0.0119	2.9
	10 µM	66.1	9.8	<0.0001	1.9	0.2	0.0003	10.3
Tunicamycin	1 µM	307.2	29.1	<0.0001	0.4	0.1	0.0078	2.1
	10 µM	148.3	77.4	<0.0001	0.9	0.5	0.0291	4.8
	25 µM	74.5	22.7	<0.0001	1.8	1.3	0.0429	9.3

3.3.4 Oxidative Stress

Hydrogen peroxide treatment was used to determine if oxidative stress can lead to RNA disruption in A375 cells. Cells were treated with 25, 50, 100, 200 and 400 µM hydrogen peroxide for 24 hours, based on unpublished observations in A2780 cells. An initial experiment revealed that A375 cells were resistant to treatment with hydrogen peroxide at these concentrations; for this reason, A2780 cells were used as a positive control in subsequent experiments. Following treatment, total RNA was isolated and analyzed by capilary gel electrophoresis (Figure 8A), total RNA was quantified (Figure 8C), and RDI values were determined (Figure 8E).

Hydrogen peroxide had little effect on RNA integrity in A375 cells at these doses. A statistically significant decrease in total RNA ($p = 0.033$) and increase in RDI ($p = 0.0286$) was only achieved at 400 µM. However, this change in RDI represented only a 2.3-fold increase from the untreated control, and there was minimal RNA disruption seen on gel images (Figure 8A). Consistent with previous observations, A2780 cells showed statistically significant decrease in

total RNA with 25 μM ($p = 0.0171$), 50 μM ($p = 0.0267$) and 100 μM ($p = 0.0292$) hydrogen peroxide treatments. A2780 cells also showed clear RNA disruption (Figure 8A), and RDI was significantly increased with 100 μM treatment ($p = 0.0490$), representing a 165-fold increase from the untreated control.

An additional experiment was conducted to determine if A375 cells respond to higher doses of hydrogen peroxide. Cells were treated with 0.5, 1, and 2 mM hydrogen peroxide for 24 hours. Total RNA (Figure 8D) was significantly reduced wtih 0.5 mM ($p = 0.0179$), 1 mM ($p = 0.0235$), and 2 mM ($p = 0.0238$) hydrogen peroxide. Treatment with 1 μM and 2 μM hydrogen peroxide induced strong RNA disruption, with almost a complete loss of the 28S and 18S rRNA bands visible with 2 mM treatment (Figure 8B). The increase in RDI values (Figure 8F) were statistically significant with 0.5 mM ($p = 0.0286$) and 1 mM ($p = 0.0140$), representing a 2.3-fold and 11.3-fold increase in RDI from the untreated control, respectively. Treatment with 2 mM hydrogen peroxide induced strong RNA disruption and a 146.5-fold increase in RDI; however, the increase was not found to be statistically significant. As mentioned previously, an RDI value cannot be calculated when there is strong RNA disruption and the 28S and 18S bands are lost. This resulted in only two RDI values being obtained with 2 mM hydrogen peroxide treatment.

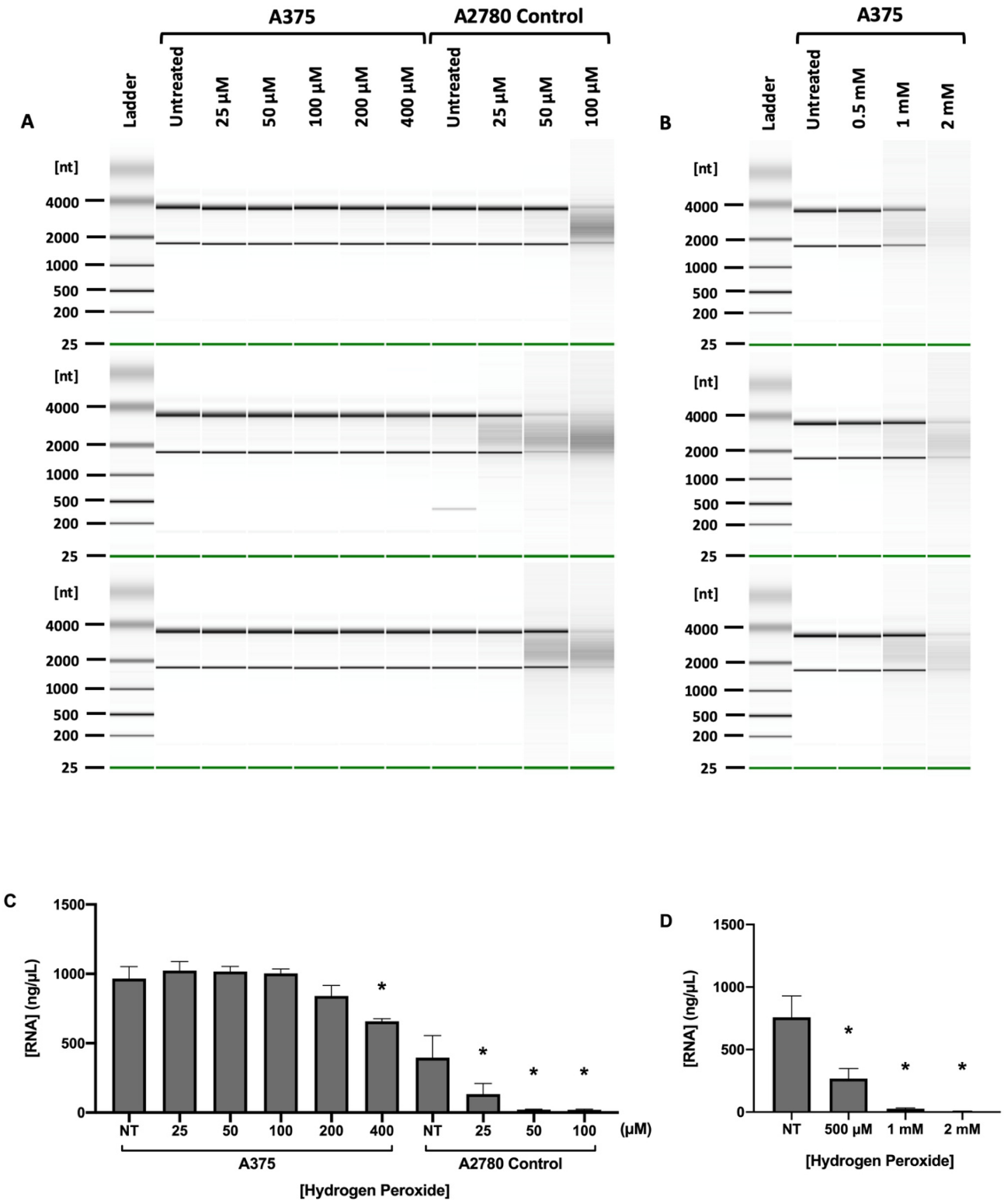
A
A375
A2780 Control
Ladder
Untreated
25 µM
50 µM
100 µM
200 µM
400 µM
Untreated
25 µM
50 µM
100 µM
[nt]
4000
2000
1000
500
200
25
B
A375
Ladder
Untreated
0.5 mM
1 mM
2 mM
C
[RNA] (ng/µL)
1500
1000
500
0
NT
25
50
100
200
400
NT
25
50
100
(µM)
A375
A2780 Control
[Hydrogen Peroxide]
D
[RNA] (ng/µL)
NT
500 µM
1 mM
2 mM
[Hydrogen Peroxide]

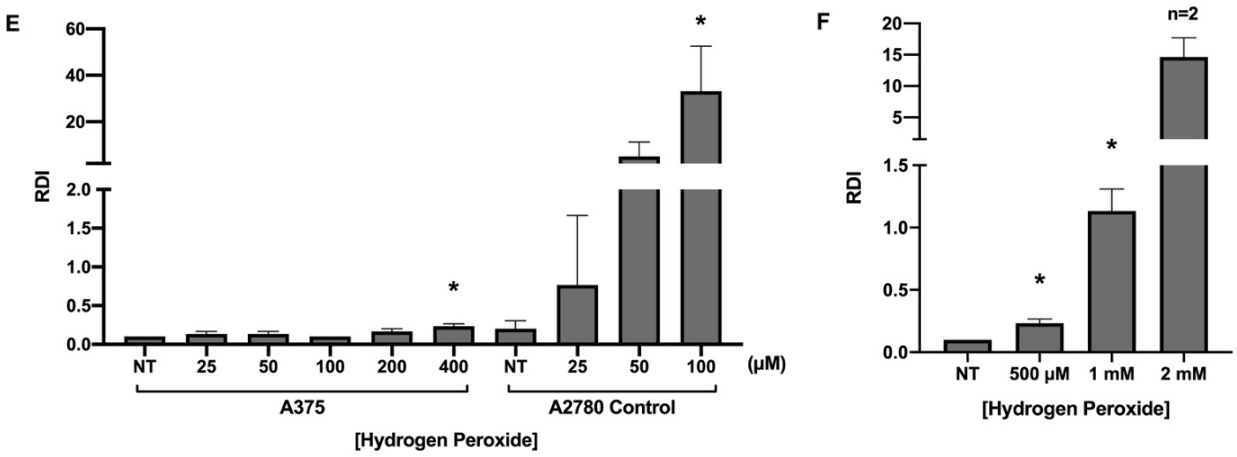

Figure 8. Effect of oxidative stress on RNA integrity after 24 hours. A375 cells were treated with 25 to 400 μM hydrogen peroxide, while A2780 cells were treated with 25 to 100 μM as a positve control for response. A375 cells were also treated with 0.5, 1, and 2 mM hydrogen peroxide in a second experiment. All treatments were 24 hours. Total RNA was isolated and samples were quantified and analyzed using capillary gel electrophoresis. 'NT' indicates the untreated controls. **(A)** Gel images demonstrating the effect of the low dose treatment on A375 and A2780 RNA integrity. (**B)** Gel images demonstrating the effect of high dose treatment on A375 RNA integrity **(C)** Effect of low dose treatment on A375 and A2780 total RNA. **(D)** Effect of high dose treatment on A375 total RNA. **(E)** RDI values obtained for low dose treatment. **(F)** RDI values obtained for high dose treatment. Error bars indicate ±SEM (paired t-test, one-tailed, unless otherwise indicated n = 3, *$p < 0.05$).

Table 8. Effect of hydrogen peroxide on total RNA and RNA disruption in A375 and A2780 cells. Average RNA concentration, RDI value, standard deviation and p value are noted for each treatment condition. "FC" represents the average fold-change from the untreated control.

		RNA Concentration (µg/µL)			RNA Disruption Index			
	[H_2O_2]	Avg.	SD	P Value	Avg.	SD	FC	P Value
A375	25 µM	1329.8	97.9	0.0751	0.1	0.1	1.3	0.2113
	50 µM	726.1	88.2	0.2336	0.1	0.1	1.3	0.2113
	100 µM	304.2	32.2	0.3130	0.1	0.0	1.0	0.5000
	200 µM	111.0	23.7	0.1626	0.2	0.1	1.7	0.0918
	400 µM	60.8	54.2	0.0330	0.2	0.1	2.3	0.0286
	500 µM	267.9	139.5	0.0179	0.2	0.1	2.3	0.0286
	1 mM	26.3	11.9	0.0235	1.1	0.3	11.3	0.0140
	2 mM	6.5	2.3	0.0238	14.7	4.3	146.5	0.0658
A2780	25 µM	133.1	76.1	0.0171	0.8	0.9	3.8	0.1743
	50 µM	20.6	3.8	0.0267	5.0	6.2	25.2	0.1530
	100 µM	19.9	4.5	0.0292	33.1	19.4	165.7	0.0490

3.3.5 Metabolic Stress

Dilution of cell culture medium was used as a method to induce metabolic stress, through nutrient deprivation and growth factor depletion, to determine if metabolic stress could lead to RNA disruption in A375 cells. Whole cell culture medium was diluted in sterile PBS to a concentration of 50, 25, 10, and 5% of normal cell culture medium. Cells were treated with whole cell culture medium, diluted medium, or with PBS alone for 72 hours. RNA integrity was assessed using capillary gel electrophoresis (Figure 9A), total RNA was quantified (Figure 9B), and RDI values were determined (Figure 9C). Dilution of cell culture medium resulted in a significant decrease in total RNA at 50% ($p = 0.0111$), 25% ($p = 0.0019$), 10 % ($p = 0.0006$), 5% ($p = 0.0003$), and 0% (PBS alone; $p = 0.0003$) of normal medum. There was very little visible RNA disruption until the cell culture medium was diluted to only 5% of normal medium or with

PBS alone; with these treatments there were visible decreases in the intensity of the 28S and 18S rRNA bands and clear RNA disruption products. RDI values were considered significant with 10% ($p = 0.0077$) and 5% ($p = 0.0100$) of normal medum, representing a 2-fold and 10.3-fold increase from the untreated control, respectively. PBS alone induced strong RNA disruption resulting in a 166.4-fold increase in RDI from the untreated control, but large variation in RDI values resulted in no statistical significance being found.

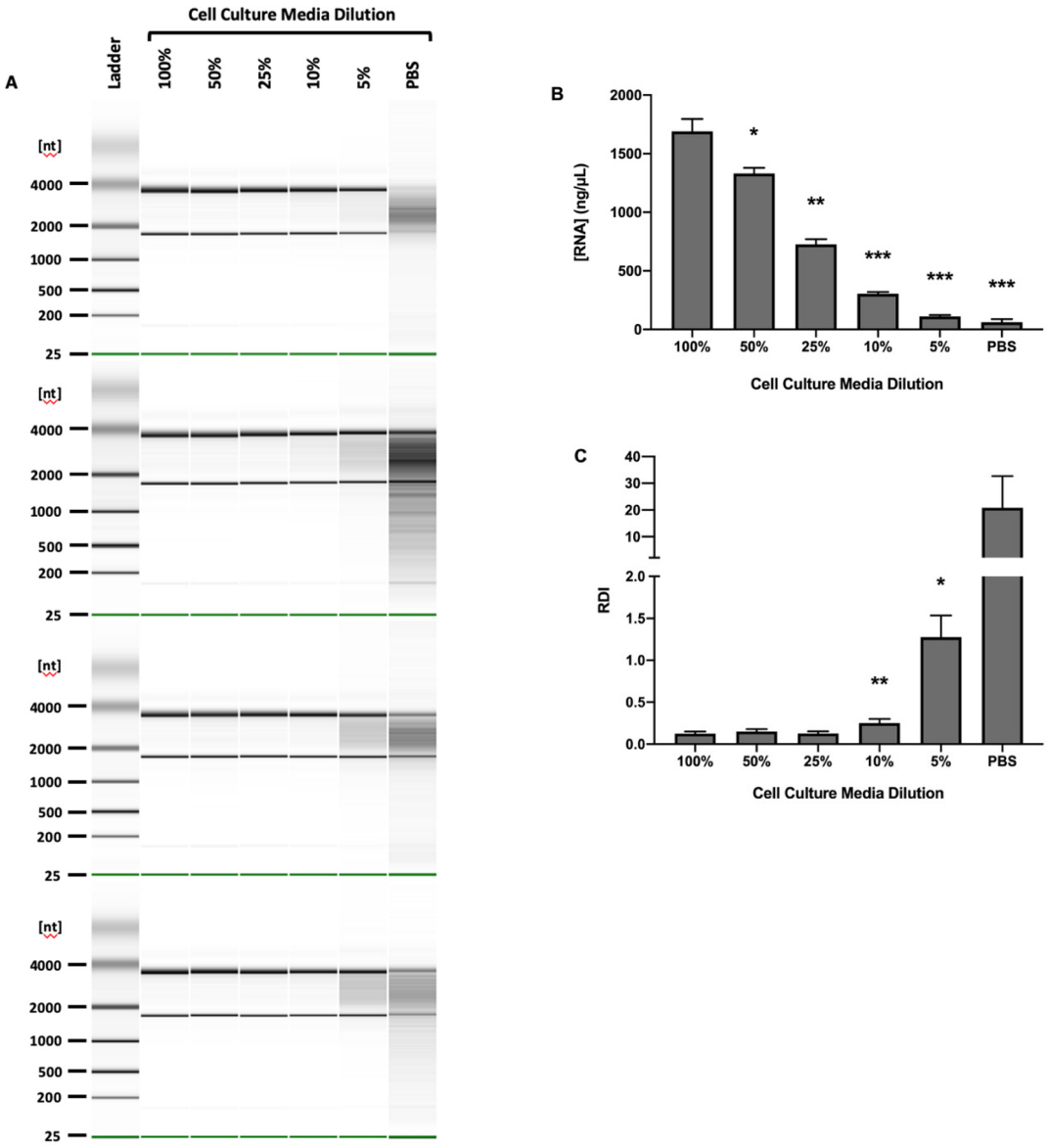

Figure 9. Effect of metabolic stress on RNA integrity after 72 hours. Cells were treated with whole cell culture medium diluted to 50, 25, 10 and 5% medium, and sterile PBS alone. Total RNA was isolated and samples were quantified and analyzed using capillary gel electrophoresis. 'NT' indicates the untreated control. **(A)** Gel images demonstrating the effect on RNA integrity for four biological replicates. (**B)** Effect of treatment on total RNA. **(C)** RDI values determined by the RDA. Error bars indicate ±SEM (paired t-test, one-tailed, n = 4, *p < 0.05, **p < 0.01, ***p < 0.001).

Table 9. Effect of metabolic stress on total RNA and RNA disruption. Average RNA concentration, RDI value, standard deviation and p value are noted for each treatment condition. "FC" represents the average fold-change from the untreated control.

		RNA Concentration (µg/µL)			RNA Disruption Index			
		Avg.	SD	P Value	Avg.	SD	P Value	FC
Media Dilution	50%	1329.8	97.9	0.0002	0.2	0.1	0.0390	1.2
	25%	726.1	88.2	<0.0001	0.1	0.0	0.0119	1.0
	10%	304.2	32.2	<0.0001	0.3	0.1	0.0003	2.0
	5%	111.0	23.7	<0.0001	1.3	0.5	0.0078	10.2
	0%	60.8	54.2	<0.0001	20.8	23.8	0.0291	166.4

3.4 Optimal Treatment Dose for Inducing RNA Disruption

In order to address the third project objective and assess the expression of eIF3f and hnRNP K with treatments that induce RNA disruption, we first conducted experiments to establish the optimal treatments to induce RNA disruption in A375 cells. Based on the results of RNA disruption with the various treatments described, doxorubicin, etoposide, staurosporine, and vincristine were selected to assess the relationship between RNA disruption and eIF3f and hnRNP K expression. Doxorubicin was selected as a positive control for RNA disruption, as it is able to induce strong RNA disruption. Staurosporine and etoposide were selected as they have been previously shown to cause the association of eIF3f and hnRNP K[64] (associated with reduced rRNA levels in cells), and also induce strong RNA disruption. Vincristine treatment was evaluated as a potential negative control for RNA disruption, as it appears to induce little RNA disruption.

To determine the optimal dose to induce RNA disruption, a dose versus response curve for each drug was performed. A375 cells were treated with 0.2, 0.4, 0.6, 0.8 and 1 µM doxorubicin for 72 hours (Figure 11). It was found that visible RNA degradation can be seen at

0.4 μM, and the presence of RNA disruption products increases with increasing dose (Figure 11A). Although changes in RDI with doxorubicin were not considered to be statistically significant in these experiments due to large variation in the RDI data, the RNA gel images and magnitude of change in RDI suggest a strong relationship between the dose of doxorubicin and the extent of RNA disruption.

For the etoposide dose curve, cells were treated with 10, 20, 50, 100 and 200 μM for 72 hours, and the effect on RNA integrity was assessed (Figure 11). RNA disruption can be seen with etoposide treatment with each increasing dose, and a decrease in the intensity of the 28S and 18S RNA bands can be seen at 100 μM and 200 μM. The increases in RDI (Figure 11C) were considered to be significant ($p < 0.05$) with 10, 20, 50, and 200 μM treatment, but not with 100 μM treatment due to the large variation in the RDI values. Etoposide treatment also resulted in a significant decrease in RNA concentration (Figure 11B) compared to the untreated control for all doses ($p < 0.01$).

Cells were treated with 0.02, 0.2, 0.5, 1 and 2 μM staurosporine for 72 hours (Figure 12). Staurosporine induced visible RNA disruption (Figure 12A) at 0.5, 1 and 2 μM doses, and the resulting increases in RDI (Figure 12C) were considered to be statistically significant at 0.5 ($p = 0.0236$) and 1 ($p = 0.0150$) μM. The change in RDI at 2 μM was not significant as there was a complete loss of the 28S ribosomal RNA band for one replicate, resulting in only two RDI values being obtained for this dose. Decreases in RNA concentration (Figure 12B) with staurosporine treatment were found to be statistically significant at 0.2, 0.5, 1 and 2 μM ($p < 0.05$).

Vincristine was selected as a potential negative control for RNA disruption, as there was little effect on RNA integrity with 50 nM treatment in preliminary experiments. To further assess

the effects of vincristine on RNA integrity, cells were treated with 20, 50, 100, 200 and 500 nM vincristine for 72 hours. Similar to the observations in initial experiments, vincristine had very little effect on RNA integrity with increasing treatment doses. RNA concentration dropped significantly with 20 nM treatment, but the RNA concentration remained relatively consistent and did not decrease much further with increasing doses up to 500 nM vincristine (Figure 13B). The changes in RDI values were considered significantly different from the untreated control at 20, 50 and 500 nM vincristine ($p < 0.05$) but the magnitude of the change was small, and there was little RNA disruption visible on the RNA gel images.

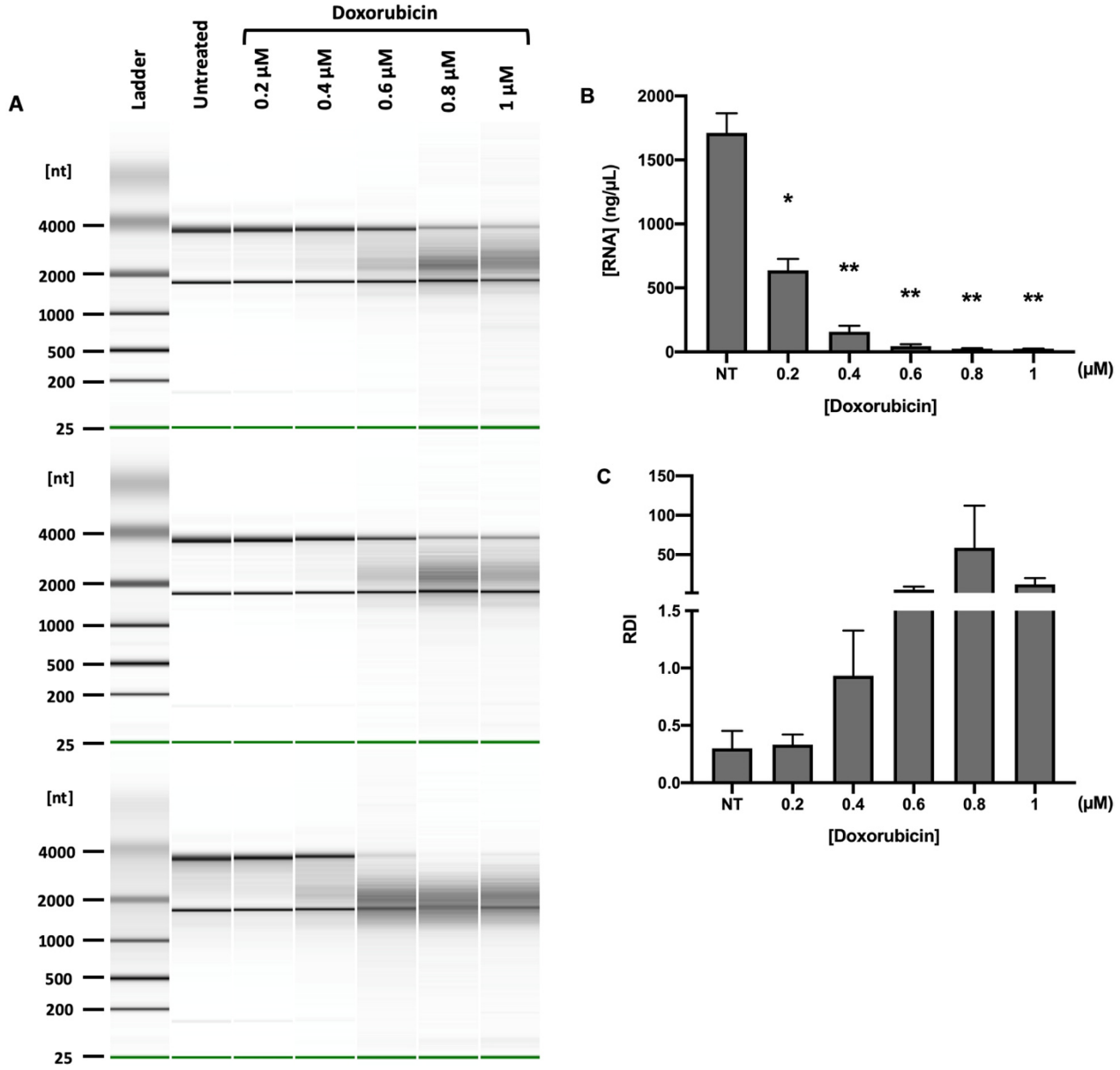

Figure 10. Effect of increasing doses of doxorubicin on RNA integrity after 72 hours. A375 cells were treated with 0.2, 0.4, 0.6, 0.8 and 1 µM doxorubicin. Total RNA was isolated and samples were quantified and analyzed using capillary gel electrophoresis. 'NT' indicates the untreated control. **(A)** Gel images demonstrating the effect on RNA integrity for three biological replicates. (**B)** Effect of treatment on total RNA. **(C)** RDI values determined by the RDA. Error bars indicate ±SEM (paired t-test, one-tailed, n = 3, *p < 0.05, **p < 0.01).

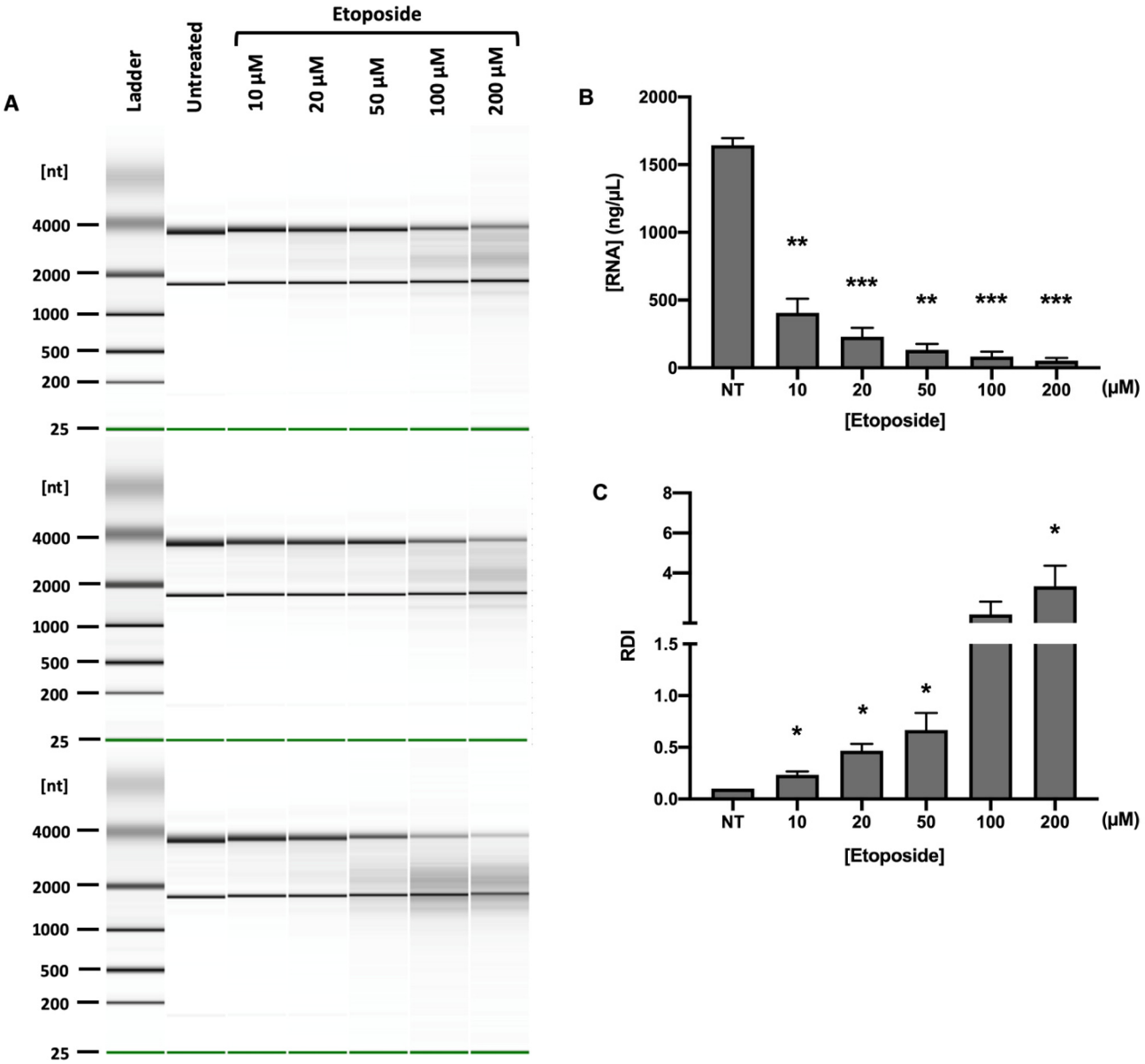

Figure 11. Effect of increasing doses of etoposide on RNA integrity after 72 hours. A375 cells were treated with 10, 20, 50, 100 and 200 µM etoposide. Total RNA was isolated and samples were quantified and analyzed using capillary gel electrophoresis. 'NT' indicates the untreated control. **(A)** Gel images demonstrating the effect on RNA integrity for three biological replicates. (**B)** Effect of treatment on total RNA. **(C)** RDI values determined by the RDA. Error bars indicate ±SEM (paired t-test, one-tailed, n = 3, *p < 0.05, **p < 0.01, ***p < 0.001).

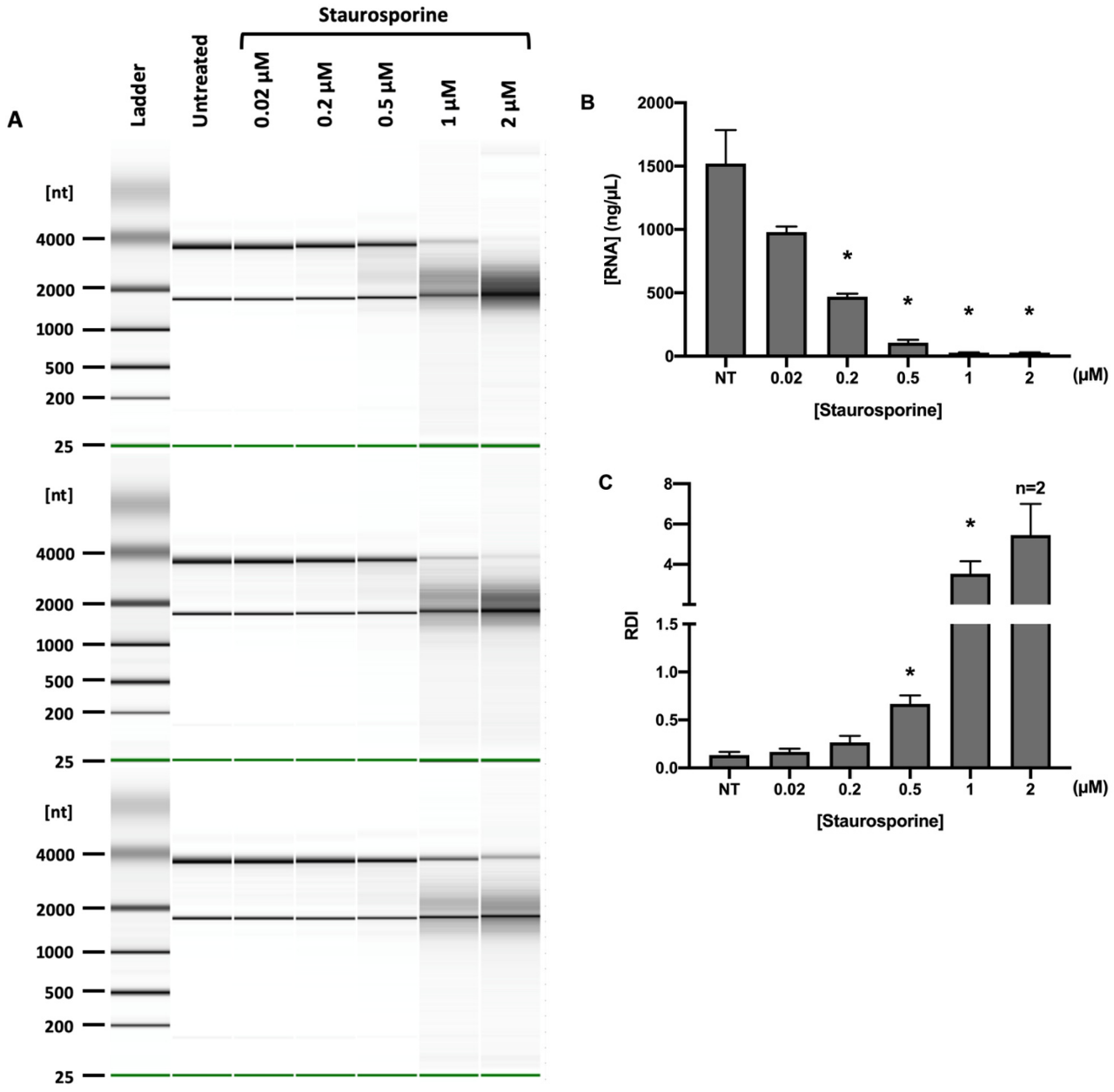

Figure 12. Effect of increasing doses of staurosporine on RNA integrity after 72 hours. A375 cells were treated with 0.02, 0.2, 0.5. 1 and 2 µM staurosporine. Total RNA was isolated and samples were quantified and analyzed using capillary gel electrophoresis. 'NT' indicates the untreated control. **(A)** Gel images demonstrating the effect on RNA integrity for three biological replicates. (**B)** Effect of treatment on total RNA. **(C)** RDI values determined by the RDA. Error bars indicate ±SEM (paired t-test, one-tailed, unless otherwise indicated n=3, *p < 0.05).

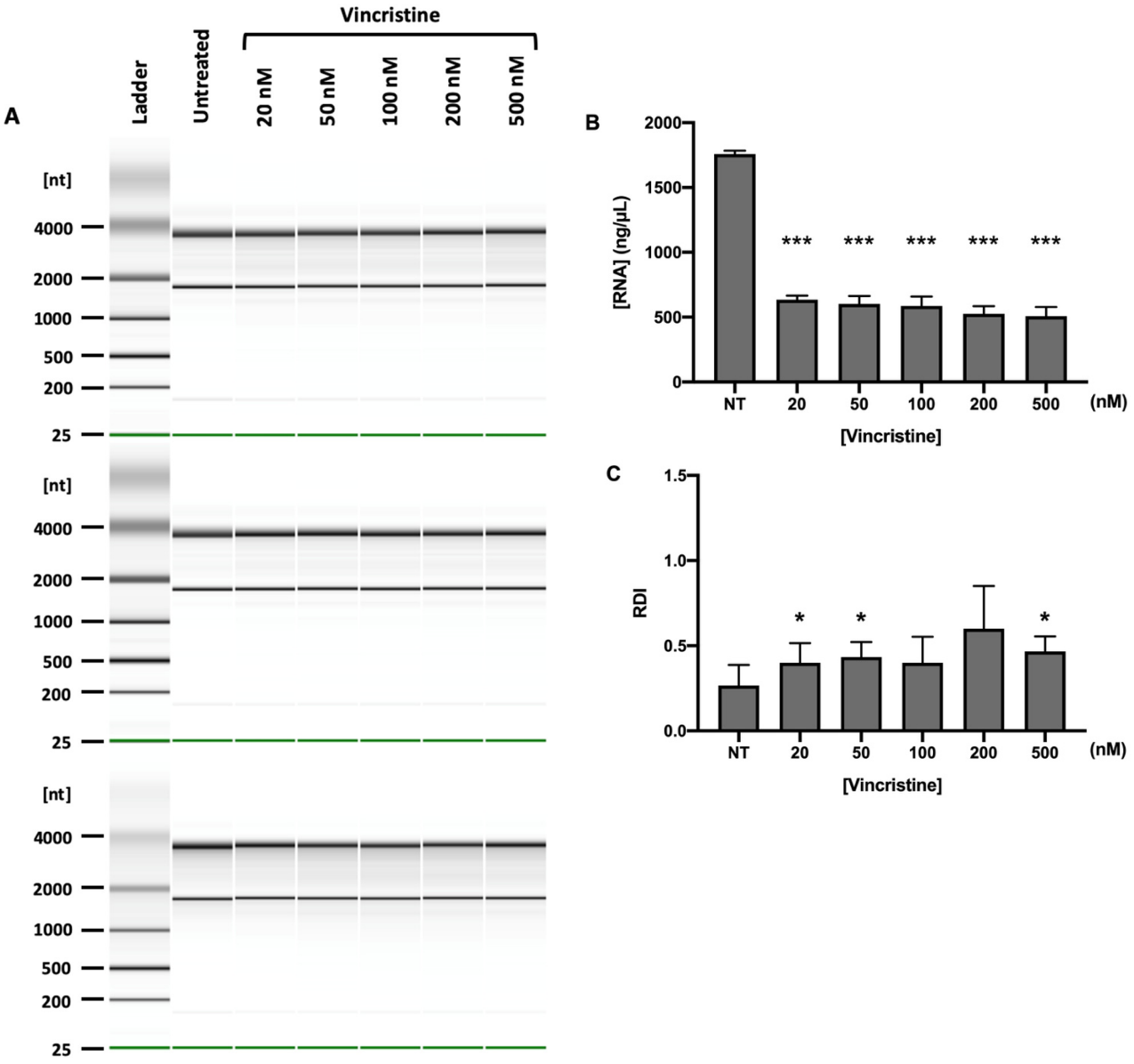

Figure 13. Effect of increasing doses of vincristine on RNA integrity after 72 hours. A375 cells were treated with 20, 50, 100, 200 and 500nM vincristine for 72 hours. Total RNA was isolated and samples were quantified and analyzed using capillary gel electrophoresis. 'NT' indicates the untreated control. **(A)** Gel images demonstrating the effect on RNA integrity for three biological replicates. (**B)** Effect of treatment on RNA concentration. **(C)** RDI values determined by the RDA. Error bars indicate ±SEM (paired t-test, one-tailed, n=3, *$p < 0.05$, ***$p < 0.001$).

Table 10. Results of the doxorubicin, etoposide, staurosporine and vincristine dose versus response curve experiments. Average RNA concentration, RDI value, standard deviation and p value are noted for each treatment condition. "FC" represents the average fold-change from the untreated control.

		RNA Concentration (µg/µL)			**RNA Disruption Index**			
		Avg.	SD	P Value	Avg.	SD	P Value	FC
	0.2 µM	637.7	154.6	0.0105	0.3	0.2	0.3333	1.1
	0.4 µM	158.0	80.1	0.0053	0.9	0.7	0.0594	3.1
Doxorubicin	0.6 µM	45.0	26.9	0.0036	5.6	6.7	0.1447	18.8
	0.8 µM	24.8	8.0	0.0041	58.6	92.8	0.1945	195.3
	1 µM	24.4	4.1	0.0042	12.5	13.7	0.1284	41.6
	10 µM	406.4	178.6	0.0015	0.2	0.1	0.0286	2.3
	20 µM	230.0	114.9	0.0009	0.5	0.1	0.0158	4.7
Etoposide	50 µM	131.4	77.7	0.0010	0.7	0.3	0.0383	6.7
	100 µM	82.4	64.1	0.0006	1.9	1.1	0.0507	19.3
	200 µM	52.5	35.5	0.0005	3.3	1.8	0.0444	33.3
	0.02 µM	979.9	75.8	0.0676	0.2	0.1	0.2113	1.3
	0.2 µM	470.0	40.4	0.0287	0.3	0.1	0.1349	2.0
Staurosporine	0.5 µM	106.5	38.9	0.0190	0.7	0.2	0.0236	5.0
	1 µM	29.5	0.6	0.0151	3.5	1.1	0.0150	26.5
	2 µM	28.9	3.0	0.0151	5.5	2.2	0.0878	40.9
	20 nM	634.4	55.0	0.0003	0.4	0.2	0.0286	1.5
	50 nM	602.2	104.7	0.0005	0.4	0.2	0.0189	1.6
Vincristine	100 nM	587.5	122.6	0.0007	0.4	0.3	0.0918	1.5
	200 nM	526.2	101.4	0.0004	0.6	0.4	0.0648	2.3
	500 nM	508.2	122.4	0.0006	0.5	0.2	0.0371	1.8

3.5 Effect of Treatment on hnRNP K and eIF3f Expression

After establishing the optimal treatments and doses for inducing RNA disruption in A375 cells, we addressed the third project objective and evaluated if eIF3f and hnRNP K expression are impacted by drug treatments that induce RNA disruption. It has been demonstrated that hnRNP K binds to rRNA and this may serve a protective function, preventing rRNA from being degraded[64]. Furthermore, the association of hnRNP K with eIF3f (instead of rRNA) under stress has been correlated with reduced rRNA levels[64]. Given these observations, we were interested in the expression of these proteins during RNA disruption.

Based on the results of the dose versus response curve experiments described, cells were treated with 1 μM doxorubicin, 200 μM etoposide, or 1 μM staurosporine. Cells were also treated with 0.02 μM staurosporine and 10 μM etoposide, as these treatments have previously been used to show the association of eIF3f and hnRNP K[64]. Treatment with 500nM vincristine was used as a negative control for RNA disruption. In addition to the lower doses of staurosporine and etoposide, 0.1 μM doxorubicin and 50 nM vincristine were also included to determine if any changes in expression were dose-dependent. Cells were treated for 48 and 72 hours, to examine the expression of eIF3f and hnRNP K when these proteins are known to associate, and when RNA disruption is at its peak. Whole cell lysates were prepared and protein expression was evaluated by western blotting with eIF3f and hnRNP K antibodies. The expression of eIF3f and hnRNP K was normalized to the GAPDH loading control.

Doxorubicin treatment resulted in significant changes in the expression of both eIF3f and hnRNP K (Figure 14). After 48 hours, there was a small (11%) but statistically significant decrease in eIF3f protein expression with 0.1 μM doxorubicin treatment ($p = 0.0044$), and a 38% decrease in expression ($p = 0.0100$) with 1 μM treatment (Figure 14B). After 72 hours, 0.1 μM

doxorubicin treatment resulted in a small (15%) but statistically significant ($p = 0.0201$) decrease in eIF3f expression, while treatment with 1 μM doxorubicin for 72 hours resulted in statistically significant ($p = 0.0006$) decrease in eIF3f protein expression, with only 11% expression remaining and almost a complete loss of eIF3f seen on the western blot images (Figure 14A). Doxorubicin treatment also resulted in a significant loss of hnRNP K protein expression (Figure 14D). While a significant effect was not observed with 0.1 μM doxorubicin treatment, 1 μM doxorubicin treatment resulted in a significant loss of hnRNP K protein expression after 48 ($p = 0.0022$) and 72 hours ($p = 0.0005$). With 1 μM doxorubicin treatment, nearly a complete loss of hnRNP K can be observed on the western blot images after 48 hours with only 10% expression remaining, and expression is completely lost at 72 hours (Figure 14C).

Etoposide treatment was also found to have an effect on eIF3f and hnRNP K expression (Figure 15). The change in eIF3f protein expression after 48 hours was not found to be statistically significant with 10 or 200 μM etoposide treatment (Figure 15B). After 72 hours, the reduction in eIF3f protein expression was statistically significant with 10 ($p = 0.0247$) and 200 ($p = 0.0039$) μM treatment; the change in eIF3f expression upon treatment with 10 μM etoposide was small with 68% expression remaining, however, western blot images (Figure 15A) show almost a complete loss of eIF3f expression with 200 μM treatment, with only 18% expression compared to the untreated control. In contrast to the changes seen in eIF3f expression, a loss of hnRNP K protein expression could be seen at both 48 and 72 hours. At 48 hours, 10 μM etoposide treatment resulted in a small (18%) but significant ($p = 0.0368$) decrease in hnRNP K expression (Figure 15D). There was a visible change in the expression of hnRNP K (Figure 15C) with 200 μM etoposide treatment after 48 hours with 46% expression remaining, however, this was not considered statistically significant due to the variation between replicate experiments.

After 72 hours of treatment, the loss of hnRNP K expression with 10 μM etoposide treatment was small and not statistically significant, with 66% expression remaining, while treatment with 200 μM etoposide for 72 hours resulted in a complete loss of hnRNP K expression ($p = 0.0050$).

Similar to findings with doxorubicin and etoposide, staurosporine treatment resulted in significant decreases in eIF3f and hnRNP K protein expression (Figure 16). Treatment with 0.02 μM staurosporine was not sufficient to cause a significant change in eIF3f expression at 48 or 72 hours (Figure 16B). However, treatment with 1uM staurosporine resulted in an 68% decrease in eIF3f expression after 48 hours, and an 85% decrease in expression after 72 hours. These decreases in eIF3f protein expression were found to be statistically significant at 48 ($p =0.0053$) and 72 ($p = 0.0448$) hours, with nearly a complete loss of eIF3f expression seen on the gel images at 72 hours (Figure 16A). Similar to eIF3f, 0.02 μM staurosporine was not sufficient to cause a significant change in hnRNP K expression at either timepoint (Figure 16D). The decrease in hnRNP K expression with 1 μM staurosporine treatment was found to be significant at 48 ($p = 0.0064$) and 72 ($p = 0.0157$) hours. There was nearly a complete loss of hnRNP K expression after just 48 hours of treatment with only 4% expression remaining, and this expression decreased further after 72 hours with only 2% expression remaining (Figure 16C).

In contrast to the other three agents tested, vincristine did not result in visible changes in eIF3f or hnRNP K protein expression (Figure 17). Treatment with 50 and 500 nM vincristine was not sufficient to cause a statistically significant change in eIF3f expression after 48 or 72 hours (Figure 17B). Expression of hnRNP K was not affected after 48 hours of treatment, however, after 72 hours there was a small but significant change in hnRNP K expression with 50 ($p = 0.0199$) and 500 ($p = 0.0407$) nM treatment, representing a 25% and 21% decrease in expression from the untreated control, respectively (Figure 17D). While this change was found to

be statistically significant, magnitude of change was quite small and strong hnRNP K bands could still be visualized on the western blot images (Figure 17C).

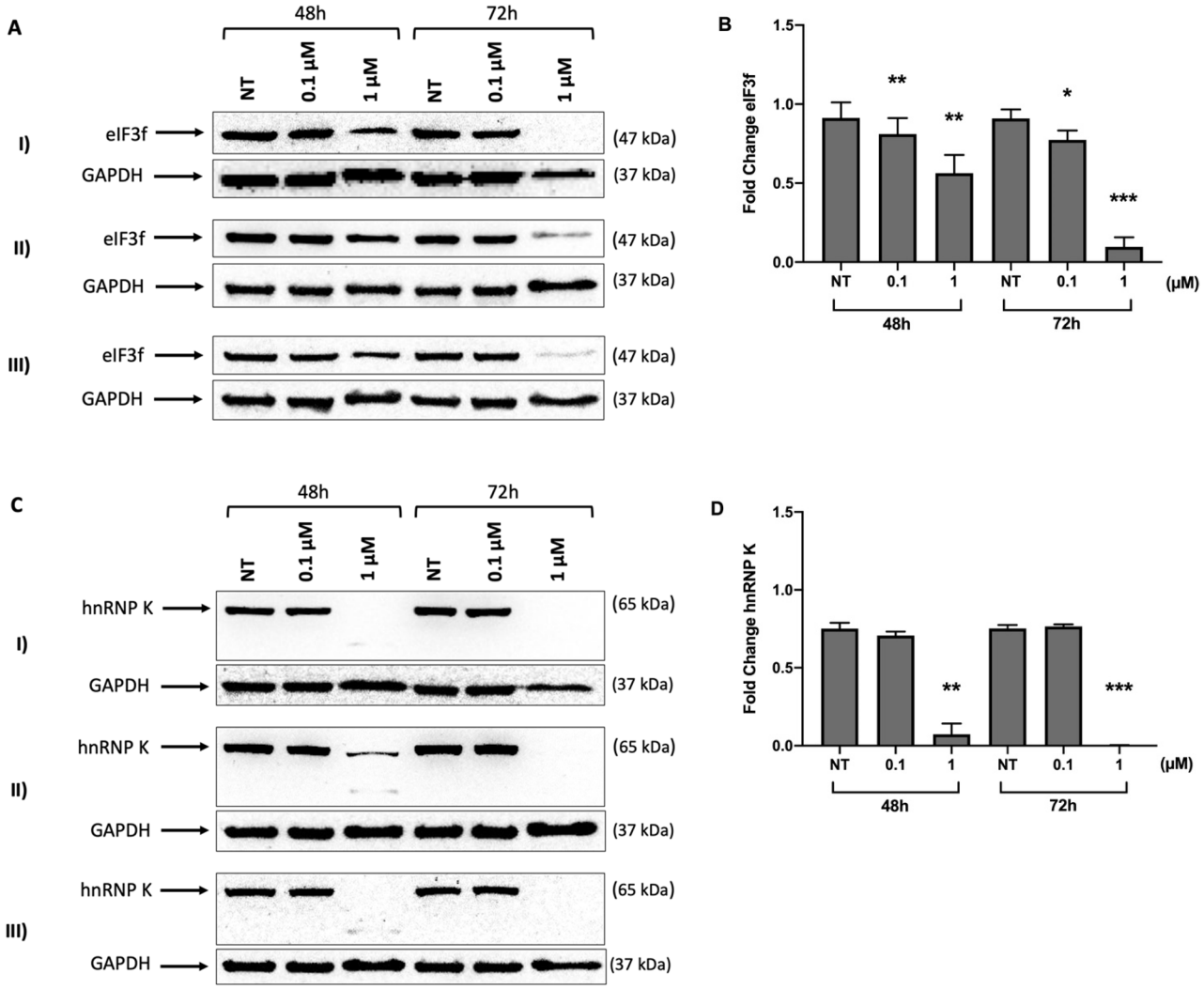

Figure 14. Expression of eIF3f and hnRNP K with doxorubicin treatment. Cells were treated for 48 and 72 hours with 0.1 and 1 µM doxorubicin. Whole cell lysates were obtained and protein expression was determined using western blotting. Fold change in eIF3f and hnRNP K compared to the GAPDH loading control were determined using ImageJ software. 'NT' indicates the untreated controls. **(A)** Three biological replicates of western blots for eIF3f expression. **(B)** Fold

change in eIF3f expression. **(C)** Three biological replicates of western blots for hnRNP K expression. **(D)** Fold change in hnRNP K expression. Error bars indicate ±SEM (paired t-test, one-tailed, n = 3, *p < 0.05, **p < 0.01, ***p < 0.001).

Table 11. Effect of doxorubicin treatment on eIF3f and hnRNP K expression. Protein expression was normalized to the GAPDH loading control. The p values and amount of protein expression relative to the untreated control in percent is noted for each condition.

		[Doxorubicin]	Avg.	SD	P Value	Expression
eIF3f	48 hours	0.1 μM	0.811	0.174	0.0044	89%
		1 μM	0.563	0.200	0.0100	62%
	72 hours	0.1 μM	0.774	0.102	0.0201	85%
		1 μM	0.097	0.105	0.0006	11%
hnRNP K	48 hours	0.1 μM	0.707	0.043	0.0669	94%
		1 μM	0.074	0.119	0.0022	10%
	72 hours	0.1 μM	0.765	0.024	0.2913	98%
		1 μM	0.003	0.003	0.0005	0%

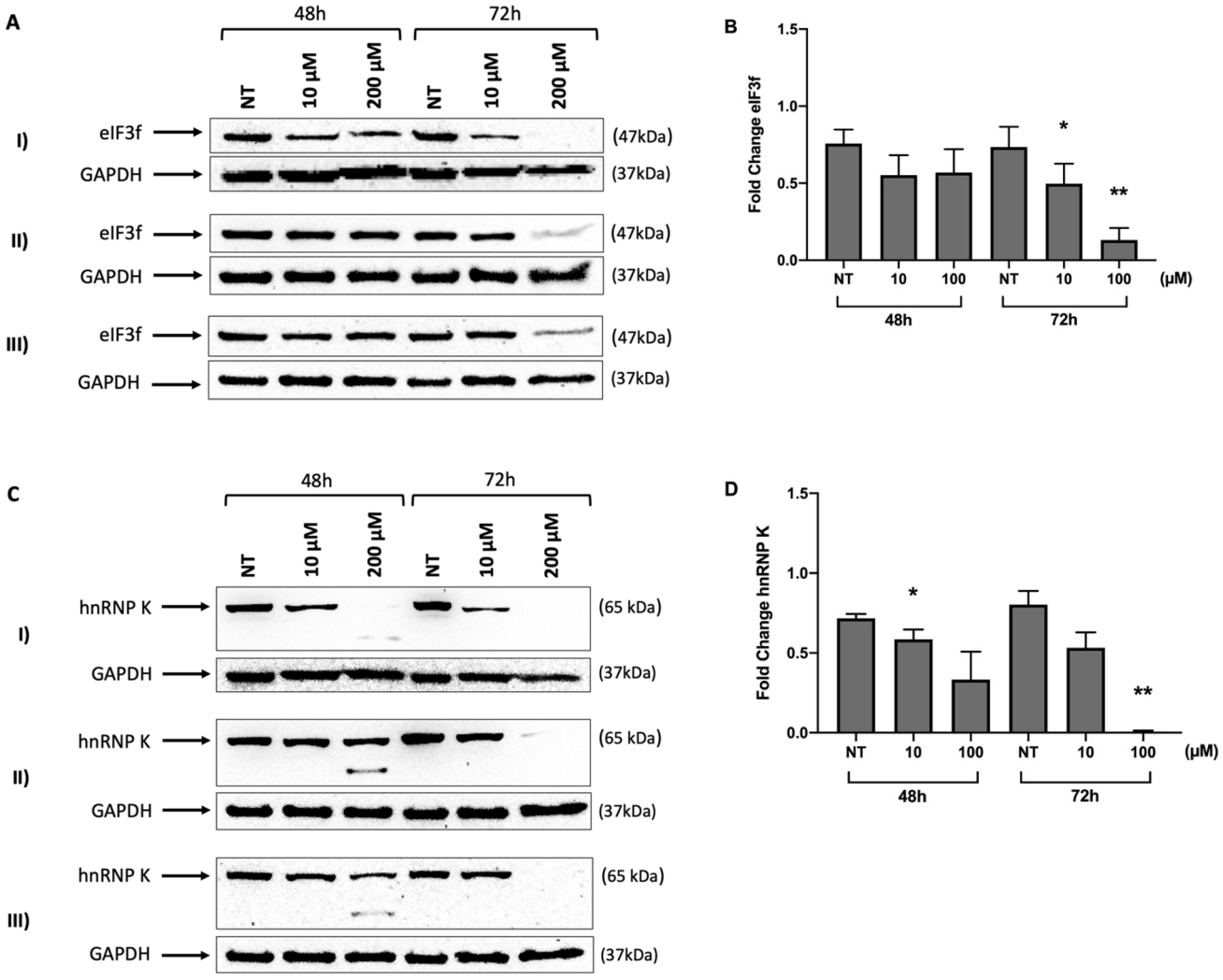

Figure 15. Expression of eIF3f and hnRNP K with etoposide treatment. Cells were treated for 48 and 72 hours with 10 and 200 µM etoposide. Whole cell lysates were obtained and protein expression was determined using western blotting. Fold change in eIF3f and hnRNP K compared to the GAPDH loading control were determined using ImageJ software. 'NT' indicates the untreated controls. **(A)** Three biological replicates of western blots for eIF3f expression. **(B)** Fold-change in eIF3f expression. **(C)** Three biological replicates of western blots for hnRNP K expression. **(D)** Fold-change in hnRNP K expression. Error bars indicate ±SEM (paired t-test, one-tailed, n = 3, *$p < 0.05$, **$p < 0.01$).

Table 12. Effect of etoposide treatment on eIF3f and hnRNP K expression. Protein expression was normalized to the GAPDH loading control. The p values and amount of protein expression relative to the untreated control in percent is noted for each condition.

		[Etoposide]	Avg.	SD	P Value	Expression
eIF3f	48 hours	10 μM	0.553	0.224	0.0717	73%
		200 μM	0.570	0.261	0.0722	75%
	72 hours	10 μM	0.496	0.225	0.0247	68%
		200 μM	0.131	0.135	0.0039	18%
hnRNP K	48 hours	10 μM	0.585	0.106	0.0368	82%
		200 μM	0.333	0.303	0.0610	46%
	72 hours	10 μM	0.532	0.168	0.0630	66%
		200 μM	0.007	0.010	0.0050	1%

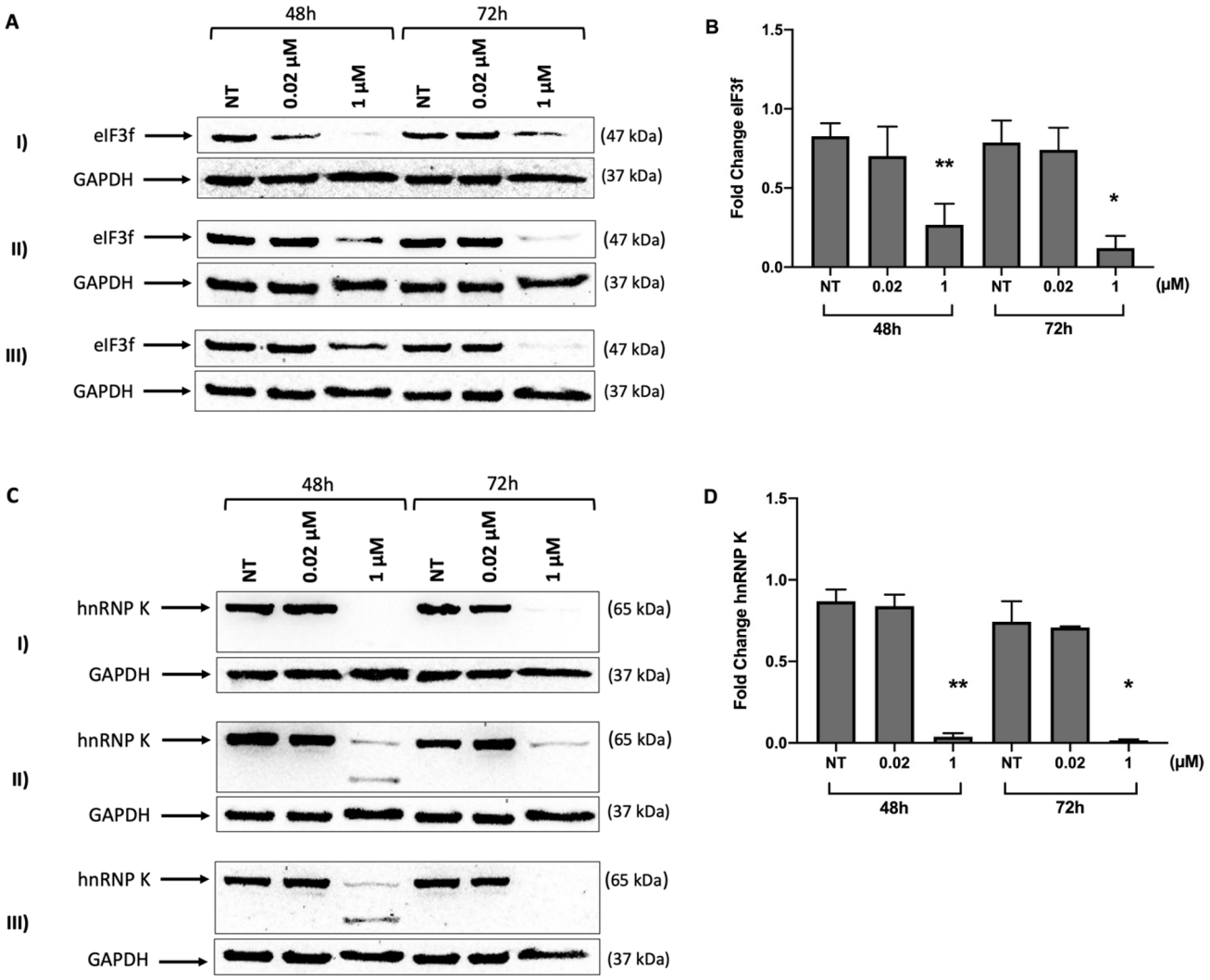

Figure 16. Expression of eIF3f and hnRNP K with staurosporine treatment. Cells were treated for 48 and 72 hours with 0.02 and 1 µM staurosporine. Whole cell lysates were obtained and protein expression was determined using western blotting. Fold change in eIF3f and hnRNP K compared to the GAPDH loading control were determined using ImageJ software. 'NT' indicates the untreated controls. **(A)** Three biological replicates of western blots for eIF3f expression. **(B)** Fold change in eIF3f expression. **(C)** Three biological replicates of western blots for hnRNP K expression. **(D)** Fold change in hnRNP K expression. Error bars indicate ±SEM (paired t-test, one-tailed, n = 3, *$p < 0.05$, **$p < 0.01$).

Table 13. Effect of staurosporine treatment on eIF3f and hnRNP K expression. Protein expression was normalized to the GAPDH loading control. The p values and amount of protein expression relative to the untreated control in percent is noted for each condition.

		[Staurosporine]	Avg.	SD	P Value	Expression
eIF3f	48 hours	0.02 μM	0.702	0.323	0.1782	85%
		1 μM	0.266	0.232	0.0053	32%
	72 hours	0.02 μM	0.741	0.243	0.2964	94%
		1 μM	0.120	0.134	0.0448	15%
hnRNP K	48 hours	0.02 μM	0.838	0.123	0.3074	97%
		1 μM	0.038	0.038	0.0064	4%
	72 hours	0.02 μM	0.708	0.011	0.3991	95%
		1 μM	0.016	0.010	0.0157	2%

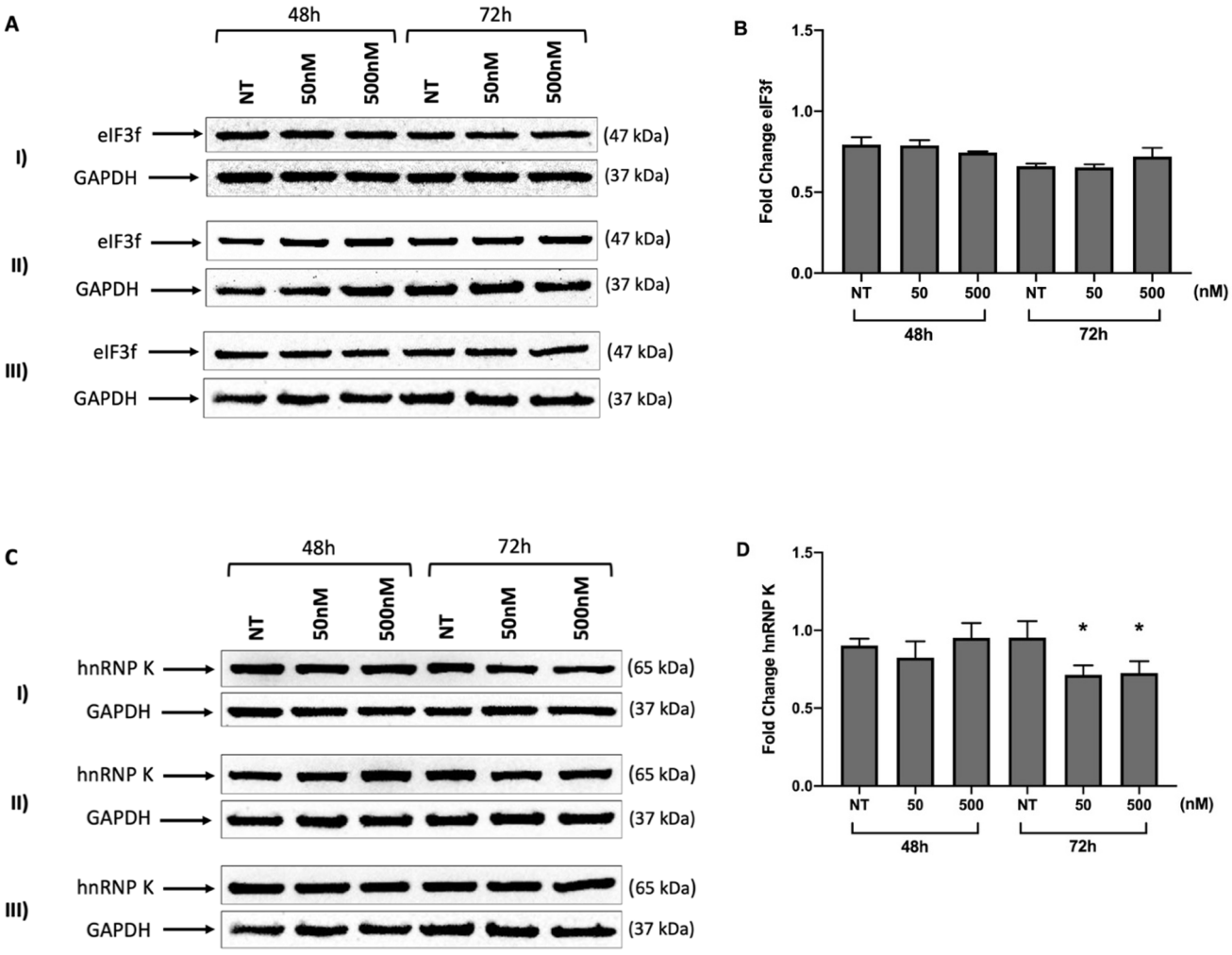

Figure 17. Expression of eIF3f and hnRNP K with vincristine treatment. Cells were treated for 48 and 72 hours with 50 and 500 nM vincristine. Whole cell lysates were obtained and protein expression was determined using western blotting. Fold change in eIF3f and hnRNP K compared to the GAPDH loading control were determined using ImageJ software. 'NT' indicates the untreated controls. **(A)** Three biological replicates of western blots for eIF3f expression. **(B)** Fold change in eIF3f expression. **(C)** Three biological replicates of western blots for hnRNP K expression. **(D)** Fold change in hnRNP K expression. Error bars indicate ±SEM (paired t-test, one-tailed, n = 3, *$p < 0.05$).

Table 14. Effect of vincristine treatment on eIF3f and hnRNP K expression. Protein expression was normalized to the GAPDH loading control. The p values and amount of protein expression relative to the untreated control in percent is noted for each condition.

		[Vincristine]	Avg.	SD	P Value	Expression
eIF3f	48 hours	50 nM	0.789	0.057	0.4763	99%
		500 nM	0.745	0.011	0.2115	94%
	72 hours	50 nM	0.653	0.032	0.4029	99%
		500 nM	0.719	0.094	0.2414	109%
hnRNP K	48 hours	50 nM	0.825	0.182	0.2218	91%
		500 nM	0.952	0.165	0.3154	105%
	72 hours	50 nM	0.713	0.107	0.0199	75%
		500 nM	0.725	0.133	0.0407	79%

3.6 Optimization of Co-Immunoprecipitation

To address the fourth and final project objective, we attempted to optimize a co-immunoprecipitation protocol to evaluate the association of eIF3f and hnRNP K and the potential relationship of this association to RNA disruption. Previous studies have provided evidence that under stress eIF3f associates with hnRNP K, displacing hnRNP K's association with ribosomal RNA[64]. Cell fractionation experiments have shown that treatment of A375 malignant melanoma cells with staurosporine causes eIF3f to co-localize with hnRNP K[64] and the direct association of these proteins was demonstrated using co-immunoprecipitation in HPDE primary cells treated with 10 μM etoposide. In this study, treatment with 0.02 μM staurosporine for either 36 or 48 hours was selected based on previous observations. There were several factors that required optimization, including the method of elution, antibody dilutions, and the quantity of protein lysate.

3.6.1 Glycine Elution

There are several methods that can be used to elute the protein of interest from the protein A/G magnetic beads after immunoprecipitation. Glycine elution uses 0.1 to 0.2 M glycine buffer with a pH of 2 to 3 in order to elute the protein of interest from the beads gently, without eluting much primary antibody[97]. In contrast, SDS elution is much more efficient in eluting the protein of interest, but is very harsh, resulting in the primary antibody being eluted along with the protein of interest[97]. Our protein of interest, eIF3f, has a molecular weight of 47 kDa, while the antibody heavy chain has a molecular weight of 50 kDa[98]. Due to their similarity in molecular weights, there was a concern that if too much primary antibody was eluted with the protein of interest, the signal might interfere with the detection of eIF3f on western blot. Under most circumstances, this issue can be avoided by using two different antibodies from different sources. For example, using a rabbit primary antibody for immunoprecipitation and a mouse primary antibody for western blotting. By doing this, the antibody that is resolved with the protein of interest would not be detected on the western blot, as the mouse secondary antibody would not bind a rabbit primary antibody. In this study, a rabbit primary antibody was used for both immunoprecipitation and western blotting, as an eIF3f antibody from another source was not commercially available.

Glycine elution was used to potentially avoid a strong signal from the primary antibody interfering with the detection of eIF3f on western blots, and experiments were conducted to determine the optimal dilution of primary antibody. A quantity of 50 µg of whole cell lysate was incubated with primary antibody at dilutions of 1 in 50, 1 in 100, and 1 in 150 (Figure 18A). Samples were incubated with primary antibody overnight, and then incubated with 25 µL of protein A/G magnetic beads for 3 hours at room temperature before elution in a 0.2 M glycine

buffer. In this experiment, eIF3f was successfully immunoprecipitated with a 1 in 50 and 1 in 100 antibody dilution using protein extracts from untreated cells; eIF3f was not detected in extracts from staurosporine-treated samples, or when a 1 in 150 dilution was used. There was also a strong signal from the antibody in this experiment.

A second experiment was conducted using only a 1 in 50 or 1 in 100 antibody dilution (Figure 18B). Samples were incubated with antibody and beads as described above, and eIF3f was eluted from beads by glycine elution. In this experiment, eIF3f was successfully detected in the untreated and staurosporine-treated samples using a 1 in 50 dilution of primary antibody. The 1 in 100 antibody dilution showed limited success in the untreated sample, and did not pull down any eIF3f in the staurosporine-treated samples. The membranes were then re-probed with an hnRNP K antibody to determine if there was any hnRNP K co-immunoprecipitated with eIF3f. Unfortunately, hnRNP K was only detected in the whole cell lysate, and was not seen in any of the immunoprecipitated samples.

With both dilutions of primary antibody, there was more eIF3f detected in the supernatant of remaining whole cell lysate than was detected in the immunoprecipitated sample. Based on these observations, a third experiment was conducted using a 1 in 25 dilution of primary antibody (Figure 18C). The primary antibody was incubated with 50 µg of lysate from both untreated and treated cells, pulled down with 25 µL of beads, and eIF3f was eluted using a glycine buffer (Figure 18C). Western blots of these samples showed an increase in the signal of the primary antibody, but did not result in an increased yield of eIF3f.

Theoretically, the protein-protein interaction of eIF3f and hnRNP K could also be detected by doing the reverse immunoprecipitation experiment, and immunoprecipitating hnRNP K. This was an appealing alternative, as there are antibodies from different sources available for

hnRNP K. Since the hnRNP K antibody already obtained for western blotting was also suitable for immunoprecipitation, experiments were conducted to determine if hnRNP K could be successfully immunoprecipitated. Similar to the methods described for eIF3f, 50 µg of lysates from untreated and staurosporine-treated cells were incubated with a 1 in 50 dilution of primary antibody overnight. Lysates and primary antibody were then incubated with 25 µL of magnetic beads and eluted with a glycine buffer. The first replicate of this experiment (Figure 19A) was not successful in immunoprecipitating hnRNP K, and hnRNP K was only detected in the untreated supernatant. A second replicate of this experiment (Figure 19B) showed similar results, with hnRNP K only being detected in the supernatant. Finally, a third replicate of this experiment was conducted with a 1 in 25 primary antibody dilution (Figure 19C), however, this experiment was also unsuccessful in immunoprecipitating hnRNP K.

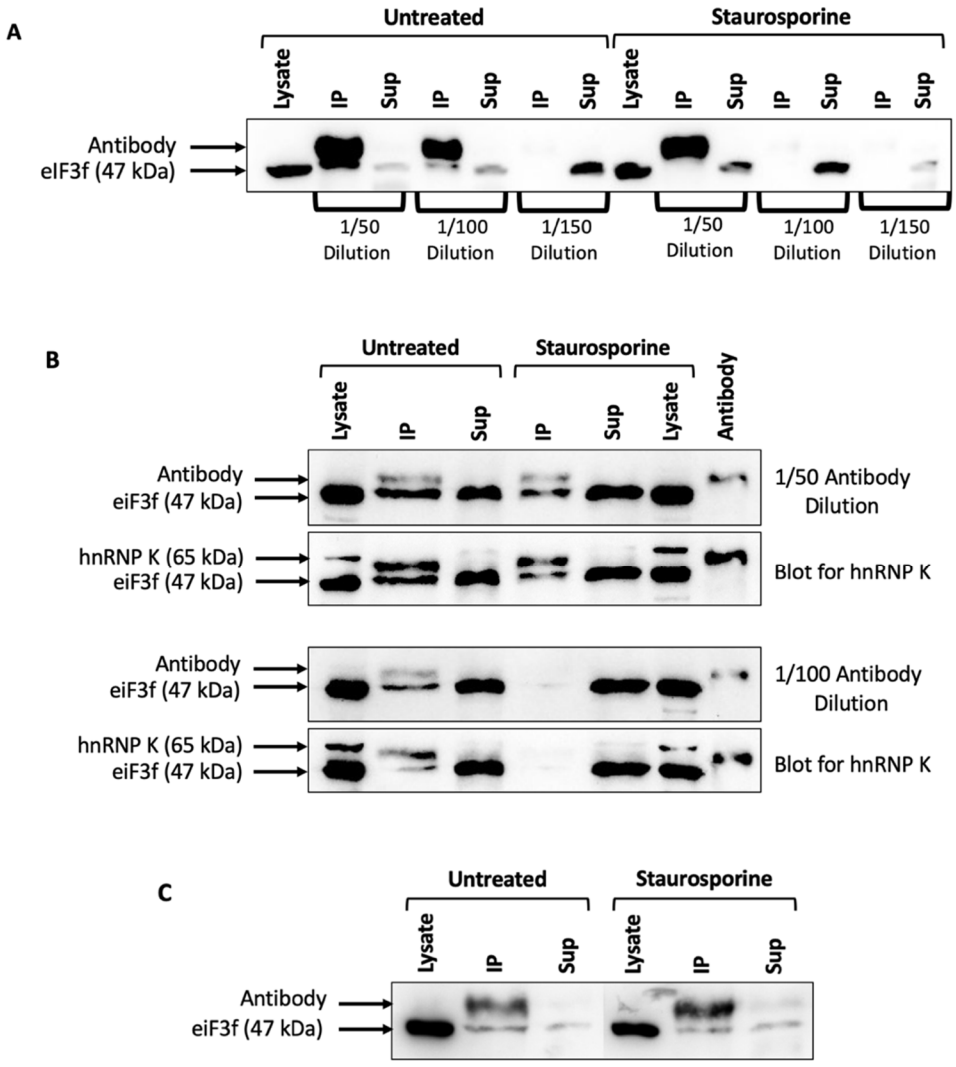

Figure 18. Optimization of immunoprecipitation of eIF3f using glycine buffer elution. The eIF3f primary antibody was incubated with 50 µg of whole cell lysate and pulled down with magnetic beads. For both treated and untreated samples 25 µg of whole cell lysate was used as a loading control. 'IP' indicates the sample of protein eluted from the beads, and 'Sup' indicates the supernatant after immunoprecipitation containing the remaining protein lysate. **(A)** Western blot of immunoprecipitation using a 1 in 50, 1 in 100 and 1 in 150 dilution of antibody. **(B)** Western blot of immunoprecipitation using a 1 in 50 and 1 in 100 dilution of primary antibody.

Membranes were re-probed with hnRNP K to determine if it was co-immunoprecipitated. (**C**) Western blot of immunoprecipitation using a 1 in 25 dilution of antibody.

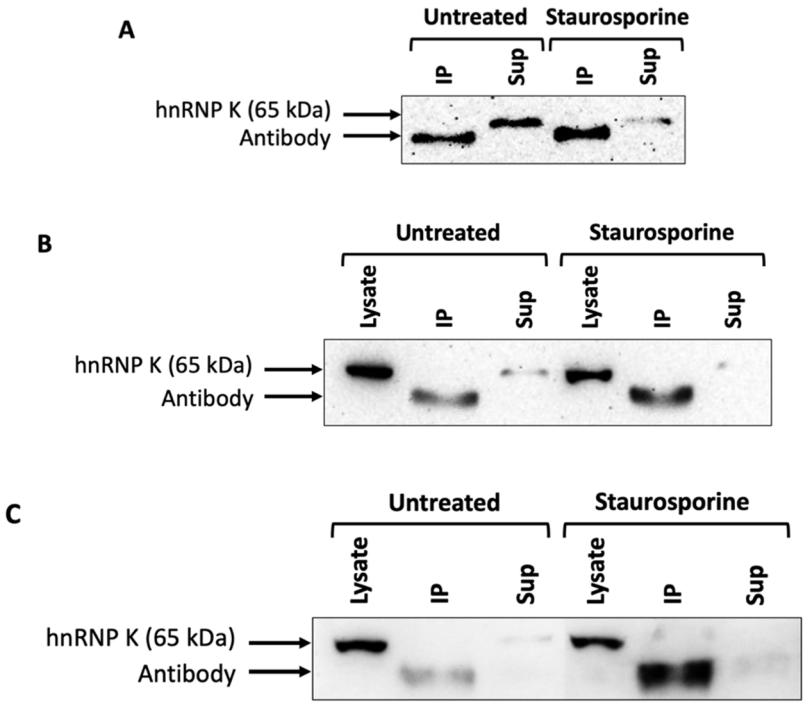

Figure 19. Optimization of immunoprecipitation of hnRNP K using glycine buffer elution. The hnRNP K primary antibody was incubated with 50 µg of whole cell lysate and pulled down with magnetic beads. For both treated and untreated samples 25 µg of whole cell lysate was used as a loading control. 'IP' indicates the sample of protein eluted from the beads, and 'Sup' refers to the supernatant after immunoprecipitation containing the remaining protein lysate. **(A)** First replicate of immunoprecipitation using 1 in 50 antibody dilution **(B)** Second replicate of immunoprecipitation using a 1 in 50 antibody dilution. **(C)** Immunoprecipitation using a 1 in 25 antibody dilution.

3.6.2 SDS Elution

With limited success in immunoprecipitating an adequate amount of eIF3f using the glycine elution method, SDS elution was used for subsequent experiments. In addition to the change in method of elution, a few additional adjustments were made to the protocol. The quantity of protein lysate was increased from 50 µg to 100, 250, and 500 µg of protein lysate, in order to optimize the amount of lysate required to pull-down a sufficient quantity of eIF3f. It was also determined based on the binding capacity of the beads and concentration of the primary antibody, that although the manufacturer recommends 25 µL of beads, 100 µL of beads would be required to pull down 3 µL of antibody. In all subsequent experiments, 3 µL of primary antibody (approximately a 1 in 50 dilution) and 100 µL of magnetic beads were used for immunoprecipitation.

A preliminary experiment was conducted using 100 µg of whole cell lysate from untreated and staurosporine-treated cells. Samples were incubated with 3 µL of primary antibody, and the antibody was precipitated using 100 µL of magnetic beads. The protein of interest was eluted by boiling twice with 25 µL of 2X sample buffer for 2 minutes. Samples were then resolved on a 12% polyacrylamide gel for 2 hours. Results of this experiment (Figure 20A) showed successful immunoprecipitation of eIF3f and limited eIF3f in the supernatant of remaining protein lysate from both treated and untreated cells. To optimize the amount of protein lysate required to obtain a high yield of eIF3f, 100, 250, and 500 µg of untreated protein lysates were used in a second experiment (Figure 20B). Ideally, the amount of eIF3f obtained would be greater than, or similar to the whole cell lysate loading control containing 25 µg of protein. Immunoprecipitation of eIF3f using 100 µg of protein lysate was again successful, but the yield of eIF3f with 250 µg and 500 µg of lysate was much greater. Since 250 and 500 µg of untreated

lysate yielded a similar amount of eIF3f, an additional experiment was conducted to determine if treatment would impact the yield of eIF3f (Figure 20C). In this experiment, eIF3f was immunoprecipitated from 250 and 500 µg of lysates from untreated and staurosporine-treated cells as previously described. Western blots of these samples indicated that a similar yield of eIF3f could be obtained with 250 and 500 µg of protein from both treated and untreated cells. Similar yields in eIF3f with both protein concentrations suggested that the binding capacity of the antibody was met with 250 µg of protein lysate, so 250 µg of protein was used in all subsequent experiments. Experiments conducted with a larger volume of antibody resulted in a high background signal from the primary antibody that overpowered the signal of eIF3f (data not shown).

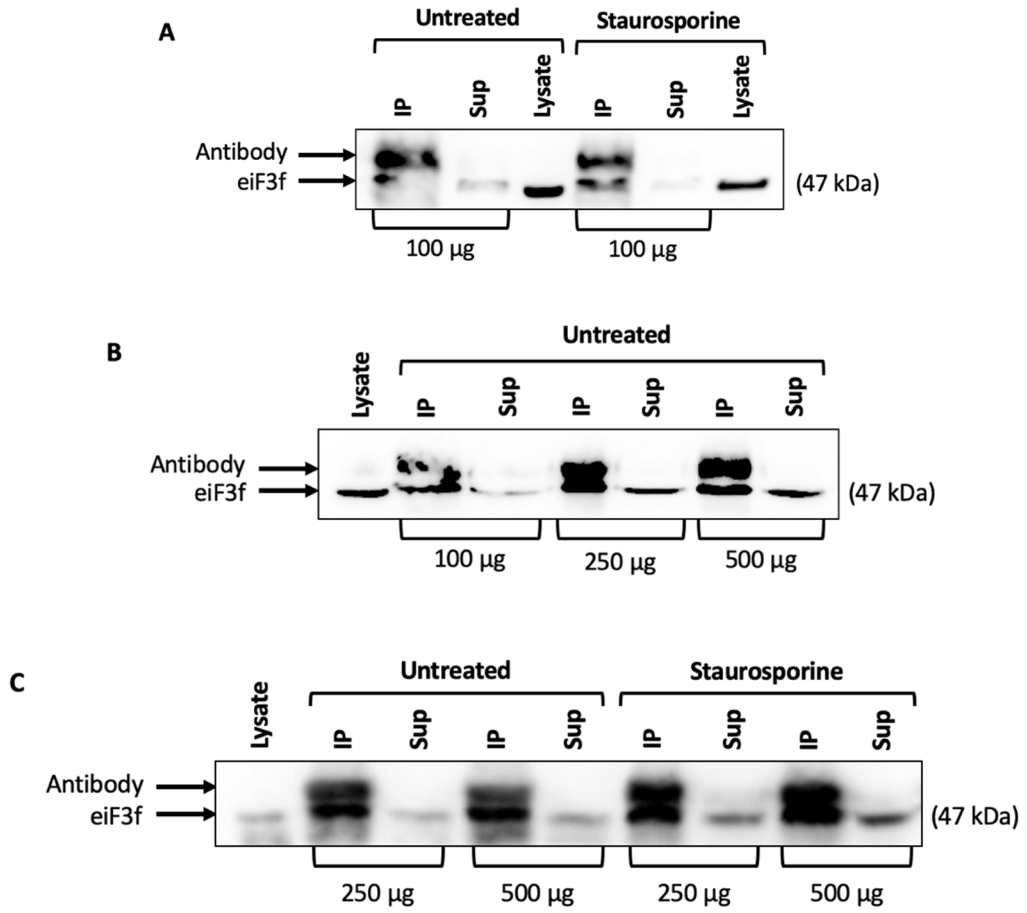

Figure 20. Optimization of immunoprecipitation of eIF3f using SDS buffer elution. The eIF3f primary antibody was incubated with 100, 250, or 500 µg of whole cell lysate and pulled down with magnetic beads. For both treated and untreated samples 25 µg of whole cell lysate was used as a loading control. 'IP' indicates the sample of protein eluted from the beads, and 'Sup' indicates the supernatant after immunoprecipitation containing the remaining protein lysate. **(A)** Western blot of immunoprecipitation using 100 µg treated and untreated lysate. **(B)** Western blot of immunoprecipitation comparing eIF3f yield with 100, 250, and 500 µg of untreated lysate. (**C)** Western blot of immunoprecipitation comparing eIF3f yield with 250 and 500 µg of treated and untreated lysates.

3.6.3 Optimization of Detection of hnRNP K

The use of a rabbit primary antibody to detect hnRNP K on immunoprecipitation western blots after immunoprecipitation with a rabbit eIF3f antibody proved to be problematic, as the anti-rabbit secondary antibody also detected the primary eIF3f antibody that was used for immunoprecipitation. If hnRNP K was successfully co-immunoprecipitated with eIF3f, the hnRNP K signal would likely be weak, and the signal would be overpowered by the signal from the primary antibody that was resolved along with the immunoprecipitated eIF3f. For this reason, a mouse primary antibody was obtained for the detection of hnRNP K.

To determine if hnRNP K can be co-immunoprecipitated with eIF3f, eIF3f was immunoprecipitated from 250 µg of whole cell lysate from untreated or staurosporine-treated cells, isolated after 36 or 48 hours of incubation (Figure 21). A volume of 3 µL of primary antibody was added to each sample, and the primary antibody was pulled down with 100 µL of magnetic beads. The protein of interest was eluted from the beads by SDS elution, and samples were resolved by polyacrylamide gel electrophoresis. Western blots were first probed with the mouse hnRNP K antibody to obtain a clear image without any background signal. The membranes were then re-probed with eIF3f and GAPDH antibodies. GAPDH was used as a loading control, to show that the pull down of eIF3f was specific and did not pull down any non-specific proteins.

The immunoprecipitation of eIF3f appeared to be successful, with a yield of eIF3f greater than the signal from the whole cell lysate loading control. The use of the hnRNP K mouse antibody proved to be superior in detecting hnRNP K when compared to the rabbit antibody. Interestingly, in these experiments hnRNP K was detected in both the immunoprecipitated sample and the remaining supernatant from lysates of treated and untreated cells. At the 36 hour

timepoint (Figure 21A), GAPDH was also detected in both the immunoprecipitated sample and supernatant, indicating that there was likely contaminating protein lysate in the immunoprecipitated sample. However, at 48 hours (Figure 21B) there was a loss of GAPDH in the immunoprecipitated samples, and hnRNP K was still detected in both the immunoprecipitated sample and supernatant. This is the first result that suggests our protocol is able to successfully demonstrate the association of hnRNP K with eIF3f.

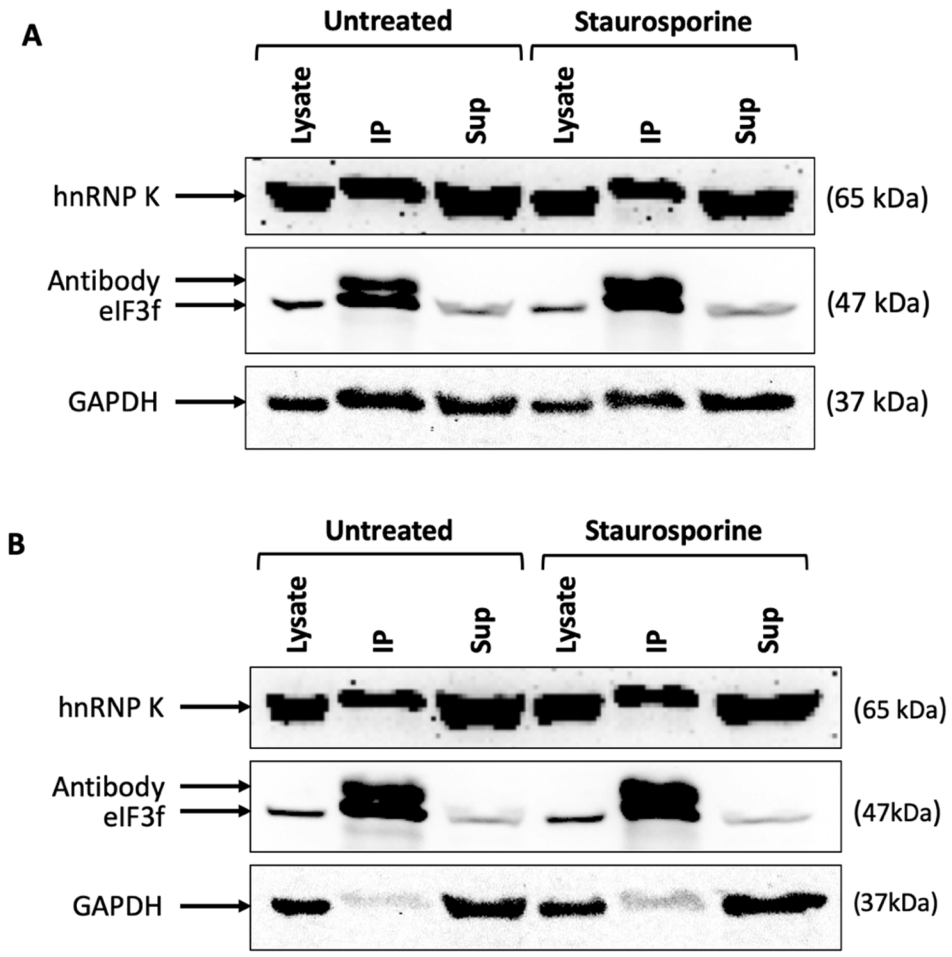

Figure 21. Optimization of co-immunoprecipitation of eIF3f and hnRNP K at 36 and 48 hours. The eIF3f primary antibody was incubated with 250 µg of whole cell lysate and pulled down with magnetic beads. For both treated and untreated samples 25 µg of whole cell lysate was used as a loading control. 'IP' indicates the sample of protein of interest eluted from the beads, and 'Sup' indicates the supernatant after immunoprecipitation containing the remaining protein lysate. The membrane was first probed with a mouse antibody to hnRNP K then re-probed for eIF3f and GAPDH. **(A)** Western blot of immunoprecipitation of samples treated for 36 hours. **(B)** Western blot of immunoprecipitation of samples treated for 48 hours.

3.6.4 Results of Biological Replicates of Co-Immunoprecipitation Experiments

Based on the success of co-immunoprecipitating eIF3f with hnRNP K at 48 hours in the previous experiment, the protocol was repeated. In these experiments, A375 cells were either untreated, or treated with 0.02 μM staurosporine or 10 μM etoposide for 48 hours, after which protein lysates were obtained. As described previously, eIF3f was immunoprecipitated from 250 μg of whole cell lysates, by incubation with 3 μL of primary antibody and immunoprecipitation with 100 μL of magnetic beads. The protein of interest was eluted from the beads by SDS elution, and samples were resolved by polyacrylamide gel electrophoresis. Western blots were first probed with the mouse hnRNP K antibody to obtain a clear image without any background signal. The membranes were then re-probed with eIF3f and GAPDH antibodies. GAPDH was used as a loading control, to show that the pull down of eIF3f was specific.

In this experiment (Figure 22), eIF3f was successfully immunoprecipitated and an adequate yield was obtained for extracts from both treated and untreated cells for all three biological replicates. Minimal GAPDH was detected in the immunoprecipitated samples in select replicates, suggesting that the immunoprecipitation was largely specific to eIF3f. In contrast to the optimization experiments (Figure 21), hnRNP K was not detected in both the immunoprecipitated sample and supernatant, and was only detected in the supernatant, meaning it was not successfully co-immunoprecipitated. The one exception is the first replicate of this experiment, where hnRNP K was detected in the IP of the staurosporine treated sample. This result is promising, however, when the western blot was re-probed with eIF3f, a significant yield was not detected for this sample, so this result is inconclusive.

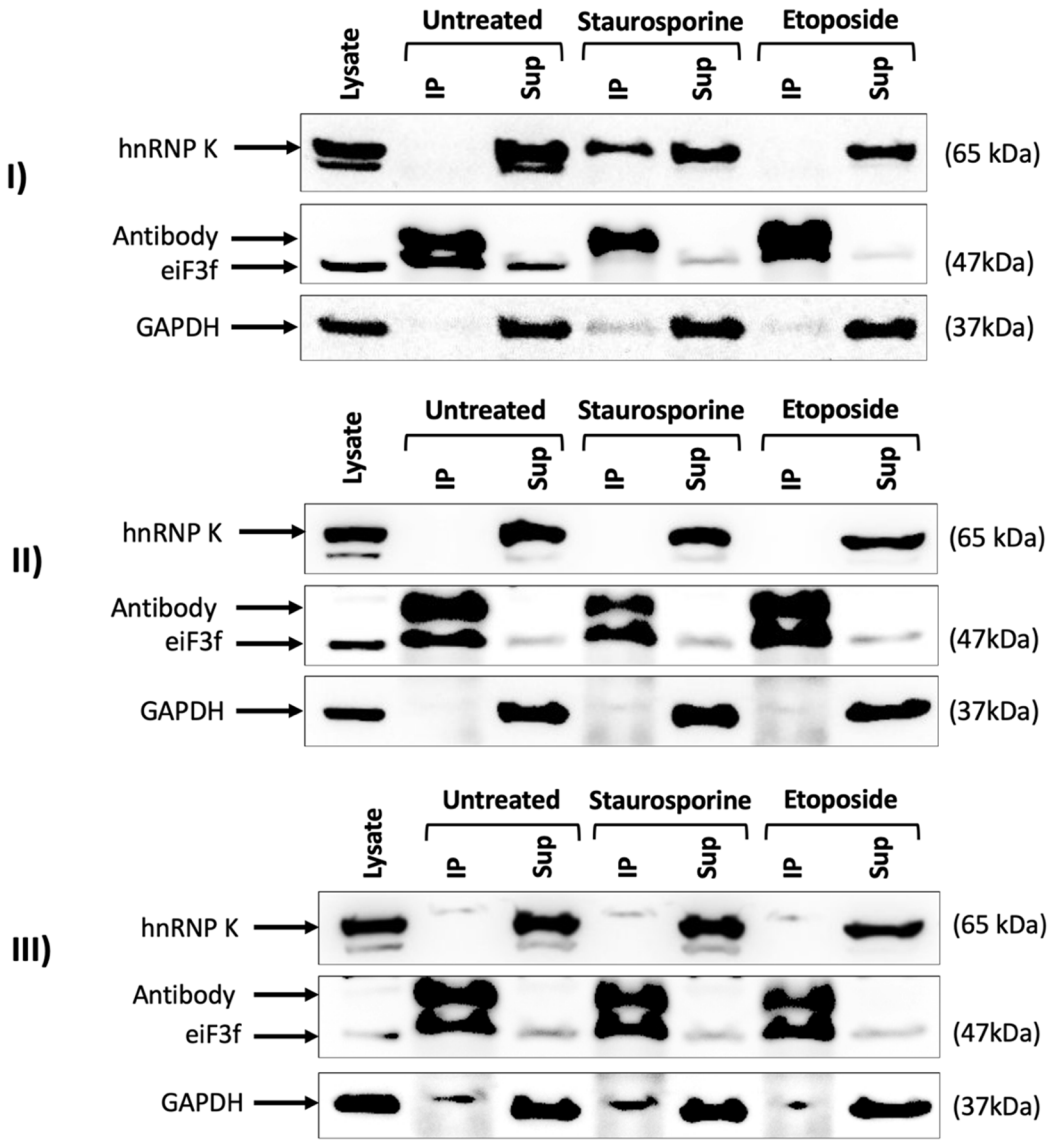

Figure 22. Co-immunoprecipitation of eIF3f and hnRNP K after 48 hours. Samples were treated with 0.02 µM staurosporine or 10 µM etoposide. The eIF3f primary antibody was incubated with 250 µg of whole cell lysate and pulled down with magnetic beads. For both treated and untreated samples 25 µg of whole cell lysate was used as a loading control. 'IP' indicates the sample of protein of interest eluted from the beads, and 'Sup' indicates the supernatant after immunoprecipitation containing the remaining protein lysate supernatant. The membrane was first probed with a mouse antibody to hnRNP K then re-probed for eIF3f and GAPDH.

4.0 Discussion

Cancer remains to be a major public health problem worldwide and the leading cause of death in Canada, despite significant advancements in early detection and therapy over the last decade. The incidence of skin cancer is rising, and although melanoma represents only 1% of skin cancers, it is the most deadly of all skin cancer subtypes. Malignant melanoma is an aggressive cancer which has a limited response to chemotherapy treatment. Parissenti and colleagues demonstrated for the first time that monitoring RNA integrity in breast tumour cells biopsied mid-treatment with chemotherapy can predict patient outcome[39]. The decreased RNA integrity in response to chemotherapy treatment has been termed RNA disruption, and RNA Diagnostics, Inc. has developed the RNA Disruption Assay (RDA) to quantify the level of RNA disruption as an RNA Disruption Index (RDI)[40]. RNA disruption has been shown to occur in response to chemotherapy agents in several breast and ovarian cancer cell lines, but has not been assessed in malignant melanoma cells[89]. Furthermore, the molecular mechanisms behind RNA disruption in response to chemotherapy treatment are not well understood. The aim of this study was to assess whether a variety of mechanistically distinct chemotherapy agents and cell stress can induce RNA disruption in malignant melanoma cells *in vitro*, and to investigate the potential role of eIF3f and hnRNP K in this phenomenon. We surveyed the A375 malignant melanoma cell line for RNA disruption after treatment with nine different chemotherapy agents and after inducing various forms of cell stress. Then, we determined which of the chemotherapy agents are the most effective at inducing RNA disruption (at various doses), and monitored the effects of these chemotherapy agents on the expression of eIF3f and hnRNP K, as these proteins may be involved in regulating rRNA levels under stress. Finally, we attempted to optimize a protocol to assess the effect of chemotherapy agents and stress on the association of eIF3f with hnRNP K, in

order to investigate whether this may be a mechanism involved in chemotherapy- or stress-induced RNA disruption.

4.1 Chemotherapy Induced RNA Disruption in A375 Cells

In this study, we assessed the response of the A375 malignant melanoma cell line to treatment with mechanistically distinct chemotherapy agents. Cells were treated with nine chemotherapy agents, at doses 10-fold higher and 10-fold lower than those shown to induce RNA disruption in other cell lines[89]. A375 cells demonstrated RNA disruption in response to several of the chemotherapy agents tested, with some agents being more effective at inducing RNA disruption than others (Table 15). Strong RNA disruption is characterized by a loss of the 28S and 18S rRNA bands, and the presence of high molecular weight RNA degradation products[40]. While most of the chemotherapy agents tested caused statistically significant changes in RDI, the magnitude of this change for some agents was quite small. Even at the highest doses, most agents did not increase RDI by more than 2. While an RDI of 2 is an approximately 10-fold increase from the untreated control and is considered statistically significant, there is minimal RNA degradation products or loss of the 28S and 18S rRNA bands. A statistically significant change in RDI may indicate complete or partial loss of cell viability, however, we are interested in uncovering the mechanisms behind the formation of unique high molecular weight rRNA degradation products. Therefore, we considered RDI values greater than 2, accompanied by visible RNA degradation products and loss of the 28S and 18S rRNA bands to be strong RNA disruption.

Table 15. Summary of the ability of various chemotherapy agents to induce RNA disruption in A375 cells. The ability of each treatment to cause RNA disruption was considered weak (RDI < 1), intermediate (RDI ≥ 1), or strong (RDI ≥ 2).

	[Drug]	Avg. RDI	RNA Disruption
Alkylating Agents			
Carboplatin	2 µM	0.2	*
	20 µM	0.2	*
	200 µM	1.0	**
Cisplatin	0.17 µM	0.2	*
	1.7 µM	0.2	*
	17 µM	1.3	**
Topoisomerase Inhibitors			
Irinotecan	0.4 µM	0.2	*
	4 µM	0.3	*
	40 µM	1.2	**
Etoposide	1 µM	0.2	*
	10 µM	0.9	*
	100 µM	3.1	***
Doxorubicin	0.1 µM	0.3	*
	1 µM	8.7	***
	10 µM	7.8	***
Epirubicin	0.1 µM	0.3	*
	1 µM	1.9	**
	10 µM	9.6	***
Mitotic Inhibitors			
Vincristine	0.5 nM	0.2	*
	5 nM	0.3	*
	50 nM	0.5	*
Paclitaxel	0.02 µM	0.6	*
	0.2 µM	1.0	**
	2 µM	0.9	*
Docetaxel	0.02 µM	1.0	**
	0.2 µM	1.1	**
	2 µM	0.8	*

*Ability of treatment to cause RNA disruption: * Weak (RDI < 1), ** Intermediate (RDI ≥ 1), *** Strong (RDI ≥ 2)*

The alkylating agents assessed, cisplatin and carboplatin, are both platinum based compounds. These agents at their highest doses of 200 µM carboplatin and 17 µM cisplatin

promoted a significant decrease in total RNA, suggesting a cytotoxic effect. Induction of RNA disruption was limited for both of these agents, with average RDI values of less than 2, and could be considered to have an intermediate ability to induce RNA disruption. Minimal RNA disruption products could be seen with both treatments and only 17 μM cisplatin treatment significantly increased RDI values compared to untreated control. The microtubule targeting agents also did not induce high levels of RNA disruption in A375 cells at the doses assessed. Treatment with vincristine was particularly ineffective at inducing RNA disruption, even at the highest dose; with 50 nM vincristine treatment there was a statistically significant decrease in total RNA when compared to the untreated control, but the yield of RNA suggests this treatment did not kill all cells. This is also reflected by the average RDI value of less than 1 that was observed for cells treated with vincristine. Treatment with 2 μM paclitaxel and docetaxel resulted in statistically significant increases in RDI values and considerably reduced total RNA, but the magnitude of increase in RDI was also small (average RDI ≤ 2). These above-mentioned agents were not found to be strong inducers of RNA disruption at the concentrations tested, but further studies could determine if these agents may result in greater increases in RDI with higher dose treatments or with longer treatment times.

Treatment with topoisomerase II inhibitors proved to be the most effective at inducing RNA disruption in A375 cells. Irinotecan, a topoisomerase I inhibitor, was not able to induce strong RNA disruption at the doses assessed in this study. Even at the highest dose of 40 μM where the increase in RDI and the decrease in total RNA were statistically significant, the average RDI value was less than 2. In contrast, treatment with topoisomerase II inhibitors proved to cause much greater increases in RDI. Treatment with 100 μM etoposide resulted in both significant reductions in RNA yield and a significant and large increase in RDI. The

anthracyclines, doxorubicin and epirubicin, were even more effective than etoposide at inducing a large increase in RDI at a dose of 10 μM. The average RDI with the highest dose of etoposide was 3.1±0.7, while it was 7.8±6.5 and 9.6±3.2, for doxorubicin and epirubicin respectively. While all three topoisomerase II inhibitors resulted in a higher RDI values than all other classes of chemotherapy agents tested, the anthracyclines were superior to etoposide at inducing RNA disruption. We also demonstrated that similar to other cell lines[89], the induction of RNA disruption in A375 cells is both dose- and time-dependent. A time course experiment conducted with doxorubicin treatment revealed that RNA disruption products can be seen as early as 24 hours, and the magnitude of the RDI increased with increasing dose and treatment time, being more prominent at 48 hours, and greatest at 72 hours.

The RDA has been demonstrated to be an excellent cell viability assay, and has been shown to be more effective at determining the cytotoxic concentrations of drug treatments when compared to commonly used cell viability assays, including the Trypan blue exclusion, and CCK8 and clonogenic assays[92]. In this study, we assessed total RNA yield as a method of monitoring cellular response to treatment, in parallel with monitoring RDI. Decreases in total RNA compared to untreated control cells likely indicate that treatment resulted in significant cell death or suppression of cell replication. The three agents found to be the most effective at inducing high RDI values, also resulted in very little RNA being obtained when total RNA was isolated from treated cells (< 100 μg/μL). This is consistent with high RDI values being associated with cytotoxic treatments. This also implies that the other chemotherapy agents used in this study would likely increase RDI at higher, more cytotoxic concentrations. Interestingly, some agents (taxanes) resulted in similar reductions in RNA yield, but very low levels of RNA disruption. Unlike the topoisomerase inhibitors, these agents likely suppress cell replication, or

induce cell death without inducing strong RNA disruption. One important difference between these two classes of agents may be their ability to generate ROS. While the anthracyclines and etoposide are known to induce significant amounts of ROS, the ROS generated by the taxanes is limited[99,100]. Furthermore, while ROS are associated with DNA damage, they have also been shown to lead to significant RNA damage[101]. It is possible that rRNA damage caused by ROS may lead to activation of the 28S NRD pathway, and the subsequent degradation of the 28S rRNA. This would explain the differences seen between these two agents, however, further experiments would be required in order to demonstrate the role of ROS in chemotherapy induced RNA disruption.

A375 cells appear to be more resistant to chemotherapy treatment, and therefore to RNA disruption, when compared to other cell lines[89]. Dacarbazine and temozolomide have been the only chemotherapy agents proven to increase overall survival in malignant melanoma patients, and even with these agents a complete response only occurs in 5-10% of patients[102]. Since patients with malignant melanoma frequently exhibit innate or acquired resistance to chemotherapy treatment *in vivo*[102], it is not surprising that malignant melanoma cells are more resistant to treatment *in vitro* as well. Differences in response to chemotherapy treatment in different tumour cell lines can be explained by the fact that different cell types may have adapted different or more effective mechanisms of resistance. For instance, adaptive mechanisms including reduced accumulation of chemotherapy drugs within tumour cells, drug inactivation, or alterations in drug targets, are common among many cancers exhibiting drug resistance[16].

Many studies have been conducted in an effort to gain insight into how malignant melanoma has adapted to become so resistant to therapy. A common mechanism of resistance to chemotherapy in many cancers is an overexpression of drug transporters, including the ATP-

binding cassette (ABC) transporters, which facilitate the efflux of drugs from the cell[16]. Studies of these transporters in melanoma have revealed that one of the most common ABC transporters associated with resistance, P-glycoprotein (P-gp), is not overexpressed in primary or metastatic melanoma tissues, or in most melanoma cell lines[103]. Furthermore, chemotherapy treatment does not increase the expression of P-gp, suggesting that drug efflux is not a primary mechanism of innate or acquired drug resistance in melanoma[103]. Another mechanism for chemotherapy resistance is the enzymatic inhibition of chemotherapy drugs within the cell. Overexpression of the detoxifying enzyme glutathione-S-transferase (GST), which inhibits drug action through conjugation to glutathione, is a common mechanism of resistance to alkylating agents in many cancers[104]. Studies of GST enzyme expression in melanoma revealed that while the expression is increased in select melanoma tissues and cell lines, its expression varies greatly and cannot be correlated with outcome or chemotherapy response[105]. This suggest that glutathione metabolism is not a major mechanism of resistance to chemotherapy in melanoma. Finally, cancerous cells are known to have innate or acquired modifications to important chemotherapy drug targets, such as topoisomerase II. This mechanism has also been investigated in melanoma, and studies have revealed that acquired resistance to etoposide in melanoma cell lines can be associated with both a decrease in the activity of topoisomerase II[106] and the expression of mutated forms of topoisomerase II[107]. However, studies of topoisomerase II expression in choroidal melanoma revealed that loss of topoisomerase II expression is not correlated with resistance to anthracylcines[108].

Studies to identify specific mechanisms involved in chemoresistance in melanoma cells have been inconclusive. However, melanoma has innate resistance to many chemotherapy agents, and although they are mechanistically distinct, they are all known to lead to the activation

of apoptotic pathways[109]. One of the important hallmarks of cancer cells is a resistance apoptotic signalling, in order to sustain uncontrolled proliferation[1]. This suggests that melanoma is not resistant to the specific actions of chemotherapeutic agents, but is resistant to chemotherapy as a result of strong inherent resistance to apoptosis[102].

4.2 Stress-Induced RNA Disruption in A375 Cells

Several stress pathways have been associated with a decrease in protein synthesis and ribosome biogenesis, but the role of these pathways in RNA disruption remains unclear. In this study, we used various treatments to activate stress pathways in A375 malignant melanoma cells in order to determine if they would result in RNA disruption. We found RNA disruption can occur in response to the inhibition of translation and cyclin dependent kinases, ER stress, oxidative stress, and metabolic stress, with some forms of stress being more effective at inducing RNA disruption than others (Table 16). This indicates that RNA disruption can result from the activation of several stress response pathways.

Table 16. Summary of the ability of various forms of cell stress to induce RNA disruption in A375 cells. The ability of each treatment to cause RNA disruption was considered weak (RDI < 1), intermediate (RDI ≥ 1), or strong (RDI ≥ 2).

	[Drug]	Avg. RDI	RNA Disruption
Cycloheximide	10 µM	0.8	*
	100 µM	1.3	**
	1 mM	3.3	***
Palbociclib	5 µM	0.2	*
	10 µM	0.2	*
	20 µM	0.8	*
Staurosporine	0.02 µM	0.3	*
	0.2 µM	0.6	*
	1 µM	5.4	***
Thapsigargin	0.1 µM	0.3	*
	1 µM	0.6	*
	10 µM	1.9	**
Tunicamycin	1 µM	0.4	*
	10 µM	0.9	*
	25 µM	1.8	**
Media Dilution	50%	0.2	*
	25%	0.1	*
	10%	0.3	*
	5%	1.3	**
	0%	20.8	***
H2O2	25 µM	0.1	*
	50 µM	0.1	*
	100 µM	0.1	*
	200 µM	0.2	*
	400 µM	0.2	*
	500 µM	0.2	*
	1 mM	1.1	**
	2 mM	14.7	***

*Ability of treatment to cause RNA disruption: * Weak (RDI < 1), ** Intermediate (RDI ≥ 1), *** Strong (RDI ≥ 2)*

Cycloheximide was used in this study to determine the effect of the inhibition of protein synthesis on RNA disruption. Cycloheximide inhibits the translation of proteins at the elongation step, through its inhibitory actions on eukaryotic elongation factor 2 (eEF2)[110]. In this study, we

showed that inhibition of protein synthesis with 72 hour cycloheximide treatment resulted in a significant reduction in RNA yield, suggesting that inhibition of protein synthesis had a significant effect on cell replication. Further, we demonstrated that inhibition of protein synthesis leads to significant RNA disruption. RNA disruption products can be seen with all three doses of cycloheximide treatment, although particularly strong RNA disruption was observed with 1 mM treatment. These results suggest that inhibition of protein synthesis, which is known to ultimately lead to the activation of apoptosis, can lead to RNA disruption.

Palbociclib has recently been shown to be a promising therapy in the treatment of hormone-receptor-positive breast cancer, particularly when used in combination with other agents[111]. Through the specific inhibition of CDK4 and CDK6 and subsequent prevention of Rb phosphorylation, palbociclib inhibits cell cycle progression[111]. We used a 72 hour treatment with palbociclib to determine if the specific inhibition of CDK4 and CDK6 could result in RNA disruption. Although treatment with a high dose of the drug (20 μM) resulted in a significant reduction in RNA yield compared to the untreated control, the increase in RDI was quite small. The reduction in total RNA with 20 μM palbociclib treatment was comparable to that with cycloheximide treatment, which induced strong RNA disruption. As previously mentioned, high treatment-induced RDI values are associated with cytotoxicity (cell death), indicating that palbociclib treatment likely acted in a cytostatic manner, inhibiting proliferation but not causing cell death. This is consistent with the known role of CDK4 and CDK6 in cell-cycle progression. Further experiments would be required to determine if increased concentrations of palbociclib or longer treatment time would be cytotoxic to A375 cells, and induce RNA disruption.

Staurosporine is a non-selective inhibitor of CDKs and protein kinase C (PKC) that causes cell cycle arrest at the G2/M checkpoint, ultimately leading to activation of apoptosis. In

this study, we found that a 72 hour treatment with staurosporine induced strong RNA disruption. Treatment with 1 μM staurosporine caused a visible decrease in the intensity of the 28S and 18S rRNA bands and produced high molecular weight RNA degradation products, resulting in a large increase in the RDI. Treatment with 0.02 μM staurosporine, the dose used in previous studies to show the interaction of eIF3f and hnRNP K, resulted in a significant increase in RDI but the magnitude of the increase was small. While 0.02 μM may have been sufficient to induce the hnRNP K and eIF3f interaction, this dose may not be cytotoxic and therefore only caused a small increase in RDI. Furthermore, while 1 μM treatment may be the dose optimal for inducing strong RNA disruption, this dose appears to be quite cytotoxic and significant cell loss may impede the detection of the eIF3f and hnRNP K interaction.

To determine if ER stress can lead to RNA disruption, we treated A375 cells with increasing concentrations of two ER stress-inducing agents (thapsigargin and tunicamycin). Through different mechanisms, both of these agents are known to activate ER stress and induce a subsequent unfolded protein response. Tunicamycin inhibits N-linked glycosylation of proteins, leading to an accumulation of misfolded proteins in the ER[90], while thapsigargin inhibits the ER Ca^{2+}-ATPase and results in a depletion of ER calcium[91]. Treatment with 10 μM thapsigargin and 25 μM tunicamycin both resulted in the production of visible RNA disruption products. At these concentrations, both agents promoted significant increases in RDI, and a reduced cellular RNA yield. However, the observed increases in RDI (average RDI > 2) were not indicative of strong RNA disruption by these agents. It is important to mention that ER stress will only lead to apoptotic cell death if the ER stress is significant and prolonged, as the UPR is activated in an attempt to restore homeostasis[71]. Therefore, A375 cells may require a higher dose or longer

treatment time for cytotoxic concentrations to be reached, and a large increase in RDI to be observed.

We also assessed the ability of oxidative stress to induce RNA disruption using 24 hour hydrogen peroxide treatment. A375 cells were significantly resistant to oxidative stress induced RNA disruption when compared to the A2780 ovarian carcinoma cell line (Figure 8). While A2780 cells displayed a large statistically significant increase in RDI with 100 μM hydrogen peroxide treatment, a dose of 2 mM was required to have similar effects on A375 cells. These increases in RDI were also associated with reduced RNA yield, suggesting that hydrogen peroxide treatment at these doses was cytotoxic to the respective cells. It is well established that cancer cells have higher levels of ROS than normal cells, due to the high metabolic demands associated with uncontrolled cell growth[73]. In order to prevent ROS-mediated cell damage, cancer cells also need to upregulate their antioxidant systems to maintain REDOX homeostasis[73]. Therefore, differences between these two cell lines may be related to differences in their antioxidant systems, with A375 cells having a greater capacity to detoxify ROS and prevent oxidative DNA damage.

In order to assess if metabolic stress activation can lead to RNA disruption, A375 cells were subjected to reduction in cellular nutrients and growth factors by diluting the cell culture medium with PBS. These cells were able to withstand almost complete nutrient/growth factor deprivation before a loss of RNA integrity was observed. Significant RNA disruption did not occur until the cell culture medium was diluted by 95% with PBS, and a large magnitude increase in RDI was only observed with a complete lack of cell culture medium for 72 hours (PBS only). These observations are consistent with the ability of cancerous cells to adapt to a

decrease in nutrient availability due to modifications in key cell signalling pathways such as mTOR[70].

We have demonstrated that specific activation of several different stress pathways can result in a strong induction of RNA disruption. Many of these pathways ultimately lead to the activation of apoptotic pathways (if the stress is not resolved), suggesting that RNA disruption may induce, accompany, or follow the activation of apoptotic pathways. This is supported by observations in many studies that have reported rRNA degradation in response to apoptosis. In 1995, Houge et al. demonstrated that alongside the DNA fragmentation that occurs during apoptosis, specific 28S rRNA cleavage also occurs[84]. This rRNA degradation was observed in several cell lines in response to the activation of apoptosis with multiple agents[84]. Furthermore, studies conducted in oat cells demonstrated that specific rRNA cleavage occurs during apoptosis, and this can be differentiated from the random cleavage that occurs during necrotic cell death[85]. However, studies conducted in HL-60 cells clearly demonstrated that rRNA cleavage can occur independently of apoptosis, and investigators observed extensive DNA fragmentation in the absence of rRNA degradation[86]. Additional studies in thymoma cells have provided evidence that 28S rRNA degradation can occur with the suppression of key apoptotic pathways[87]. This conflicting evidence suggests that there may be multiple pathways associated with the degradation of rRNA, which may or may not impinge on apoptotic pathways.

It has been demonstrated that ribophagy can occur in response to cell stress, including nutrient deprivation and disturbances in protein homeostasis[46]. Therefore, it is possible that the induction of RNA disruption by metabolic stress and treatments that impair protein synthesis or lead to ER stress may lead to the activation of ribophagy. ER stress has also been shown to lead to the generation of ROS, and could potentially cause rRNA damage that leads to the activation

of the NRD pathway[112]. Hydrogen peroxide proved to be a strong inducer of RNA disruption at the higher doses, further suggesting a role of ROS and the NRD pathway in RNA disruption, as described above. However, ROS can also damage proteins and lead to disturbances in protein homeostasis and potentially leading to the activation of ribophagy[113]. Although our findings provide insight into the potential mechanism(s) that ultimately lead to RNA disruption, the exact mechanisms involved remain unclear.

4.3 Loss of hnRNP K and eIF3f Expression with RNA Disruption

Based on the proposed mechanism of the involvement of eIF3f and hnRNP K in rRNA degradation[64], we decided to monitor eIF3f and hnRNP K expression under stress. Four treatments were selected for this experiment, based on both previous observations and the results of this study. Doxorubicin was selected as it was found to be one of the most effective agents for inducing RNA disruption, while vincristine was selected as a negative control for RNA disruption, as it is a very poor inducer of RNA disruption. Staurosporine treatment has been shown to cause the translocation of eIF3f with hnRNP K in A375 cells, while etoposide has been shown to cause the association of eIF3f and hnRNP K in HPDE cells[64], and both of these agents can cause a robust increase in RDI. Prior to protein expression experiments, additional RNA disruption studies were conducted to confirm that RNA disruption with these agents is reproducible, and to explore a wider range of doses for each of these agents. To induce RNA disruption in A375 cells, we first determined that 1 μM doxorubicin, 200 μM etoposide, and 1 μM staurosporine were the appropriate doses to induce RNA disruption. Treatment with 10 μM etoposide and 0.02 μM staurosporine have been shown to cause the interaction of eIF3f and hnRNP K, and we also selected treatment with 0.1 μM doxorubicin to determine the dose

dependency of any changes in protein expression that were observed. Finally, 50 and 500 nM vincristine treatments were used as a negative control.

The association of eIF3f with hnRNP K has been shown to be time-dependent, occurring between 24 and 48 hours post-treatment[64]. In our studies, RNA disruption was found to be detectable at 24 hours and was considerably higher at 48 and 72 hours; therefore, we selected 48 and 72 hour treatment times for assessment of hnRNP K and eIF3f expression. Interestingly, we found that treatment with doses of doxorubicin, etoposide and staurosporine that induce RNA disruption, had significant effects on the expression of hnRNP K and eIF3f. hnRNP K expression was significantly reduced after 48 hours of treatment with high doses of doxorubicin and staurosporine. Although the change was not significant due to variability in the data, 200 μM etoposide treatment also reduced hnRNP K expression at 48 hours. By 72 hours the expression of both hnRNP K and eIF3f were lost. Treatment with vincristine resulted in very little change in expression of these proteins at both doses and timepoints. GAPDH expression was unaffected by doxorubicin, staurosporine, and etoposide, indicating that these stressors did not induce a general reduction in the protein content of cellular extracts.

This timing could potentially support our proposed mechanism for RNA disruption. RNA disruption in response to doxorubicin treatment is visible by 24 hours after treatment and increases at 48 and 72 hours. Therefore, we propose that after 24 hours of treatment when we begin to see RNA disruption, eIF3f forms a complex with hnRNP K removing a protective protein from the 28S rRNA and allowing it to be degraded by RNases. After 48 hours, when we see an increase in RNA disruption products, eIF3f has removed hnRNP K from the ribosome and its expression is lost as a result of proteolysis. After 72 hours, there is strong RNA disruption and eIF3f is lost as a consequence of protein synthesis being suspended due to activation of survival

mechanisms. It has been shown that the 28S NRD pathway involves ubiquitination of 60S ribosomal proteins and activation of the proteasome, which degrades ubiquitinated ribosomal proteins and allows rRNA to be accessed by RNases[52]. The activation of the NRD pathway and associated proteasome activation may explain the loss of hnRNP K and eIF3f that is seen with treatments that induce RNA disruption. Similar studies using other agents and timepoints would help us gain further insight into the potential role of these proteins in RNA disruption. Furthermore, we would need to assess if this loss of eIF3f and hnRNP K can occur in response to other mechanistically distinct chemotherapy agents or forms of cell stress that cause RNA disruption, and if these agents can induce the association of eFI3f and hnRNP K.

4.4 Optimization of Co-Immunoprecipitation of eIF3f and hnRNP K

In previous studies by Wen et al., it was shown that treatment of A375 cells with 0.02 μM staurosporine caused hnRNP K to co-localized with eIF3f[64]. This interaction was also demonstrated in HPDE primary cells treated with 10 μM etoposide using co-immunoprecipitation studies. In addition, knockdown of eIF3f in normal cells resulted in features of malignant transformation, while restoration of eIF3f in cancerous cells resulted in rRNA degradation, suggesting reduced expression of eIF3f may facilitate tumorigenesis by preventing rRNA degradation. hnRNP K was shown to bind to the 28S rRNA and overexpression of hnRNP K was protective against rRNA degradation. Based on their observations the authors proposed that under stress eIF3f dissociates hnRNP K from the ribosome, allowing rRNA to be degraded. We propose that this mechanism may play a role in chemotherapy-induced RNA disruption.

In order to evaluate the potential role of the association of eIF3f and hnRNP K in RNA disruption, we attempted to show the association of these proteins using co-immunoprecipitation.

Despite the clear improvements in the protocol throughout the course of optimization, the ability of this protocol to successfully study the co-immunoprecipitation of these proteins is not clear. We determined that although glycine elution resulted in less interfering signal of the primary antibody run alongside eIF3f, this protocol did not yield sufficient eIF3f. We showed that SDS elution was superior to glycine elution, and optimized the amount of protein lysate, antibody and beads required to pulldown sufficient eIF3f. Finally, we determined that using a mouse primary antibody to hnRNP K was needed to detect the weaker signals due to limited expression of this protein, and to avoid the background signal from the rabbit primary eIF3f antibody from interfering with detection. However, we had limited success in demonstrating this protein-protein interaction under stress. While we did show in some experiments that hnRNP K could be successfully co-immunoprecipitated with eIF3f, these results could not be consistently replicated. Further experiments will be required in order to assess the reproducibility of this protocol and to determine if additional modifications to the protocol are necessary to effectively monitor eIF3f binding to hnRNP K.

5.0 Summary and Conclusions

In this study, we present the first evidence that a variety of structurally and mechanistically distinct chemotherapy agents can induce RNA disruption can occur in malignant melanoma cells *in vitro.* Furthermore, we found that RNA disruption can occur in response to other forms of cell stress, including the inhibition of protein translation, suppression of cell cycle progression with inhibitors of cyclin dependent kinase, ER stress, oxidative stress, and metabolic stress. We showed that the time and dose dependent loss of hnRNP K and eIF3f may support our proposed theory for a mechanism involved in RNA disruption. Finally, we successfully immunoprecipitated eIF3f, however, additional experiments will be required to determine if hnRNP K can be consistently co-immunoprecipitated under stress. Our findings give some insight into a potential mechanism involved in RNA disruption, however, at this time we do not have sufficient evidence to make any definitive conclusions.

Malignant melanoma is an aggressive cancer that has a high tendency for metastasis, and once the disease is metastatic the prognosis for patients is very poor, with an average survival of less than one year. While immunotherapy has become the first-line treatment for malignant melanoma, only about 10% of melanoma patients respond to immunotherapy, and chemotherapy is used often as a second line of treatment. Chemotherapy also continues to be the primary treatment for many cancers, despite its limited efficacy in many patients and its toxic adverse effects. Increased RNA disruption (loss of RNA integrity) in patient tumour samples during chemotherapy treatment can be correlated with increased in overall survival in breast cancer patients, and the BREVITY clinical trial currently underway will hopefully validate the utility of the RNA Disruption Assay (RDA) as a chemotherapy response biomarker. If this assay proves to be useful clinically, it could significantly improve the quality of life in cancer patients by

reducing the use of ineffective chemotherapy regimens that are toxic to host tissues. This would be particularly useful in the case of cancers such as malignant melanoma, where patients have limited benefit from chemotherapy treatment due to the presence of innate of acquired chemotherapy resistance mechanisms.

6.0 References

1. Hanahan, D. & Weinberg, R. A. Hallmarks of cancer: The next generation. *Cell* **144**, 646–674 (2011).
2. Siegel, R. L., Miller, K. D. & Jemal, A. Cancer statistics, 2019. *CA. Cancer J. Clin.* **69**, 7–34 (2019).
3. Brenner, D. R. *et al.* Projected estimates of cancer in Canada in 2020. *Can. Med. Assoc. J* **192**, E199–E205 (2020).
4. Sandru, A., Voinea, S., Panaitescu, E. & Blidaru, A. Survival rates of patients with metastatic malignant melanoma. *J. Med. Life* **7**, 572–576 (2014).
5. Cummins, D. L. *et al.* Cutaneous malignant melanoma. *Mayo Clin. Proc.* **81**, 500–507 (2006).
6. Domingues, B., Lopes, J., Soares, P. & Populo, H. Melanoma treatment in review. *ImmunoTargets Ther.* **Volume 7**, 35–49 (2018).
7. Bandarchi, B., Ma, L., Navab, R., Seth, A. & Rasty, G. From melanocyte to metastatic malignant melanoma. *Dermatol. Res. Pract.* **2010**, (2010).
8. Costin, G.-E. & Hearing, V. J. Human skin pigmentation: melanocytes modulate skin color in response to stress. *FASEB J.* **21**, 976–994 (2007).
9. Liu, J., Fukunaga-Kalabis, M., Li, L. & Herlyn, M. Developmental pathways activated in melanocytes and melanoma. *Arch. Biochem. Biophys.* **563**, 13–21 (2014).
10. Tas, F. Metastatic behavior in melanoma: Timing, pattern, survival, and influencing factors. *J. Oncol.* **2012**, (2012).
11. Wilson, M. A. & Schuchter, L. M. Chemotherapy for Melanoma. in *Cancer Treatment and Research: Melanoma* vol. 167 107–129 (2016).

12. Knackstedt, T., Knackstedt, R. W., Couto, R. & Gastman, B. Malignant melanoma: Diagnostic and management update. *Plast. Reconstr. Surg.* **142**, 202E-216E (2018).

13. Disis, M. L. Mechanism of action of immunotherapy. *Semin. Oncol.* **41**, S3–S13 (2014).

14. Couty, E. *et al.* Safety assessment of anticancer drugs in association with radiotherapy in metastatic malignant melanoma: a real-life report: Radiation/systemic drug combo in metastatic melanoma. *Cancer Chemother. Pharmacol.* **83**, 881–892 (2019).

15. Fu, D., Calvo, J. A. & Samson, L. D. Balancing repair and tolerance of DNA damage caused by alkylating agents. *Nat. Rev. Cancer* **12**, 104–120 (2012).

16. Pan, S. T., Li, Z. L., He, Z. X., Qiu, J. X. & Zhou, S. F. Molecular mechanisms for tumour resistance to chemotherapy. *Clin. Exp. Pharmacol. Physiol.* **43**, 723–737 (2016).

17. Patel, P. M. *et al.* Extended schedule, escalated dose temozolomide versus dacarbazine in stage IV melanoma: Final results of a randomised phase III study (EORTC 18032). *Eur. J. Cancer* **47**, 1476–1483 (2011).

18. Tomco, D. *et al.* Molecular mechanisms of resistance and toxicity associated with platinating agents. *Changes* **29**, 997–1003 (2012).

19. Rabik, C. A. & Dolan, M. E. Molecular mechanisms of resistance and toxicity associated with platinating agents. *Cancer Treat. Rev.* **33**, 9–23 (2007).

20. Qin, Z. *et al.* Systemic evaluation on the pharmacokinetics of platinum-based anticancer drugs from animal to cell level: Based on total platinum and intact drugs. *Front. Pharmacol.* **10**, 1–11 (2019).

21. Hartmann, J. T. & Lipp, H. P. Toxicity of platinum compounds. *Expert Opin. Pharmacother.* **4**, 889–901 (2003).

22. Boddy, A. V. & Yule, S. M. Metabolism and pharmacokinetics of oxazaphosphorines.

Clin. Pharmacokinet. **38**, 291–304 (2000).

23. Giraud, B. *et al.* Oxazaphosphorines: New therapeutic strategies for an old class of drugs. *Expert Opin. Drug Metab. Toxicol.* **6**, 919–938 (2010).
24. Pommier, Y., Leo, E., Zhang, H. & Marchand, C. DNA topoisomerases and their poisoning by anticancer and antibacterial drugs. *Chem. Biol.* **17**, 421–433 (2010).
25. Martins-Teixeira, M. B. & Carvalho, I. Antitumour Anthracyclines: Progress and Perspectives. *ChemMedChem* **15**, 933–948 (2020).
26. Khasraw, M., Bell, R. & Dang, C. Epirubicin: Is it like doxorubicin in breast cancer? A clinical review. *Breast* **21**, 142–149 (2012).
27. Kaklamani, V. G. & Gradishar, W. J. Epirubicin versus doxorubicin: Which is the anthracycline of choice for the treatment of breast cancer? *Clin. Breast Cancer* **4**, S26–S33 (2003).
28. Marinello, J., Delcuratolo, M. & Capranico, G. Anthracyclines as Topoisomerase II poisons: From early studies to new perspectives. *Int. J. Mol. Sci.* **19**, (2018).
29. Cragg, G. M. & Newman, D. J. Plants as a source of anti-cancer agents. *J. Ethnopharmacol.* **100**, 72–79 (2005).
30. Smith, N. A., Byl, J. A. W., Mercer, S. L., Deweese, J. E. & Osheroff, N. Etoposide quinone is a covalent poison of human topoisomerase IIβ. *Biochemistry* **53**, 3229–3236 (2014).
31. Rezonja, R., Knez, L., Cufer, T. & Mrhar, A. Oral treatment with etoposide in small cell lung cancer-dilemmas and solutions. *Radiol. Oncol.* **47**, 1–13 (2013).
32. Ulukan, H. & Swaan, P. W. Camptothecins: A review of their chemotherapeutic potential. *Drugs* **62**, 2039–2057 (2002).

33. Kweekel, D., Guchelaar, H. J. & Gelderblom, H. Clinical and pharmacogenetic factors associated with irinotecan toxicity. *Cancer Treat. Rev.* **34**, 656–669 (2008).

34. Downing, K. H. & Nogales, E. Tubulin and microtubule structure. *Curr. Opin. Cell Biol.* **10**, 16–22 (1998).

35. De Weger, V. A., Beijnenb, J. H. & Schellensa, J. H. M. Cellular and clinical pharmacology of the taxanes docetaxel and paclitaxel -A review. *Anticancer. Drugs* **25**, 488–494 (2014).

36. Joerger, M. Treatment regimens of classical and newer taxanes Cytotoxic Reviews Godefridus J. Peters and Eric Raymond. *Cancer Chemother. Pharmacol.* **77**, 221–233 (2016).

37. Moudi, M., Go, R., Yien, C. Y. S. & Nazre, M. Vinca alkaloids. *Int. J. Prev. Med.* **4**, 1131–1135 (2013).

38. Martino, E. *et al.* Vinca alkaloids and analogues as anti-cancer agents: Looking back, peering ahead. *Bioorganic Med. Chem. Lett.* **28**, 2816–2826 (2018).

39. Parissenti, A. M. *et al.* Association of low tumor RNA integrity with response to chemotherapy in breast cancer patients. *Breast Cancer Res. Treat.* **119**, 347–356 (2010).

40. Pritzker, K. *et al.* RNA disruption and drug response in breast cancer primary systemic therapy. *J. Natl. Cancer Inst. - Monogr.* **2015**, 76–80 (2015).

41. Parissenti, A. M. *et al.* Tumor RNA disruption predicts survival benefit from breast cancer chemotherapy. *Breast Cancer Res. Treat.* **153**, 135–144 (2015).

42. Pelletier, J., Thomas, G. & Volarevic, S. Ribosome biogenesis in cancer: new players and therapeutic avenues. *Nat. Publ. Gr.* **18**, 51–63 (2017).

43. Henras, A. K., Plisson-Chastang, C., O'Donohue, M. F., Chakraborty, A. & Gleizes, P. E.

An overview of pre-ribosomal RNA processing in eukaryotes. *Wiley Interdiscip. Rev. RNA* **6**, 225–242 (2015).

44. Zhou, X., Liao, W. J., Liao, J. M., Liao, P. & Lu, H. Ribosomal proteins: Functions beyond the ribosome. *J. Mol. Cell Biol.* **7**, 92–104 (2015).

45. Ruggero, D. & Pandolfi, P. P. Does the ribosome translate cancer? *Nat. Rev. Cancer* **3**, 179–192 (2003).

46. Kazibwe, Z., Liu, A. Y., MacIntosh, G. C. & Bassham, D. C. The Ins and Outs of Autophagic Ribosome Turnover. *Cells* **8**, 1–14 (2019).

47. Klinge, S. & Woolford, J. L. Ribosome assembly coming into focus. *Nat. Rev. Mol. Cell Biol.* **20**, 116–131 (2019).

48. Denton, D. & Kumar, S. Ribophagy: New receptor discovered. *Cell Res.* **28**, 699–700 (2018).

49. Beese, C. J., Brynjólfsdóttir, S. H. & Frankel, L. B. Selective Autophagy of the Protein Homeostasis Machinery: Ribophagy, Proteaphagy and ER-Phagy. *Front. Cell Dev. Biol.* **7**, 1–12 (2020).

50. Lafontaine, D. L. J. A 'garbage can' for ribosomes: how eukaryotes degrade their ribosomes. *Trends Biochem. Sci.* **35**, 267–277 (2010).

51. LaRiviere, F. J., Cole, S. E., Ferullo, D. J. & Moore, M. J. A late-acting quality control process for mature eukaryotic rRNAs. *Mol. Cell* **24**, 619–626 (2006).

52. Fujii, K., Kitabatake, M., Sakata, T. & Ohno, M. 40S subunit dissociation and proteasome-dependent RNA degradation in nonfunctional 25S rRNA decay. *EMBO J.* **31**, 2579–2589 (2012).

53. Lafontaine, D. L. J. & Tollervey, D. The function and synthesis of ribosomes. *Nat. Rev.*

Mol. Cell Biol. **2**, 514–520 (2001).

54. Aitken, C. E. & Lorsch, J. R. A mechanistic overview of translation initiation in eukaryotes. *Nat. Struct. Mol. Biol.* **19**, 568–576 (2012).

55. Ali, M. U., Ur Rahman, M. S., Jia, Z. & Jiang, C. Eukaryotic translation initiation factors and cancer. *Tumor Biol.* **39**, (2017).

56. Jackson, R. J., Hellen, C. U. T. & Pestova, T. V. The mechanism of eukaryotic translation initiation and principles of its regulation. *Nat. Rev. Mol. Cell Biol.* **11**, 113–127 (2010).

57. Silvera, D., Formenti, S. C. & Schneider, R. J. Translation control in cancer. *Nat. Rev. Cancer* **10**, 254–266 (2010).

58. Shi, J. *et al.* Decreased expression of eukaryotic initiation factor 3f deregulates translation and apoptosis in tumor cells. *Oncogene* **25**, 4923–4936 (2006).

59. Marchione, R., Leibovitch, S. A. & Lenormand, J. L. The translational factor eIF3f: The ambivalent eIF3 subunit. *Cell. Mol. Life Sci.* **70**, 3603–3616 (2013).

60. Spilka, R., Ernst, C., Mehta, A. K. & Haybaeck, J. Eukaryotic translation initiation factors in cancer development and progression. *Cancer Lett.* **340**, 9–21 (2013).

61. Cheng, Y., Jia, C., Li, G. & Li, H. Expression of eukaryotic initiation factor 3f is associated with prognosis in gastric carcinomas. *Oncol. Res. Treat.* **37**, 198–202 (2014).

62. Doldan, A. *et al.* Loss of the eukaryotic initiation factor 3f in pancreatic cancer. *Mol. Carcinog.* **47**, 235–244 (2008).

63. Doldan, A. *et al.* Loss of the eukaryotic initiation factor 3f in melanoma. *Mol. Carcinog.* **47**, 806–813 (2008).

64. Wen, F. *et al.* The tumor suppressive role of eIF3f and its function in translation inhibition and rRNA degradation. *PLoS One* **7**, (2012).

65. Nigg, E. A. Cyclin-dependent protein kinases: Key regulators of the eukaryotic cell cycle. *BioEssays* vol. 17 471–480 (1995).

66. Otto, T. & Sicinski, P. Cell cycle proteins as promising targets in cancer therapy. *Nat. Rev. Cancer* **17**, 93–115 (2017).

67. Harbour, J. W. & Dean, D. C. Rb function in cell-cycle regulation and apoptosis. *Nat. Cell Biol.* **2**, 65–67 (2000).

68. Joerger, A. C. & Fersht, A. R. The p53 Pathway: Origins, Inactivation in Cancer, and Emerging Therapeutic Approaches. *Annu. Rev. Biochem.* **85**, 375–404 (2016).

69. DuRose, J. B., Scheuner, D., Kaufman, R. J., Rothblum, L. I. & Niwa, M. Phosphorylation of Eukaryotic Translation Initiation Factor 2α Coordinates rRNA Transcription and Translation Inhibition during Endoplasmic Reticulum Stress. *Mol. Cell. Biol.* **29**, 4295–4307 (2009).

70. Saxton, R. A. & Sabatini, D. M. mTOR Signaling in Growth, Metabolism, and Disease. *Cell* **168**, 960–976 (2017).

71. Sano, R. & Reed, J. C. ER stress-induced cell death mechanisms. *Biochim. Biophys. Acta - Mol. Cell Res.* **1833**, 3460–3470 (2013).

72. Zhang, X. *et al.* Endoplasmic reticulum stress induced by tunicamycin and thapsigargin protects against transient ischemic brain injury: Involvement of PARK2-dependent mitophagy. *Autophagy* **10**, 1801–1813 (2014).

73. Castaldo, S. A., Freitas, J. R., Conchinha, N. V. & Madureira, P. A. The Tumorigenic Roles of the Cellular REDOX Regulatory Systems. *Oxid. Med. Cell. Longev.* **2016**, (2016).

74. Cerella, C. *et al.* Multiple mechanisms for hydrogen peroxide-induced apoptosis. *Ann. N.*

Y. Acad. Sci. **1171**, 559–563 (2009).

75. Glisovic, T., Bachorik, J. L., Yong, J. & Dreyfuss, G. RNA-binding proteins and post-transcriptional gene regulation. *FEBS Lett.* **582**, 1977–1986 (2008).

76. Burd, C. G. & Dreyfuss, G. Conserved structures and diversity of functions of RNA-binding proteins. *Science (80-.).* **265**, 615–621 (1994).

77. Carpenter, B. *et al.* Heterogeneous nuclear ribonucleoprotein K is over expressed, aberrantly localised and is associated with poor prognosis in colorectal cancer. *Br. J. Cancer* **95**, 921–927 (2006).

78. Bomsztyk, K., Denisenko, O. & Ostrowski, J. hnRNP K: One protein multiple processes. *BioEssays* **26**, 629–638 (2004).

79. Barboro, P., Ferrari, N. & Balbi, C. Emerging roles of heterogeneous nuclear ribonucleoprotein K (hnRNP K) in cancer progression. *Cancer Lett.* **352**, 152–159 (2014).

80. Wang, Z. *et al.* The emerging roles of hnRNPK. *J. Cell. Physiol.* **235**, 1995–2008 (2020).

81. Gao, R. *et al.* Heterogeneous nuclear ribonucleoprotein K (hnRNP-K) promotes tumor metastasis by induction of genes involved in extracellular matrix, cell movement, and angiogenesis. *J. Biol. Chem.* **288**, 15046–15056 (2013).

82. Zhou, R., Shanas, R., Nelson, M. A., Bhattacharyya, A. & Shi, J. Increased expression of the heterogeneous nuclear ribonucleoprotein K in pancreatic cancer and its association with the mutant p53. *Int. J. Cancer* **126**, 395–404 (2010).

83. Li, M. *et al.* Downregulation of HNRNPK in human cancer cells inhibits lung metastasis. *Anim. Model. Exp. Med.* **2**, 291–296 (2019).

84. Houge, G. *et al.* Fine mapping of 28S rRNA sites specifically cleaved in cells undergoing apoptosis. *Mol. Cell. Biol.* **15**, 2051–2062 (1995).

85. Hoat, T. X., Nakayashiki, H., Tosa, Y. & Mayama, S. Specific cleavage of ribosomal RNA and mRNA during victorin-induced apoptotic cell death in oat. *Plant J.* **46**, 922–933 (2006).

86. Samali, A., Gilje, B., Døskeland, S. O., Cotter, T. G. & Houge, G. The ability to cleave 28S ribosomal RNA during apoptosis is a cell-type dependent trait unrelated to DNA fragmentation. *Cell Death Differ.* **4**, 289–293 (1997).

87. King, K. L., Jewell, C. M., Bortner, C. D. & Cidlowski, J. A. 28S ribosome degradation in lymphoid cell apoptosis: Evidence for caspase and Bcl-2-dependent and -independent pathways. *Cell Death Differ.* **7**, 994–1001 (2000).

88. Wen, F. *et al.* Higher expression of the heterogeneous nuclear ribonucleoprotein K in melanoma. *Ann. Surg. Oncol.* **17**, 2619–2627 (2010).

89. Narendrula, R. *et al.* RNA disruption is associated with response to multiple classes of chemotherapy drugs in tumor cell lines. *BMC Cancer* **16**, 1–17 (2016).

90. Wu, J. *et al.* Tunicamycin specifically aggravates ER stress and overcomes chemoresistance in multidrug-resistant gastric cancer cells by inhibiting N-glycosylation. *J. Exp. Clin. Cancer Res.* **37**, 1–12 (2018).

91. Kijima, Y., Ogunbunmi, E. & Fleischer, S. Drug action of thapsigargin on the Ca2+ pump protein of sarcoplasmic reticulum. *J. Biol. Chem.* **266**, 22912–22918 (1991).

92. Mapletoft, J. P. J. *et al.* The RNA disruption assay is superior to conventional drug sensitivity assays in detecting cytotoxic drugs. *Sci. Rep.* **10**, 1–12 (2020).

93. Sun, Y. *et al.* Potent anti-tumor efficacy of palbociclib in treatment-naïve H3.3K27M-mutant diffuse intrinsic pontine glioma. *EBioMedicine* **43**, 171–179 (2019).

94. Elango, R. *et al.* Concurrent targeting of BMI1 and CDK4/6 abrogates tumor growth in

vitro and in vivo. *Sci. Rep.* **9**, 1–13 (2019).

95. Thuret, G. *et al.* Mechanisms of staurosporine induced apoptosis in a human corneal endothelial cell line. *Br. J. Ophthalmol.* **87**, 346–352 (2003).

96. Antonsson, A. & Persson, J. L. Induction of apoptosis by staurosporine involves the inhibition of expression of the major cell cycle proteins at the G2/M checkpoint accompanied by alterations in Erk and Akt kinase activities. *Anticancer Res.* **29**, 2893–2898 (2009).

97. Abcam. Immunoprecipitation Protocol. 1–4 (2010).

98. Janeway, C., Travers, P., Walport, M. & Shlomchik, M. The Structure of a Typical Antibody Molecule. in *Immunology: The Immune System in Health and Disease* 1–10 (Garland Science, 2001).

99. Conklin, K. A. Chemotherapy-associated oxidative stress: Impact on chemotherapeutic effectiveness. *Integr. Cancer Ther.* **3**, 294–300 (2004).

100. Mizutani, H., Tada-Oikawa, S., Hiraku, Y., Kojima, M. & Kawanishi, S. Mechanism of apoptosis induced by doxorubicin through the generation of hydrogen peroxide. *Life Sci.* **76**, 1439–1453 (2005).

101. Li, Z. *et al.* Recent Advances: Molecular Mechanism of RNA Oxidation and Its Role in Various Diseases. *Front. Mol. Biosci.* **7**, 1–7 (2020).

102. Soengas, M. S. & Lowe, S. W. Apoptosis and melanoma chemoresistance. *Oncogene* **22**, 3138–3151 (2003).

103. Schadendorf, D., Herfordt, R. & Czarnetzki, B. M. P-glycoprotein expression in primary and metastatic malignant melanoma. *Br. J. Dermatol.* **132**, 551–555 (1995).

104. Helmbach, H., Rossmann, E., Kern, M. A. & Schadendorf, D. Drug-resistance in human

melanoma. *Int. J. Cancer* **93**, 617–622 (2001).

105. Schadendorf, D., Jurgovsky, K., Kohlmus, C. M. & Czarnetzki, B. M. Glutathione and related enzymes in tumor progression and metastases of human melanoma. *J. Invest. Dermatol.* **105**, 109–112 (1995).

106. Lage, H., Helmbach, H., Dietel, M. & Schadendorf, D. Modulation of DNA topoisomerase II activity and expression in melanoma cells with acquired drug resistance. *Br. J. Cancer* **82**, 488–491 (2000).

107. Campain, J. A. *et al.* Acquisition of multiple copies of a mutant topoisomerase IIα allele by chromosome 17 aneuploidy is associated with etoposide resistance in human melanoma cell lines. *Somat. Cell Mol. Genet.* **21**, 451–471 (1995).

108. Satherley, K. *et al.* Relationship between expression of topoisomerase II isoforms and chemosensitivity in choroidal melanoma. *J. Pathol.* **192**, 174–181 (2000).

109. Fisher, D. E. Apoptosis in cancer therapy: Crossing the threshold. *Cell* **78**, 539–542 (1994).

110. Schneider-Poetsch, T. *et al.* Inhibition of eukaryotic translation elongation by cycloheximide and lactimidomycin. *Nat. Chem. Biol.* **6**, 209–217 (2010).

111. Turner, N. C. *et al.* Palbociclib in hormone-receptor-positive advanced breast cancer. *N. Engl. J. Med.* **373**, 209–219 (2015).

112. Zeeshan, H. M. A., Lee, G. H., Kim, H. R. & Chae, H. J. Endoplasmic reticulum stress and associated ROS. *International Journal of Molecular Sciences* vol. 17 (2016).

113. Cabiscol, E., Piulats, E., Echave, P., Herrero, E. & Ros, J. Oxidative Stress Promotes Specific Protein Damage inSaccharomyces cerevisiae. *J. Biol. Chem.* **275**, 27393–27398 (2000).